2010

University of Nevada - Reno

Development, Analysis and Use of a Distributed Wireless Sensor Network for Quantifying Spatial Trends of Snow Depth and Snow Water Equivalence Around Meteorological Stations With and Without Snow Sensing Equipment

A thesis submitted in partial fulfillment of the requirements for the degree of Master of Science in Hydrology

By:
C. David Moeser

Thesis Advisor:
Dr. Mark Walker

December 2010

THE GRADUATE SCHOOL

We recommend that the thesis
prepared under our supervision by

C. DAVID MOESER

entitled

Development, Analysis And Use Of A Wireless Sensor Network For Quantifying Spatial Trends Of Depth And Snow Water Equivalence Around Meteorological Stations With And Without Snow Sensing Equipment

be accepted in partial fulfillment of the
requirements for the degree of

MASTER OF SCIENCE

Dr. Mark Walker, Advisor

Dr James Carr, Committee Member

Dr. Christian Skalka, Graduate School Representative

Marsha H. Read, Ph. D., Associate Dean, Graduate School

December, 2010

Development, Analysis and Use of a Distributed Wireless Sensor Network for Quantifying Spatial Trends of Snow Depth and Snow Water Equivalence Around Meteorological Stations With and Without Snow Sensing Equipment

Abstract:

Snow accumulated in the mountainous portions of the Western United States is an extremely important source of water supply. Federal resource management agencies (USFS, BLM, USGS, NRCS, Federal water master), non-governmental organizations (stakeholder groups) and private contractors quantify and predict future stream and river flows throughout the Western United States for water use allocated to water supply, recreational waters, and water to sustain aquatic life. These agencies devote substantial resources to estimating snowpack depth and snow water equivalence during the winter and spring months to allocate water through river and irrigation systems. Forecasts are based on measurements collected from a network of meteorological stations, some of which also measure snow water equivalence and snow depth. Such stations are expensive to establish and maintain and provide data from a single point of measurement. Accordingly, forecasts cannot account for spatial variability associated with snowpack depth and water content. Information about spatial variability could be extremely useful in water supply forecasts, especially if measurements from meteorological stations, with or without snow sensing equipment, could be extended by simple, low cost data collection efforts.

A prototype wireless sensor network, Snowcloud, was deployed in the Sagehen Creek experimental field station, CA. Snowcloud was developed by the University of Vermont and deployed in fall, 2009 in collaboration with the University of Nevada-Reno, for

a single season study in the Sagehen Creek Field Station, near Truckee, CA. The network was set up around a meteorological station to sense and report snow depth and temperature from a distributed set of independent nodes.

The Snowcloud deployment within the Sagehen Creek Field Station examined small scale variability in snow depth and SWE arising from temporal changes in state variables, including canopy cover, aspect, temperature, solar radiation, wind speed, wind direction and relative humidity. The Snowcloud nodes were tested to estimate SWE from SD around a fixed based meteorological station acting as a station (1) with snow sensing equipment and (2) without snow sensing equipment.

Within the field site, neither a snow pillow that was part of the meteorological station nor manual snow course transects represented the spatial mean SWE of the study area. The snow pillow overestimated SWE values an average of 30% with a maximum overestimation of 40%.

The six Snowcloud nodes in conjunction with regression and kriging effectively captured the spatial and temporal variability of SWE with a resolution much greater than the snow pillow. Both estimation methods accurately extrapolated SWE at the node sites and at 48 points in a sampling grid covering the site, with a maximum RMSE of 2.7%. A simple estimate based only on SWE at the meteorological station and SD throughout the site predicted SWE with greater accuracy than regression models that included state variables from the meteorological station and site characteristics. Aspect with canopy closure percentage was an important predictor of SWE at meteorological stations without snow sensing equipment. Significantly decreased correlation between measured and estimated SWE was seen within the models with only the use of a generalized canopy closure qualifier, and the quality of the correspondence were not increased by the addition of a generalized

qualifier. With the exception of SD, percent canopy closure to the north (P = 0.000+) was the most important qualifier for predicting SWE around meteorological stations without snow sensing equipment.

Acknowledgments

The contributions and assistance from numerous professionals involved with water forecasts, snow surveys, geo-statistics, snow sensing equipment and the Snowcloud platform have been invaluable to the thoughts, methods and results presented here. Specifically, the following people contributed through interviews, email/phone correspondence, sensor network site tours and field work help. Their input and feedback has been integral to the completion of this document. Thank you all.

- Dr. Mark Walker, *adviser and committee member* – Associate Professor and Interim Chair, Department of Natural Resources and Environmental Science, University of Nevada-Reno
- Dr. James Carr, *committee member* –Professor, Geological Sciences and Engineering, University of Nevada-Reno, creator of Visual Data, an integrated software platform for data analysis and digital image processing
- Dr. Christian Skalka, *committee member* - Associate Professor, Department of Computer Science, University of Vermont, co-creator of Snowcloud
- Dr. Douglas Boyle – Associate Professor, Division of Hydrologic Sciences, Desert Research Institute, P.I. and developer of Sagehen Creek sensing network
- Faerthen Felix, Jeff Brown – Sagehen Creek Field Station managers
- Dr Jeff Frolik –Associate Professor, School of Engineering, University of Vermont, co-creator of Snowcloud
- Dan Greenlee- Hydrologist/ Water Forecaster, Natural Resource Conservation Service, Reno, NV
- Brad Lyles- Researcher, Desert Research Institute, Sagehen Creek sensing network caretaker

- Yuichiro Miyata – GIS professional, University of Nevada-Reno, co-developer of Python script for ArcGIS time series kriging
- Bob Rice – Assistant Researcher, School of Engineering, University of California- Merced
- Michaela Woerndl – Environmental Engineer, University of Natural Resources and Life Sciences, Austria, field help

Development, Analysis and Use of a Wireless Sensor Network for Quantifying Spatial Trends of Depth and Snow Water Equivalence Around Meteorological Stations With and Without Snow Sensing Equipment

Table of Contents

List of tables

List of figures

Development, Analysis and Use of a Wireless Sensor Network for Quantifying Spatial Trends of Depth and Snow Water Equivalence Around Meteorological Stations With and Without Snow Sensing Equipment

Introduction

Hypothesis and research goals

This project tested two hypotheses, using a prototype wireless sensor network of ultrasonic snow depth sensors (Snowcloud), in Sagehen Creek, California. It also evaluated the Snowcloud system with respect to data output reliability and utility for snow research. The hypotheses tested with electronically sensed data and field measurements are stated below. A research objective is stated as 3, below.

(1) *Hypothesis:* Snow depth measurements from distributed sensors can be used to develop areal estimates of snow water equivalence and snow depth surrounding (A) fixed-base meteorological stations with snow density sensing equipment and (B) fixed base meteorological stations without snow density sensing equipment.

(2) *Hypothesis:* Spatial and temporal trends in snow depth measurements and snow water equivalence estimates from distributed sensors can be modeled with site characteristics as predictors using numerical techniques.

(3) *Research Objective:* This research evaluated the utility of the prototype Snowcloud platform for snow pack research.

Background

Water supply

Snow storage in the mountainous portions of the Western United States is an extremely important source of water supply. Federal resource management agencies (United States Forest Service, Bureau of Land Management, United States Geological Survey, Natural Resources Conservation Service, The Federal Water Master), non-governmental organizations and private contractors quantify and predict stream and river flows throughout the Western United States for water use allocated as water supply, allocated water rights, recreational waters, and water to sustain aquatic life. These agencies devote substantial resources to estimate snowpack depth and snow water equivalence during winter and spring to formulate operating policies for water allocation through river and irrigation systems.

Precipitation amounts in the Sierra Nevada Mountains vary annually from 50% to 200% of climatological averages (Lundquist, et al., 2003). Current water supply forecasts in the Sierra Nevada operate relatively well when snow accumulations are within the long term mean (Elder, et al., 1991, Rice, et al., 2010). However, when annual accumulations fall out of this range the forecasts are less likely to be accurate (Rice, et al., 2010). The precision and accuracy of prediction is likely to decrease in the future, given that hydrological observations indicate trends of earlier runoff, and increases in the annual average elevation of the transition zone between rain and snow (Lundquist, et al., 2003). Consequently, it is imperative to consider large scale variability of snow pack accumulation and ablation to anticipate increased weather variability in the future associated with climate change.

Meteorological stations

Low cost, low power wireless sensor networks have potential to revolutionize environmental data collection and analysis. They can be used to collect data at sub-basin, basin and regional scales at much higher resolutions than networks currently in use (e.g. snow telemetry sites and remote automated weather systems). Snowpack telemetry sites (Snotel) maintained by the Natural Resources Conservation Service throughout the Western United States, utilize fixed based systems to measure and report snow depth (SD) and snow water equivalence (SWE). However, due to the large distances between sites and logistical constraints associated with building and maintaining sites, estimation of snow pack depth and snow water equivalence and the physical processes of snow accumulation and ablation are subject to large spatial uncertainties.

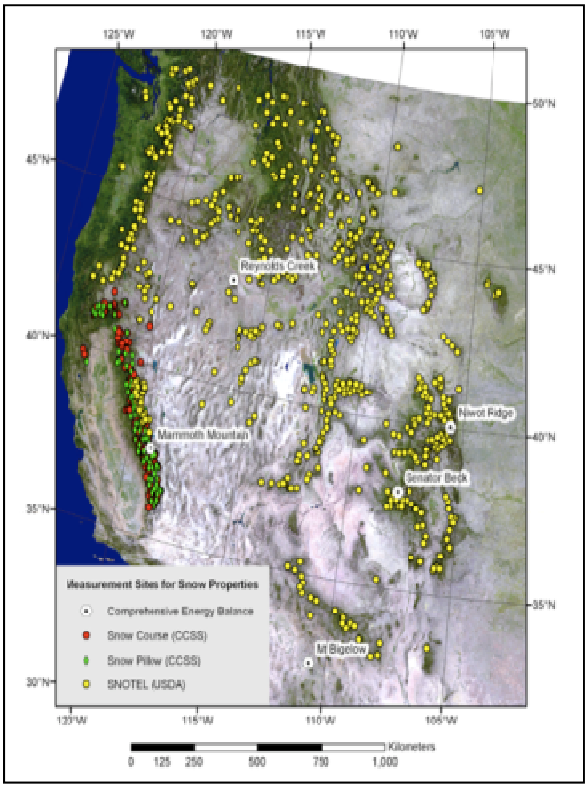

Figure 1: Snow measurement sites within the Western U.S. (Boyle, 09).

Many data collection networks do not have SWE or SD measurement capacity. The RAWS sites (remote automated weather stations) maintained and managed collaboratively by the United States Forest Service, Bureau of Land Management, National Oceanic and Atmospheric Administration, National Interagency Fire Center, The Weather Information Management System and the Western Regional Climate Center and state cooperative sites report weather information

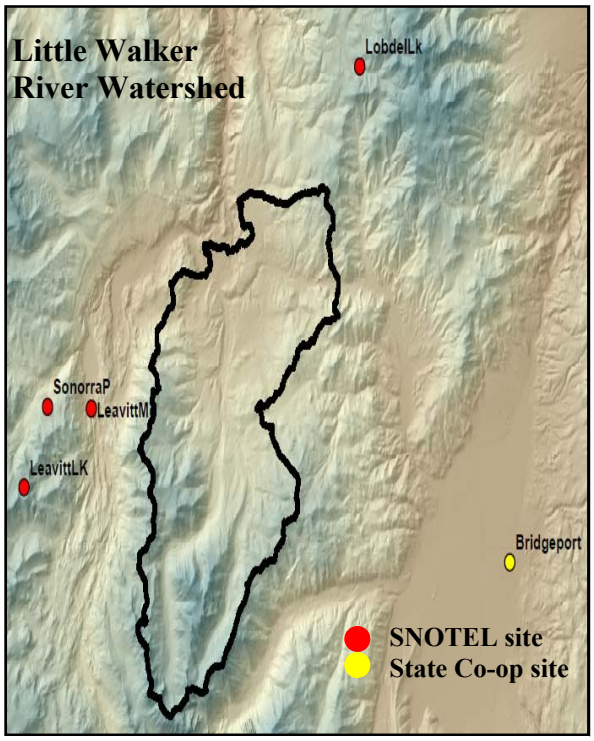

Figure 2: The Little Walker River Watershed is an example of a snow dominated watershed without meteorological or snow measurement stations within the basin.

including temperature, relative humidity, wind speed, solar radiation and precipitation in the form of rain.

In total, SWE is measured at 1,700 sensor stations throughout the Western United States (Figure 1) (Molotch, et al., 2005). These stations, in conjunction with remotely sensed snow cover data, provide reasonable estimations of SD and SWE on small scales, but extrapolations from these points to basin scales include much more uncertainty and leave some montane catchments severely undersampled or not sampled at all (Figure 2).

Snotel sites utilize snow pillows for SWE measurement. Snow pillows must have a large measuring surface to avoid the effects of snow bridging. SNOTEL snow pillows are approximately 3 meters by 3 meters and measure SWE from the overlying hydrostatic pressure of the snow (Figure 3). The sealed pillows are equipped with a pressure transducer or exterior based manometer and are filled with approximately 800 liters of a water-glycol mixture (Sommer, 2010). The size and weight of the snow pillows and associated equipment necessitates placement in flat open areas with good access. In some

Figure 3: Example of an NRCS snow pillow.

watersheds manual SD and SWE measurement courses are used to augment snow pillow measurements and may be used in place of snow pillows. Snow courses are typically 1000 feet long with at least 10 measurement points. These transects are sampled at approximately monthly intervals and give little information about the heterogeneous nature of snow pack due to uniform sampling areas (NRCS, 2010).

There are almost 2,200 RAWS stations located throughout the United States. While these stations do not currently have snow sensing capabilities, the addition of low cost wireless snow sensor networks could more than double the current snow sensing suite of instruments throughout the Western US.

The fixed base platform of the Snotel and RAWS data networks hinders higher spatial resolution of SD and SWE monitoring because measurements occur at one point on the land surface. The costs of initial installation and yearly maintenance also prohibit a more extensive array. The SNOTEL system and installation cost from $12,000 - $15,000 with yearly maintenance fees of $2,000/ year. The RAWS systems also cost between $12,000 – $15,000 for installation with estimated yearly maintenance fees of $525/ year (USEPA., 2010). In order to equip a site with a snow pillow, the equipment alone (snow pillow and affiliated parts, not including site preparation and set-up) costs $8,000.

Spatial snow water equivalence and snow depth extrapolation

Ground based measurement techniques are being increasingly supplemented and replaced with remote sensing technology (Rice, et al., 2010). Remote sensing technology such as areal LIDAR (light detection and ranging) and satellite based MODIS (moderate resolution imaging spectroradiometer) imagery supports SD and subsequent SWE

extrapolation with high resolution and is currently only limited by the frequency of requested “fly-overs.”

Remotely sensed information does not provide sufficient information to estimate SWE in certain areas because of the lack of resolution of the imagery and the distribution and variation in factors on the landscape that affect SWE (for example, canopy cover). Pixel scales are typically very coarse (ranging from 30m – 100km grid scale), and individual pixels are normally assigned a snow cover of either 0% or 100% (Elder, et al., 1998). This binary classification masks SD and SWE variability on small and large scales (Rice, et al., 2010, Shi et al., 2000). The loss of SD resolution is especially noticeable in areas with highly variable ground cover, because aerial and satellite techniques cannot sense snow pack under canopy. Remotely sensed data are also subject to atmospheric variation such as cloud cover. Due to this, remote data collection via satellites has limited utility, being most reliable when the sky is clear and ground cover is limited. Augmenting the existing snow pack analysis framework will help account for snow pack variability characteristic of larger scales.

Emphasis should be placed on sensor networks under canopy and at the margins of open area and canopy to supplement current and future remote sensing advances, existing meteorological stations (SNOTEL, RAWS) and snow course data collection efforts. The open area – canopy margin is a dynamic zone where snow accumulation can be greater than beneath canopies and where snowpack ablation is likely to last much longer than in open areas (Veatch, et al., 2009). Thus, the timing and amounts of moisture releases from the snowpack at the open area - canopy margin are likely to be important, especially in Sierra mountain systems in which forested areas are interspersed with meadows. As this paper will demonstrate, the open area canopy interface has both the minima and maxima of snow

accumulation and the quickest and slowest ablation rates. Part of this extreme variability is due to shading, which is a direct function of aspect (north, south, east and west). However, no research has linked canopy cover directly to aspect as a predictor for estimating both SD and SWE. This relationship while understudied may prove to be an important qualifier for SD and SWE estimation on an areal basis.

Physical characteristics related to SD and SWE accumulation and ablation include latitude, elevation, aspect, slope, canopy cover, wind, temperature and solar radiation. According to Erikson et al (2005) the relationships between SD, SWE, topography, canopy cover, and to a lesser extent wind, is constant year to year. Consequently, spatial and temporal trends in snow accumulation are similar in areas with similar topography, canopy cover and wind patterns. Therefore if small scale variability can accurately be characterized within an area surrounding a meteorological station, SD and SWE measurements at a point could be extended to surrounding areas with a high degree of confidence.

Canopy cover directly influences the amount of snow accumulation. In forested areas, snow accumulation and ablation are influenced the surrounding vegetative structure. Musselman et al (2008) found 56% differences in snow depth in open areas vs. under canopy at maximum accumulation in Northern New Mexico. Within the forest canopy maximum accumulation occurs in areas with cover densities of 25 to 40%, even though maximum snow accumulation has historically been thought to occur only in open areas. However, Veatch et al (2009) demonstrated that forest edges (canopy-open area interface) in mid-latitude sites have the ability to hold up to 25% more snow than open and forested areas. Snow accumulation and ablation is directly affected by wind speeds, directions and solar radiation fluxes at the surface, all of which are influenced by canopy structure (Musselman, et al., 2008, Woods, et al., 2006). Canopy density has an inverse relationship to

SWE and SD during the accumulation phase. However, during the ablation phase, lower solar radiation fluxes reduce melt rates in comparison to canopy-free areas. Consequently, to accurately model SWE and trends in SWE through time it is essential to quantitatively evaluate the overlying canopy density.

Canopy cover is not the only site specific control on SWE and SD accumulation and ablation. Elevation and aspect can have equal impacts on SWE and SD. Jost et al (2007) reported that elevation, aspect and canopy cover accounted for 80% - 90% of the variability of snow accumulation in a forested watershed, with aspect having the greatest influence during the accumulation phase. Elevation, while not as important in the accumulation phase, can be the most important factor during the snow ablation phase.

Rice et al (2010) demonstrated 50% differences in accumulation and ablation rates within a 0.4 hectare area in a subalpine basin within Yosemite National Park. Aspect has been identified as a key determinant of snow depth within clearings and on slopes (Anderton, et al., 2004, Cline, et al., 1998, Elder, et al., 1991, Erickson, et al., 2005, Golding, et al., 1986, Jost, et al., 2007, Molotch et al., 2005). Other factors with potential relationships to SWE such as temperature, solar radiation and wind have different effects during the accumulation and ablation phases, changing with sites, and seasons. This indicates a need for further research to understand the effects of topography, and canopy density on snow pack.

SWE has been accurately extrapolated based on statistical approaches that use snow depth and other independent variables. Regression tree models provide estimates of SWE when supported by extensive site characterization (Molotch, et al., 2005). Some research has demonstrated that SWE point measurements (for example, from snow pillows) can be used to directly model SWE in an area if combined with snow depth measurements.

According to Molotoch et al (2005) and Elder et al (1991, 1998) snow density did not correlate as well as snow depth with factors such as temperature, solar radiation and wind and, when the snowpack has a uniform temperature approaching 32°C, snow density is conservative compared to snow depth. Jonas et al (2009) found that density of snow did not correlate well with topography, though density increased with increasing snow depth and with duration on the ground.

If season and spatial variability of snow density are ignored, SWE for an area can be indirectly determined by: $SWE_p = d_\rho \; x \; \frac{\rho_s}{\rho_w} \left(SCA_p \right)$ where d_p = snow depth at point, ρ_s = density of snow for an area, ρ_w= density of water , SCA_p= snow covered area and SWE_p = volumetric SWE (Molotoch 2005). This equation can be augmented by increasing SD measurements within the field area (dp) and creating an average depth for the site.

Wireless sensor networks coupled with existing snow sensing infrastructure could greatly increase accuracy of areal and point based estimates of SWE simply by increasing the number of SD measurement points. Furthermore, if meteorological stations without snow sensing capabilities were augmented with wireless sensor networks, SWE estimates could be based on SD and physical site characteristics to increase the accuracy of water supply forecasting even in years where precipitation falls out of the historical mean.

A variety of methods are used for water supply forecasting. These include both physically and statistically based models. Physical models represent processes that affect snow melt and accumulation including mass and energy balances. Statistical models rely on correlations and historical trends. Many water supply forecasts, such as those from the Natural Resources Conservation Service, are statistical models. Statistical models such as bivariate regression modeling only require two inputs, precipitation at specific points

within a basin (in this case, observed SWE) and outflow in order to generate a probability distribution model for future flow.

More complex models have been created to estimate precipitation based on topography and weather information. Regression models such as the parameter – elevation regressions on independent slopes model (PRISM) operated by Oregon State University estimates precipitation on an 800 meter to 4 km grid scale on 24 hr intervals (PRISM, 2010). The snow data assimilation system (SNODAS) operated from the National Snow and Ice Data Center is a physically based energy balance model that estimates snow water equivalence values on a 1 km grid at 24 hr intervals (NOHRSC, 2004).

PRISM and SNODAS estimates can be used as precipitation inputs for physical water runoff models to increase the accuracy and resolution of the estimated stream flow predictions. However, both models require surface precipitation information from meteorological stations such as the Snotel or RAWS stations. The expansion of meteorological data collection networks would allow for greater inputs into not only surface water runoff models such as the Hydrologic engineering Center Hydrologic Model System (HEC-HMS) from the United States Army Corp of Engineers and the Precipitation Runoff Modeling System (PRMS) from the United States Geologic Survey but also to individual parameter estimation models such as the SNODAS and PRISM models (HEC-HMS, 2010, Leavesley et al., 1983).

Thesis overview

With the goal of improving the accuracy of SD and SWE estimations, a pilot project investigating the applicability of extending meteorological stations with low cost highly portable sensor networks was initiated in the Fall of 2009. The pilot project addressed three goals:

(1) Assess the utility of a wireless sensor network (WSN) to extend SWE measurements from a fixed based SNOTEL meteorological station to any point within the field area using statistical and numerical techniques.

(2) Assess the potential of a wireless sensor network (WSN) to estimate SWE from a fixed based RAWS meteorological station with no snow sensing equipment to any point within the field area using statistical and numerical techniques.

(3) Assess the utility of the prototype WSN used.

The WSN, Snowcloud, developed by Dr. Jeff Frolik and Dr. Christian Skalka from the University of Vermont, was deployed in the Fall of 2009. It consisted of six wireless sonar nodes surrounding a meteorological station on a 0.77 ha site within Sagehen Creek experimental Field Station north of Truckee, CA. The meteorological station is further described in chapter 2. Methods for deployment were designed by a collaborative team from the University of Nevada-Reno and the University of Vermont, including C. David Moeser, Dr. Christian Skalka and Dr. Mark Walker. Snowcloud was left in place until May 2010.

Methods for data analysis of both the WSN and the meteorological station data were developed and carried out at the University of Nevada–Reno. The meteorological station acted as both a RAWS and a SNOTEL station. The data from the meteorological station were integrated with the WSN to estimate SWE at each of the WSN nodes and within a sampling grid in the field area. These data were then geostatistically analyzed to transform the WSN point data into areal data.

Field data measurements, comprised of weekly manual SD and SWE measurements at 58 points within the field area, were used to verify Snowcloud SD estimates and to provide data to verify the statistical model predictions of SWE.

Finally, the SWE point measurement from the onsite snow pillow was compared against the interpolated and averaged areal SWE for the site.

The structure of this pilot project is depicted as three phases in figure 4.

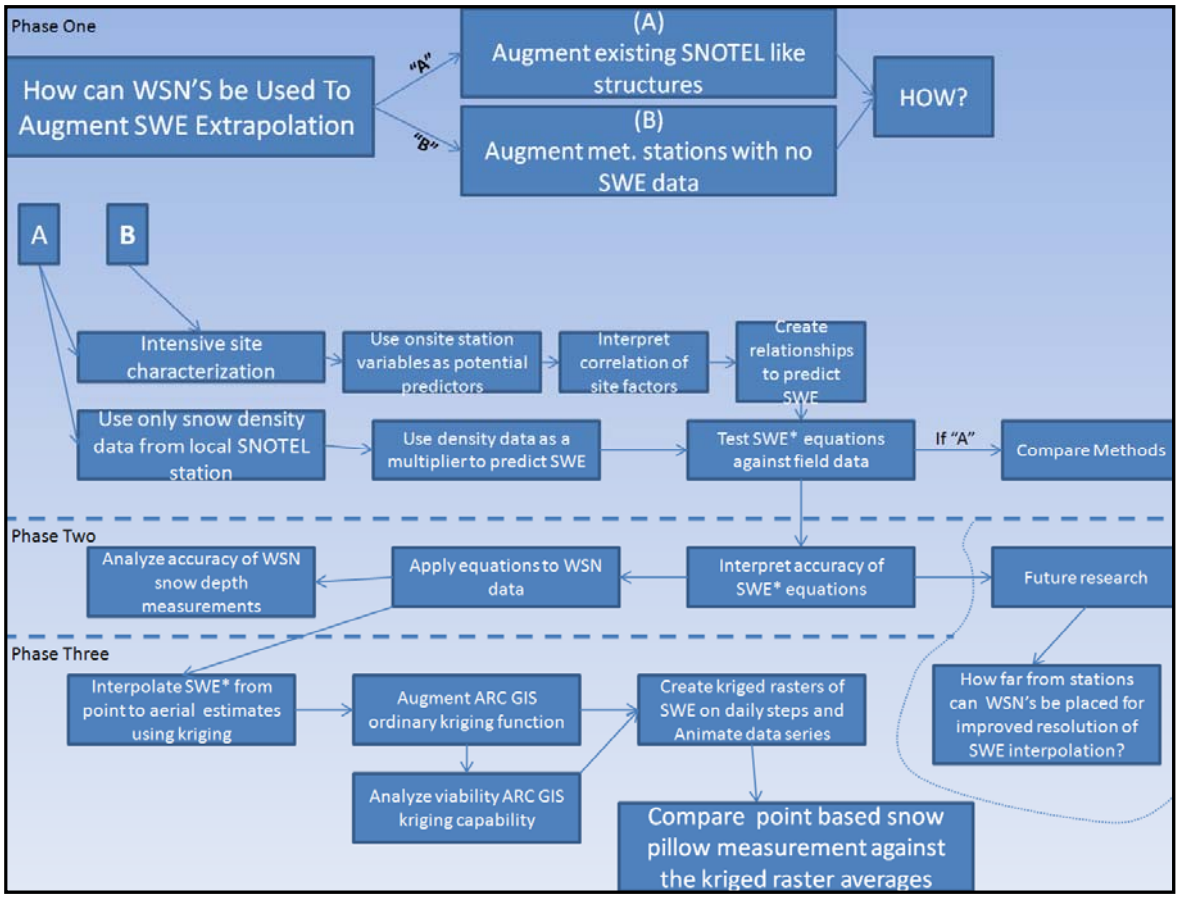

Figure 4: Flow chart of the three phases of the project.

Results of this pilot project are aimed at agencies responsible for data collection from meteorological stations, water budget analysts and the development team of the Snowcloud wireless sensor network. It is hoped the results will be a useful step in assessing

the feasibility of integrating these low cost systems into the framework of meteorological stations within the Western United States. It aims to demonstrate an effective approach for SWE extrapolation and areal estimation of SWE to supplement information from meteorological stations. This study should give the developers of the Snowcloud prototype an assessment of the functionality and utility of the system, with suggestions for improving the current design.

Throughout the document, language has been simplified to reduce redundancy and improve general readability. The terms "Snotel," and "RAWS" are meant to be inclusive. "Snotel" denotes not only snowpack telemetry sites but any site which is equipped in a similar nature such as state cooperative survey sites. "RAWS" includes not only Remote Automated Weather Station sites but any other meteorological station similarly equipped. The term "Transect" is equivalent to a snow course or any other line of pre-established snow sampling points for either SWE or SD measurement.

Methods and materials

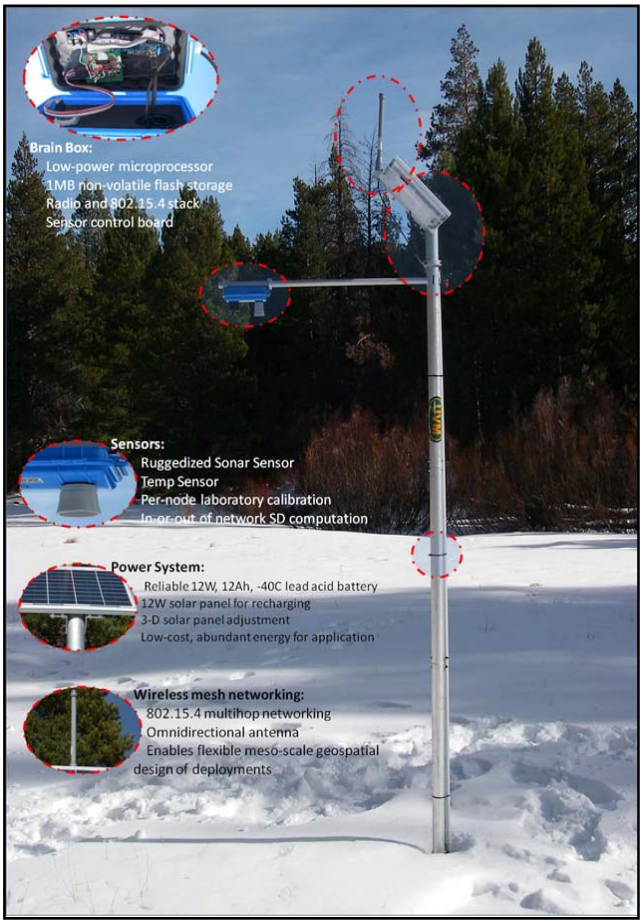

Figure 5: A Snowcloud node within the Sagehen Creek field area.

The Snowcloud system

A wireless system network is a set of small autonomous sensor nodes, that cooperate singularly and network individually or in tandem with a base station to perform at least one task (Haenselmann, 2005, Jindal et al., 2006).

The prototype Snowcloud system used in this research is a wireless self assembling network of six sensor nodes and one base station (Figure 5) designed and constructed by Dr. Jeff Frolik and Dr. Christian Skalka from the University of Vermont. The sensor nodes collect and communicate snow depth and temperature data using low frequency radio signals. Each node can connect directly to a base station or can deliver information packets from node to node (multi-hop) to the base station. This multi-hop communication structure extends the potential range of the Snowcloud network and allows the system to continue data collection and transport in the event of partial network failure or loss.

Most aspects of the Snowcloud sensors are controllable in real time, including sampling interval changes. Each node is connected to an omni-directional antenna with radio ranges of 50-100 meters.

All nodes include a temperature sensor and sonar emitter and receiver. The temperature sensor allows for temperature compensated depth-to-snow measurements. This compensated distance is paired with the total distance from the sonar emitter to soil surface for snow depth estimates. The current configuration costs ~$500 per node.

Snowcloud support structure

The Snowcloud support structure is made of lightweight aluminum. It consists of a vertical support shaft terminating in a solar panel and antenna support frame, an elevated horizontal sensor arm and a buried anchor system. The vertical support shaft is modular to allow for additional sections to be added depending on snow depth at a field site. The vertical shaft used within Sagehen creek was 9 feet. The distance between the sonar and the anchor system was 8 feet, which allowed for accurate snow depth readings up to 7 feet. The horizontal arm was also adjustable. At Sagehen Creek all sensors were set at 2.75 feet from the vertical support. The solar panel support can be adjusted horizontally 360 degrees and vertically 90 degrees. The anchor system consisted of an aluminum plate that can be detached from the vertical support for set-up and removal. Four removable 1 foot steel stakes were used to anchor the aluminum plate to the ground. The aluminum plate was adjustable for level with attached nuts on the removable steel stakes. The housing for both the wireless sensor module and the battery were made of ruggedized and waterproof plastic boxes (Pelican case 1020 &1450, http://www.pelican.com/cases_detail.php?Case=1450). The waterproof box housing the sensor module and the sonar sensor was located on the end of the horizontal sensor arm.

The waterproof box housing the battery was located at ground level and was connected to the solar panel via waterproof plastic ¾ inch conduit.

Snowcloud power and electrical system

The power system consisted of a 12V, 12ah lead acid battery with a -40°C operational rating, which was connected to a 12 W solar panel for recharging. There was an external switch on the support structure that allowed the system to be manually turned on or off for winter maintenance.

Snowcloud sensors and data transmission

The "brainbox" situated on the end of the sensor arm housed the sonar sensor and the internal microprocessor, which controlled the sonar emitter and transmitted data. The internal wireless sensor module (also called a mote) was a Crossbow TeloB (Crossbow Technology Inc. www.xbow.com), with a Tiny OS operating system and 1 mb of internal flash storage. The 1 mb of flash storage retained data in case of transmission or antenna failure. The Crossbow TeloB mote was directly connected to the battery and an omni directional radio antenna capable of data transmission up to 100 meters in any direction. The mote managed the sonar emitter to measure the distance between the sonar emitter and snow or ground surface.

Sonar

Due to the compact size and low cost, the Max Sonar® – WR1™ (MB7060) from MaxBotix® Inc. (www.maxbotix.com) was utilized for Snowcloud. The MB7060 requires very low power for operation, between 3.3V and 5V. The MB7060 has a range from a minimum of 25 cm to a maximum of 765 cm (0.83 to 25.1 feet), with 1 cm resolution.

Distances less than 25 cm are reported as 25 cm. Product specifications also stated that the sonar is functional over a range of temperatures, though no bounds were specified. The manufacturer also stated that the sonar emitter is designed to operate in the presence of outside noises, though best operation is obtained when noise levels are low. It is unclear what noise strength is considered low. No further performance information regarding noise and temperature effects was available from the producer.

The Crossbow TeloB mote reads the sonar data output as a voltage signal. A signal must first be transformed into sonar to surface distances by calibrating each sonar emitter. Sonar emitter to snow surface distance can then be determined as the difference between the total distance from the sonar emitter to the land surface and the sonar to snow surface depth (eq. 1):

$$SD = (S\text{-}Ls) - (S\text{-}S)$$

in which SD= snow depth at the land surface, (S-Ls) = sonar emitter to the land surface distance and (S-S) = sonar emitter to snow surface distance.

Snowcloud installation and calibration

Snowcloud was installed jointly, by myself and Dr. Christian Skalka from the University of Vermont over a one month period in the Fall of 2009. Six nodes were installed within a 0.77 ha site within Sagehen Creek Field Station in Truckee, Ca. Upon installation, each node was tested and the network was deemed fully functional on the 17th of January 2010. Snowcloud data collection began January 18th 2010, which also marked the first day of manual measurements of SD and SWE (described in field measurement section).

Two separate sonar emitter calibration trials were run to determine the most accurate method to calibrate the sonar emitters. It was initially unclear whether similar results could be obtained utilizing a calibration inside versus a calibration outside. The first

trial (calibration one) was run prior to installation within a laboratory at the University of Nevada, Reno. The second trial (calibration two) was run after all data collection from the Snowcloud system was complete within the field area in Sagehen Creek. These are described below.

Calibration one

Each sonar emitter was calibrated on a rolling platform four feet above a lab floor. The sonar was leveled on the rolling platform and directed at a concrete wall uniformly covered by 0.5 mm thick white paper. The rolling platform was moved 10 times at one foot increments, starting at one foot and ending at 10 feet from the white paper. At each increment, 12 sonar voltage outputs were recorded along with 12 internal node voltage outputs for temperature. Each set of temperature readings was averaged and transformed into Celsius degrees using the equation specified by the manufacturer (eq. 2):

$$T_c = (0.01V_r - 53.83)$$

in which T_c= temperature in Celsius and V_r = voltage output.

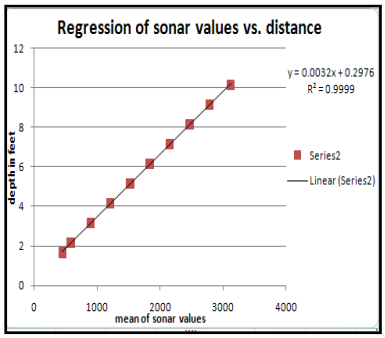

Figure 6: Example of linear relationship between sonar voltage output and distance.

A simple regression of sonar values vs. distance from sonar to wall was created in order to arrive at a linear relationship of the form: distance (ft) = m(voltage output) +b, in which m is a slope constant and b is an intercept (Figure 6). The sonar readings were further corrected for the affects of temperature on sound transmission using equation three (Ryan, et al., 2008):

in which SD= snow depth (ft), D_{gs} = distance from ground surface to sonar emitter (ft), V= voltage output, T= average temperature (°C) at sample time and $m_i x+b$ = calibration for

node i. The distance from the ground surface to the sonar emitter (D_{gs}) was measured with an avalanche probe with cm gradations.

Calibration two

Figure 7: The adjustable calibration clamp affixed to the vertical support shaft of the Snowcloud structure.

The second trial was run in field. An adjustable bracket was attached the sensor arm to the vertical support shaft to create a flexible connection (Figure 7). This clamp allowed the sensor arm to lock on any spot on the vertical support shaft and also permitted the sensor arm to be leveled. Prior to disassembly of the Snowcloud system, each of the six "brain boxes" were removed from the respective support structures, affixed to the support structure of node 5, leveled on the support structure and calibrated (Figure 8). Calibration consisted of readings at different heights on the support shaft. At each height increment, 12 sonar voltage outputs and 12 temperature voltage outputs were recorded and used to create calibration equations as in calibration one.

Calibrations and estimates of snow depth throughout the field trials were compared for accuracy against weekly field measurements of SD and distance from ground to sonar as described below in the manual SWE and SD sampling section.

Snowcloud use and data output

Snowcloud data were provided by the University of Vermont (Dr. Christian Skalka) in the following comma delimited format:

1. Node ID
2. Unix timestamp of sensor reading, indicating the real time of each report
3. Interpretation of (2) in format MM/DD/YY HH:00 with time rounded to the turn of the hour
4. Node latitude position (decimal format)
5. Node longitude position (decimal format)
6. Average raw temperature reading (volts)
7. Temperature reading converted to °C with tenths of a degree precision
8. Average raw sonar reading (volts)
9. Interpreted snow depth reading (inches)
10. Interpreted sonar-to-snow distance reading (inches)

The field site

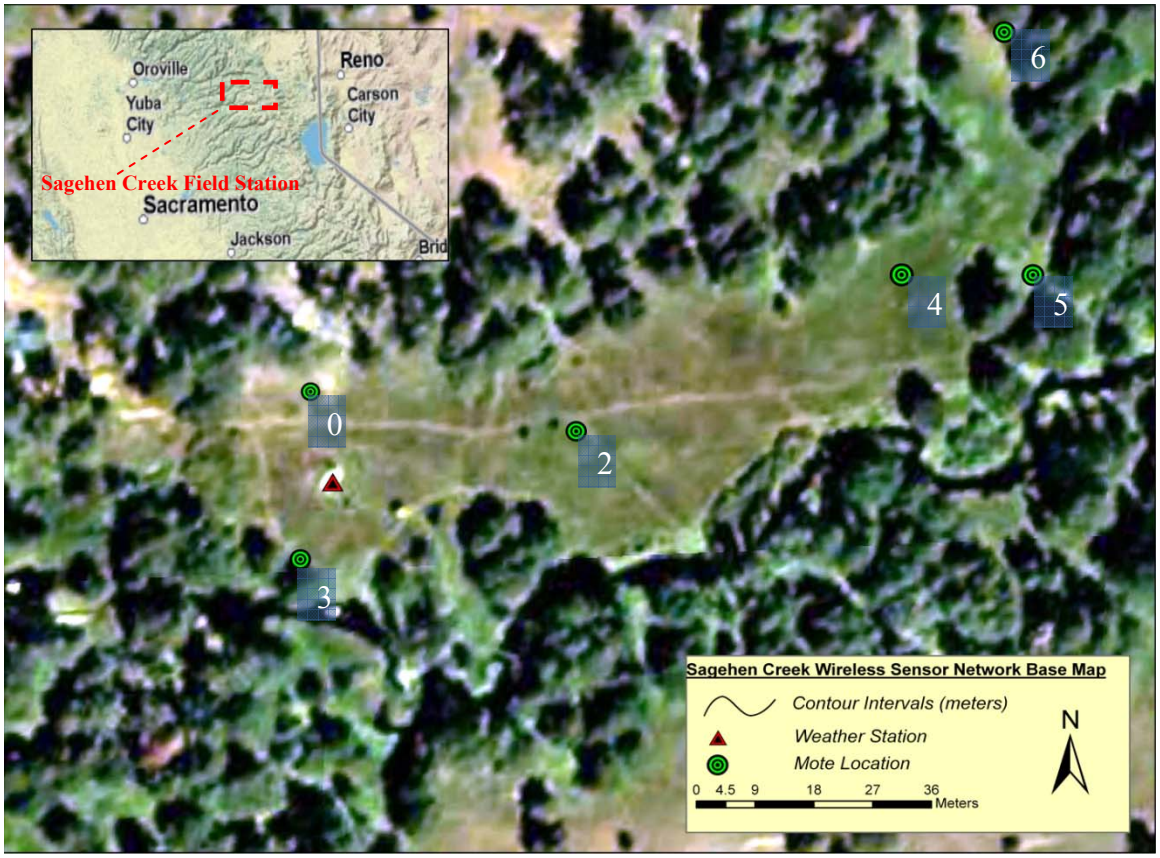

Figure 8: The field area and location of nodes within the Sagehen Creek Experimental Field Station.

The six node prototype Snowcloud system was deployed in the Central Sierra Mountains at Sagehen Creek Field Station (Sagehen) near Truckee, California. Sagehen is ideal for winter research because it is within a snow-dominated hydrologic system with year around road access (Figure 8). The research station has an extensive hydrologic research infrastructure in place, most notably a meteorological station similar to those in the Snotel network, equipped with a snow pillow that collects weather information and SWE data on ten minute time intervals. The data are available through a website and in real time.

The six Snowcloud nodes were deployed inside and around a ~0.77 ha meadow near the snow pillow (e.g. 5 - 130 meter distance from node to snow pillow). The nodes were sited to compare SD and SWE in opposing tree canopy structures and canopy–open area interfaces with varying aspects. The nodes can be seen in green and the snow pillow is a seen in red on figure 8. All nodes were located within a different aspect (north, south, east, west) relative to the centroid of the field and canopy cover regimes.

Sagehen Creek meteorological station

The meteorological station, referred to as Tower one, is a one hundred foot tower that measures 32 variables at different heights along the tower (Table 1). Access was

Ground Surface	15 feet	25 feet	100 feet
SWE at snow pillow (in)	average air temperature (°C)	wind speed (m/s)	wind speed (m/s)
snow depth* (in)	maximum air temperature (°C)	resident wind speed (m/s)	resident wind speed (m/s)
	minimum air temperature (°C)	wind direction	wind direction
	average air temperature (°C)	standard deviation of wind direction	standard deviation of wind direction
		maximum wind speed (m/s)	maximum wind speed (m/s)
		average air temperature (°C)	average air temperature (°C)
		relative humidity (%)	relative humidity (%)
		maximum relative humidity (%)	
		minimum relative humidity (%)	
		average relative humidity (%)	
		average barometric pressure (millibars)	
		average incoming shortwave radiation (kilowatts)	
		total incoming shortwave radiation (mega joules)	
		average barometric pressure (millibars)	

Table 1: Variables measured at tower one at different heights along the tower. * denotes measurement apparatus was not functioning during experimental trials.

granted to use this data by Dr. Doug Boyle at the Desert Research Institute, Reno, NV. All measurements are reported in ten minute intervals, with the exception of snow depth.

Tower one data were uploaded on a weekly basis and transformed into a series of hourly and daily averages, with the exception of total incoming shortwave radiation. For these experiments, daily averages were further aggregated into separate weekly and monthly data series along with a seasonal running average starting on December 1st. The weekly and monthly averages utilized the moving window approach, giving each day unique daily, weekly, monthly and seasonal running averages. The weekly average consisted of the average of the previous seven days daily averages and the monthly average used the previous 30 days daily averages. The seasonal running average consisted of all daily averaged values from December 1st to day i, with i representing the end of each time interval in the series. The total incoming shortwave radiation in mega joules was treated in this manner with values totaled rather than averaged.

This approach transformed the 10 minute interval data into 5 separate data series; hourly, daily, weekly, monthly and a seasonal running average or total. These data sets incorporate different levels of memory associated with each factor which could have a strong influence on SD and SWE. For example, the monthly averages capture a greater portion of the season than the weekly averages. Also, average temperatures over one month intervals contain information relevant to snow pack ablation (or other longer term events such as snow ripening and snow accumulation) more than single day measurements. These series were utilized during correspondence analysis in order to analyze correlation between variables for the purpose of creating SWE prediction equations.

Field measurements

Extensive field work was required to assess accuracy and precision of the snow pillow SWE data and the Snowcloud generated SD data. The field data were also used to validate and verify SD and SWE models for individual points within the field area and the SD and SWE areal interpolation models from kriging.

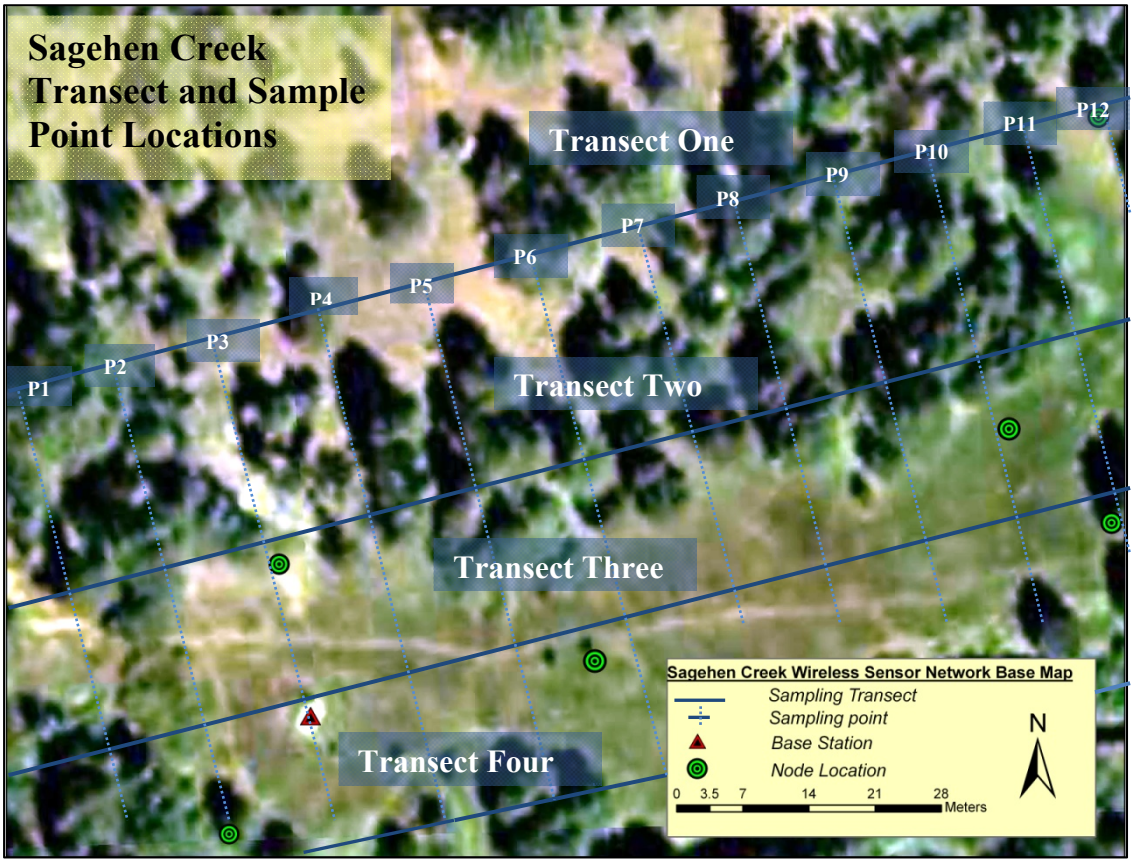

Figure 9: Transect and sample point grid within the field area.

Elevation was not considered within the analyses because of the low elevation variation of the field site (<30ft of relief within the area). Only canopy structure and aspect in relation to the canopy structure were analyzed at each sampling point. The site characterization included measurements of canopy closure in relation to aspect throughout the field area, which was considered to be a potential predictor of SWE.

Field site delineation

Four transects were created, traversing the site approximately east to west (T1 to T4) with twelve sampling points along each (P1 to P12) creating an equi-spaced 4 x 12 sampling grid (Figure 9). Six separate points were also sampled 1.5 feet away from each node. Finally, four sampling points were established on each side of the snow pillow (north, south, east and west sides) for a total of 58 sampling points. SD measurements, SWE measurements and the initial site characterization were performed at all points. SD and SWE were sampled weekly throughout the season. The initial site characterization was performed at the beginning of the season.

Each transect represented unique characteristics of the field area. For example, the points on transect one have a predominantly northern aspect in relation to canopy. Transect two points are located in the canopy – open area interface and have a southern aspect in relation to surrounding canopy. Transect three was a largely open area located in the middle of a large meadow. Transect four was predominately on the southern edge of the meadow and had a southern aspect in relation to canopy.

Site characterization

The majority of the canopy cover within the field area is mixed conifer. Because of the relatively slow growth rates of this forest type, especially in the winter, a single canopy closure analysis was sufficient to characterize all the sample points for the season.

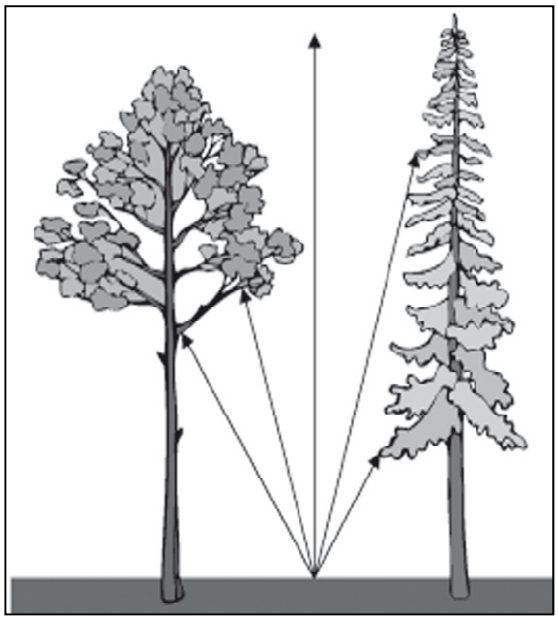

Figure 10: Canopy closure is measured in an angle of view. Adapted from Fiala et al 2006.

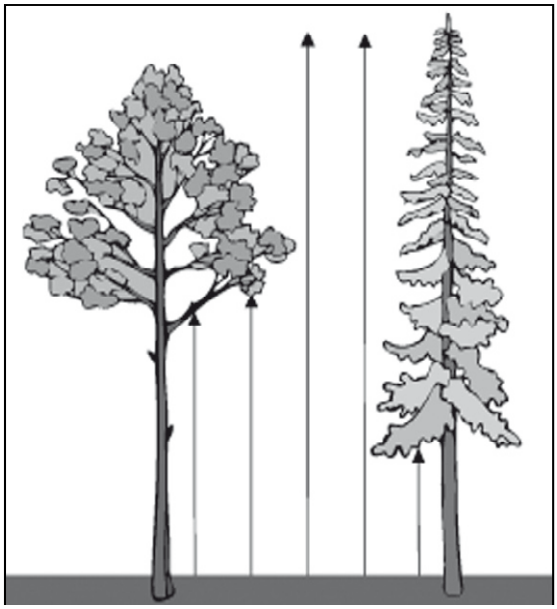

Figure 11: Canopy cover is measured in a vertical direction. Adapted from Fiala et al 2006.

A convex spherical densiometer (Model A, www.terratech.net) was used to measure canopy closure (Figure 12). Canopy closure is a measure of canopy cover from a point to represent an area. Canopy closure measurement techniques are an overhead measure of an area, reducing error involved with bias from points (see figure 10). This avoids the bias of measuring canopy cover with techniques such as crown mapping, the intercept transect method, the GRS densiometer, and narrow angle digital photography (Fiala, et al., 2006). For example, if one measured canopy cover under one tree branch, canopy cover techniques would indicate 100% canopy cover, but just inches away in an open area within the canopy, the measurement would be 0% (Figure 11). In contrast, canopy closure measurements would read neither 0 nor 100%, indicating a canopy density measurement without a point based bias.

There are several other instruments that accurately measure canopy closure, such as hemispherical photography, and aerial image processing. However, the spherical densiometer is the only method that incorporates aspect into the measurement, which

allows the combined effects of overhead canopy and aspect to be quantified and utilized as potential predictors of SWE.

Spherical densiometer use

Figure 12: Concave spherical densiometer

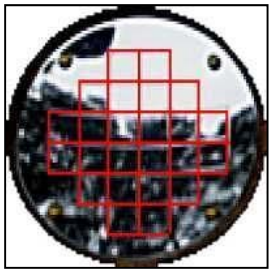

Figure 13: gridded face plate of the above densiometer. The depicted canopy closure is ~70%.

The concave densiometer measures canopy closure in a 60° radius relative to the direction of the user's eyes (Figure 12). The face plate is delineated into 24 squares and is used to quantify percentages of closure (Figure 13). Canopy closure was quantified at each point within the field site grid. At each point, the densiometer, affixed to a tripod, was leveled and placed at 4.5' above the ground surface. A compass was used to align the densiometer to each of the cardinal directions (north, south, east, west) and four readings were taken standing 16 inches away from the densiometer. There are several methods for reading the mirrored plate of the densiometer. This study utilized the dot method (Korhonen, et al., 2006), which breaks each of the 24 squares into 4 smaller squares. Each of the 96 sub gridded squares is given a canopy cover rating of either 1 for canopy cover or 0 for no canopy cover. This process was used for each cardinal direction and the ratings were added for each direction and a percentage of canopy cover was then assigned to each direction. The canopy cover percentages for each direction were then averaged to characterize total canopy cover at each sample point and Snowcloud node (Table 2).

% canopy cover	canopy cover north	canopy cover south	canopy cover east	canopy cover west	canopy cover total
Node 1	50.0	8.3	50.0	71.9	45.1
Node 2	6.3	2.1	0.0	12.5	5.2
Node 3	2.1	37.5	55.2	36.5	32.8
Node 4	12.5	3.1	26.0	41.7	20.8
Node 5	60.4	64.6	92.7	85.4	75.8
Node 6	56.3	68.8	83.3	71.9	70.1

Table 2: Estimated canopy cover linked to aspect from the concave spherical densiometer.

Manual SWE and SD sampling

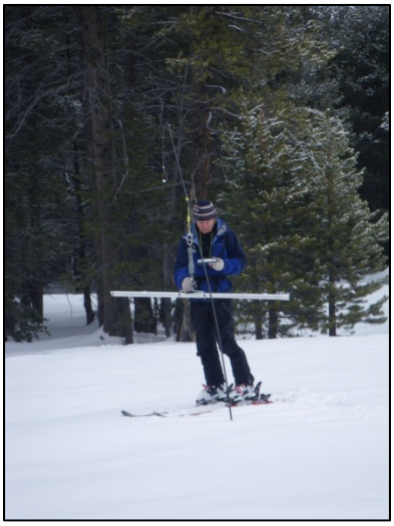

Figure 12: Use of a Mount Rose snow sampler within the field area.

A Mount Rose snow sampler was used to measure SD and SWE at each sampling point on a weekly basis. These measurements were made to compare with predictions of SWE across the site, including each Snowcloud node. The Mount Rose or Federal sampler is used by the NRCS for snow surveys and is the standard for most snow studies. The SWE and SD sampling commenced on the 18th of January 2010 and ended on the 26th of April 2010, when the site was ~85% free of snow on the ground surface. The Mount Rose snow sampler is comprised of a long tube that is inserted into the snow pack and approximately 1 inch of the underlying soil. The snow sampler is then removed from the snow pack, the underlying soil is removed and the tube and its contents are then weighed. This weight (the total weight – the tare weight of the tube) is then divided by a constant that represents the internal cross sectional area of the tube and the

density of water (1 g/cm^3). While the density of water when it is below freezing is below 1 g/ cm^3 (at 0°C the density of water is 0.99984 g/cm^3 and at -20°C the density of water is 0.9935 g/cm^3), it is an insignificant difference in comparison to the accuracy of the sampler. The Mount Rose Sampler (Rickly Hydrological Supply Inc, www.rickly.com) has an internal surface area of 1.7203 in^2, the density of water in English units is 0.036127 lb/in^3, giving a conversion constant of 0.06215 lb/in.

Due to the physical removal of snow cores at each sample point, the location of each sample point varied slightly between the weeks. However, efforts were made to consistently sample within a 1.5 foot radius of each point.

A 4 meter long avalanche probe was used to measure the distance from the sonar emitter to the snow surface directly underneath each node. These measurements were taken to verify the accuracy of the sonar to snow surface estimates. The avalanche probe has a small diameter (0.70 cm) creating very little disturbance in the snow surface underneath the sonar emitter. If any disturbance was seen after snow depth measurements, snow was added to fill holes to maintain a relatively undisturbed sonar emission target surface.

Snow pillow verification

The Mt. Rose sampler was used to measure both SD and SWE on four points surrounding the outer margin of the snow pillow. The SWE and SD measurements were moved 6" clockwise from the previous sampling points to avoid potential influences from past sampling. The SD and SWE measurements were averaged and compared to the snow pillow output for that time interval.

Data analysis

Three separate SWE prediction methods (SWE*) were developed for the field site using data collected at the Snowcloud nodes. Each equation was used to estimate SWE at the six Snowcloud nodes and the sampling points on each of the transects at all time intervals and all estimates were compared with observed data. The first approach (a) tested the feasibility of extending wireless sensor snow depth data to Snotel sites and predicted SWE* from site characteristics, tower one data and the Snowcloud generated SD. The second approach (b) also tested the feasibility of extending wireless sensor snow depth data to Snotel sites using only snow density information obtained from the snow pillow at tower one with the Snowcloud estimated SD. The third approach (c) tested the feasibility of predicting SWE from site characteristics and tower one data without snow density information (no snow pillow data to mimic a RAWS site) and the Snowcloud estimated SD. Two databases were created for data analysis.

Snowcloud data was not yet available at the start of the data analysis, so manual SD measurements at the nodes were used as a surrogate for Snowcloud. The manual SD measurements around the snow pillow were also used instead of the faulty sonar sensor on tower one.

Data aggregation

The principal data set included tower one data reduced to hourly, daily, weekly, monthly and seasonal running averages or totals for all variables, the manual SWE and SD data at each node point and snow pillow, and the spherical densiometer data for each Snowcloud node, giving 202 observations each week for 15 weeks. This data set was used for all SWE modeling.

The second data set included tower one data reduced as described above, the manual SWE and SD measurements for each sample point along all transects, the manual SWE and SD data for each Snowcloud node and snow pillow, and the spherical densiometer data for all sample points along each transect and node points, giving 536 observations each week for 15 weeks. This database was used to verify, and analyze SWE estimates generated from the Snowcloud nodes that were extended to all sampling points within the field area. Kriged areal interpolations were also verified and analyzed using this gridded data base.

Correspondence and regression analysis

SWE prediction using tower one data with and without snow pillow data were developed using multiple linear regression. Regression analysis focuses on associations between a dependent variable and one or more independent variables. Previous studies have used regression analysis to analyze the associations between environmental variables and snow depth (Elder, et al., 1991, 1998, Jonas, et al., 2009, Molotch, et al., 2005). The significance of independent variables or potential SWE predictors varies according to site, season, and available data (which have limited concurrence in previous SWE and snow density regression studies).

Multivariate linear regression is the extension of a linear least squares bivariate regression (Carr, 2002), and takes the following form (eg. 4):

$$y^* = a + b_1X_1 + b_2X_2 + \ldots\ldots + b_nX_n$$

in which a = the y intercept, b_n= the generated regression coefficient, and X_n=the independent variable.

The independent variables should be statistically independent of each other. The regression coefficients (b_n) quantify the independent contributions and relationships of each independent variable. The partial correlations, or degree of association between the

independent variables, should be minimized and the final model should include a minimum number of independent variables.

Correspondence analysis (CA) was used to identify a series of potential predictors or independent variables for the multivariate regression modeling. CA is a non parametric principle component method for analyzing correspondence or independence among variables to visually depict the degree of association between them. The significance of the associations is based on the chi-square distance between each data point and the expected value, where the expected value is equal to the value that has the highest probability of occurring within the data set (Carr, 2002, Nagpaul, 1999). Unlike other principal component methods, CA is a simultaneous examination of both rows (Q- mode) and columns (R- mode) of the data input matrix, which allows for a more robust analysis than single Q- mode or R- mode analyses. Eigenvectors (factors) associated with the Eigen decomposition of the matrix of the chi-square values from the initial data set can be plotted on independent axes of a graph. The value of the factor for the associated sample can be projected as a coordinate, allowing for a visual representation of independence. The factors (eigenvectors) also have attached values of significance indicating the amount of variability captured within the initial data set. Figure 15 shows a correspondence analysis plot in three dimensions. The circled groupings indicate clear independence from other variables,

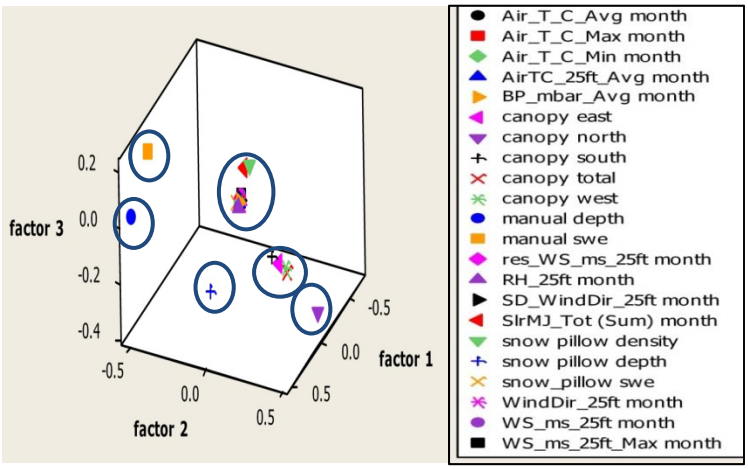

Figure 13: Example of a 3 dimensional correspondence analysis plot, the blue circles represents independent groupings of variables.

while variables that plot next to one another represent associations. In this case, factor one contains 70% of the data set's variability, factor 2 contains 17% and factor three 5%, which illustrates the importance of variable separation on the factor one axis and, to a lesser extent the factor two axis, while reducing the importance of the factor three axis.

Three dimensional box plots were created for all analyses due to the large data sets analyzed. Factors one and two accounted for the majority of the variability within the data set in all analyses. In a two dimensional analysis with factor one and two on the x and y axis, many plotted variables could be not be seen because they plotted directly on top of one another (overprinting). Even though factor three typically accounted for very little variability, this factor was included on the box plots to give the variables a third dimension, effectively minimizing overprinting and enhancing visualization of variables that might have gone unseen within the 2-D plots.

The three dimensional box plots were rotated in space on the x, y and z plane to augment visualization. A series of potential predictors for SWE was generated from these analyses and used for multiple regression analysis.

All potential predictors were initially used for the SWE regression models. Potential predictors were sequentially eliminated based on significance of the individual variables. Results from the multiple regressions were then compared with field measurements to evaluate precision and accuracy of the regression models.

Multivariate regression analysis assumes that the underlying distribution of the random component of models is normally distributed. Because of this assumption, the significance of coefficients for the independent variables can be assessed with the P value. The P value indicates the likelihood that a coefficient is not significant. Many statistical analyses adopt a threshold value of $P \leq 0.05$, which indicates that the probability of a

coefficient not being significant is less than or equal to 0.05 or that there is less than or equal to a 5% chance of having the independent variable be unrelated to the dependent variable. All independent variables with P values greater than 0.20 were initially considered statistically insignificant and only P values which were less than 0.05 were retained within the SWE* models, unless exclusion reduced significance of the overall model, indicated by the initial correspondence analysis, the correlation coefficient, the f statistic, and the t statistic for the regressions.

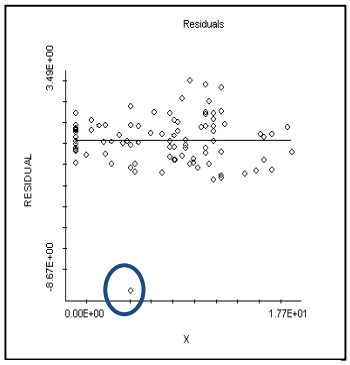

Figure 16: Example plot of residuals. The blue circle highlights an outlier within the residuals.

In order to assess the significance of the P value, the residuals, which represent the random component of the model, must be normally distributed. The residuals are computed as the difference between the observed and predicted values of the dependent variable (SWE). The residuals can be considered to be normally distributed if the coefficient of skew is less than 1.0 (calculated as $\frac{skew^2}{variance^3}$). In several cases within these analyses, the assumption of normality was not met due to outliers within the residuals, which increased the coefficient of skew above an acceptable level (see figure 16). Due to this, probability plots were created. Probability plots graph the z- scores of the data quantiles (from the residuals) against the z-scores of a perfectly normal distribution. If the plots are linear, the underlying error structure can be considered to be normal even if the coefficient of skew is above the threshold of 1.0 (Figure 17).

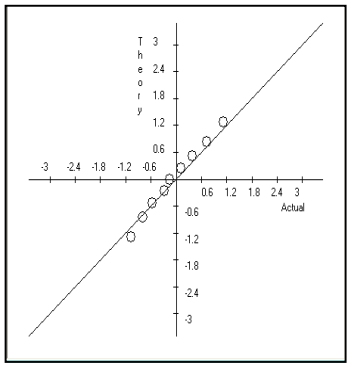

Figure 17: Example of a probability plot using the same data from the residuals plotted in figure 16.

The Spearman rank coefficient, a non parametric indicator of correlation, was also generated for all regressions and was employed in cases in which the residuals did not appear to be normally distributed. This coefficient analyzes the direction and strength of correlation for the independent variables as a whole to SWE.

Evaluation of accuracy and precision of SWE estimates

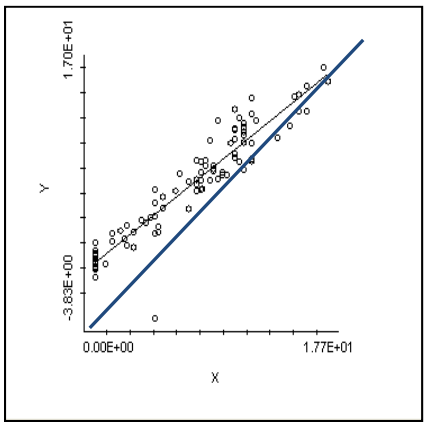

Figure 14: Example regression of manual SWE measurements on the x axis vs. estimated SWE on the y axis, with a regression line through the data cloud. The blue line is a 1:1 line for comparison.

The SWE estimates were also plotted and analyzed to evaluate correspondence to the manual measurements. The SWE measurements were plotted on the x axis vs. the SWE estimates on the y axis and compared using regression (figure 18). The regressions provided two points of comparison to evaluate accuracy and precision of the models. These were the value of the slope coefficient of the regression line, the intercept term and the 95% confidence bounds for both. Random variability introduces error in the relationship between observed and estimated SWE, which can be characterized in the confidence bounds for the slope and intercept coefficients. Ideally these bounds would be small for an accurate model, and include 1 and 0 for the slope and y intercept, respectively. However, if the confidence bounds were broad, the models the models would not be precise.

The significance of the overall regression was evaluated using the F statistic. The correlation coefficient (with 1.0 being a perfect positive correlation) was also used to evaluate the proportion of variation accounted for by the regression comparison models. Finally, the T statistic was used to determine the significance of the estimate of the slope of the regression line.

Validation

SWE* predictions were extended to all sample points on each of the transects to: (1) evaluate the significance of the SWE models, (2) assess the accuracy of the SWE models beyond the node points (3) and assess the initial site characterization and node placement. The estimates from the SWE models were regressed against the manual SWE values on a transect to transect basis.

Each transect had very different patterns of accumulation and ablation because of their unique site characteristics. Due to this, the SWE estimates and measurements were compared transect by transect ($transect_n$) rather than across all points at once. The individual transect comparisons provided greater insight into the accuracy of the SWE estimates within specific canopy and aspect regimes. The transect based observed vs. estimated SWE comparisons also provided information about the initial Snowcloud node placement, whether some of the nodes should be placed in different locations to better capture snow pack variability of the field area, if some nodes were unnecessary, or if the site should be augmented with more nodes. While this was a one year pilot study, these questions are invaluable for future use of systems like Snowcloud (see future study section).

Snowcloud and regression equation data pairing

Snowcloud data from January 18th to March 31st 2010 were used with each of the regression models on a daily time step to create a time series of estimated SWE at all node locations. Since manual SD was initially used as a surrogate for the Snowcloud SD, each SWE model at each node for the entire daily time series was compared against the weekly manual SWE measurements for verification. This daily time series was used for all areal SWE and SD interpolations.

Data interpolation

SD measurement from the Snowcloud network and the estimated SWE at each node were interpolated to provide a spatial estimate of both SD and SWE for the field area using ordinary kriging. Daily values of SWE and SD from each node were used to perform kriging with the entire time series of Snowcloud data. All kriged time steps were then animated and recorded to illustrate SD and SWE trends through time. Python script was integrated with ArcGIS to automate the kriging and animation processes.

Ordinary Kriging

Kriging is a geostatistical technique used to estimate values at locations that have not been sampled. Ordinary kriging uses a weighted average of neighboring samples to estimate a value at a known location. The weights are optimized by applying a semivariogram model, the locations of the samples, and variance between known and unknown values (Clark, 1979). Kriging minimizes the error of predicted values and is based on the regionalized variable theory, which assumes spatial variability is homogenous and can be represented by the semivariogram. Kriging is similar to inverse distance weighting (IDW) in that it assigns weights to data from surrounding measurements to derive a prediction. The general formula for both interpolative processes is (eq. 5):

$$Z^*(S_o) = \sum_{i=1}^{N} \lambda_i Z(S_i)$$

in which $Z^*(S_o)$ = the estimated value at the prediction location, λ_i= the weight for the measured value at the i^{th} location and $Z(S_i)$=the measured value at the i^{th} location.

In IDW the weight, λ_i, depends only on the distance between the known locations and the prediction locations, whereas in kriging the weights are based on the distance between the known locations and the prediction locations and the overall spatial arrangement in the

weights (ESRI, 2010). This spatial arrangement is quantified by fitting a model to the variogram allowing covariance (correlation) to be modeled between points.

The variogram

The variogram represents correlation, separated by an established distance, h (lag distance). The variogram is a graph of lag distance vs. variance (γh) expressed as (eq. 6):

$$\gamma h = \frac{1}{2N}\sum_{i=1}^{N}[Z(X_i) - Z(X_{i+h})]^2$$

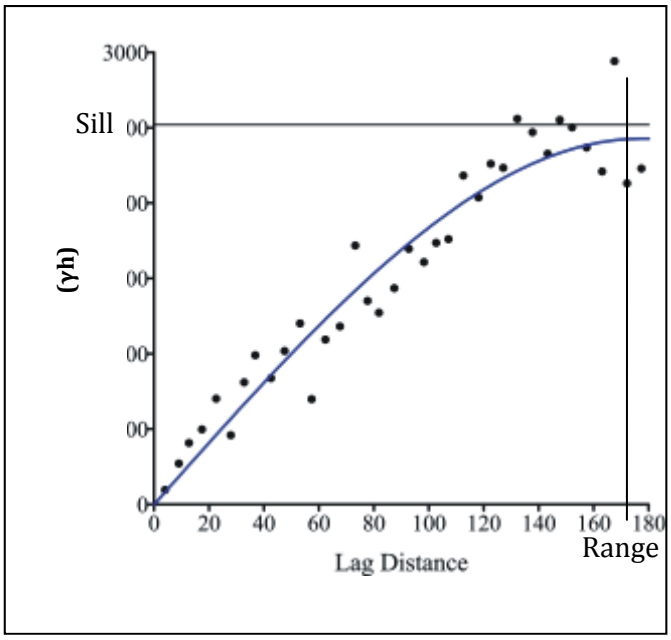

Figure 15: Example of a variogram. The blue line is the chosen, spherical model line for the data. The sill is ~2500, the range is ~165 and the nugget is ~0.

in which γh =variance, $Z(X_i)$=value at location X_i, and $Z(X_{i+h})$=value at location X_i + a distance of h, determined by the analyst.

In this model, variance can be considered ½ the average squared difference of data for all points separated by a lag distance or class size of h. Once the class size, chosen by the analyst, yields results with an apparent trend, a model can be fitted to the data to arrive at the input values for ordinary kriging. The input values used are the sill, nugget and range (Figure 19). The nugget is the value on the y axis where the data begin. The distance where the model first flattens out (on the x axis) is known as the range. The value at which the variogram model attains the range (on the y axis) is called the sill.

When performing kriging within Arcgis, the user has the option of either manually inputting the variogram parameters or having the software automatically specify the values

for the variogram parameters from an internal algorithm. However, if the variogram parameters are chosen by the program, the parameter estimates cannot be output or seen, creating a black box effect, which may lead to applying kriging inappropriately. Due to this, it was decided to perform the variogram analysis outside of ArcGIS.

Kriging was performed only on the SD and estimated SWE at each node. Using only six points on individual time steps limited the variogram output, because of minimal data input. Low numbers of sample sites at each time step can inhibit visualization of potential spatial trends and provide inadequate information for parameter estimation (nugget, range, and sill). Due to the potential for low resolution variograms on each time step, data from all time steps were used to create a "generalized" variogram for both SD and SWE for the entire time series. A model unique to each data set (SD and SWE) was then fit to the generalized variograms, and the class size, nugget, range and sill were generated for both.

Automation and animation of kriging

All aspects of kriging for each time step were automated using Python script linked to ArcGIS. The manual inputs to the script include the seasonal variogram parameters (nugget, sill, range), best fit model of the variogram, output cell size, a database file format (.dbf) of all values (SD or SWE), associated time stamps and location data. All output raster files for each time stamp were grouped, sorted and superimposed according to time. Video recordings were then created within ArcGIS of the data groupings to represent spatial and temporal SD and SWE trends within the field area.

Validation and verification

Each of the kriged time steps was compared to SD and SWE measurements at each sample point. The kriged raster outputs had a 0.1 meter resolution and created a time prohibitive analysis if each of the outputs cells (1980 raster cells per layer) were to be analyzed for accuracy at each of the 72 time steps. Due to the large size of the kriged data output, a generalized analysis was performed as explained below.

Each kriged raster output at each time step was (1) averaged, (2) the maximum value was generated and (3) the minimum value was generated. This process was also implemented for the entire manual SD and SWE data series. All average, maximum and minimum kriged SWE and SD estimates were then compared with the average, maximum and minimum observed SWE and SD. Finally, all data from the kriged raster outputs were compared with measurements from the snow pillow to determine how representative the point based snow pillow measurement was for the field site.

Results

Snowcloud calibration trials

Snowcloud calibrations were analyzed for accuracy from a comparison of Snowcloud SD and ground surface to sonar distances (s-s) to the manual SD and s-s measurements. Each sonar node had unique calibration constants included in appendix A. The manual measurements used to develop the constants can also be found within appendix A.

The first calibration trial results yielded calibration equations that were inaccurate, such that Snowcloud data did not correspond with the manual SD and S-S measurements.

The second calibration trial yielded results that were congruent with the manual measurements. Using these calibrations, the Snowcloud generated data compared well with the manual measurements from the 1/18/2010 to 5/02/2010. These measurements are included in appendix A.

Field work

Site characterization

All values and bar graphs generated from the field data can be found in appendix B.

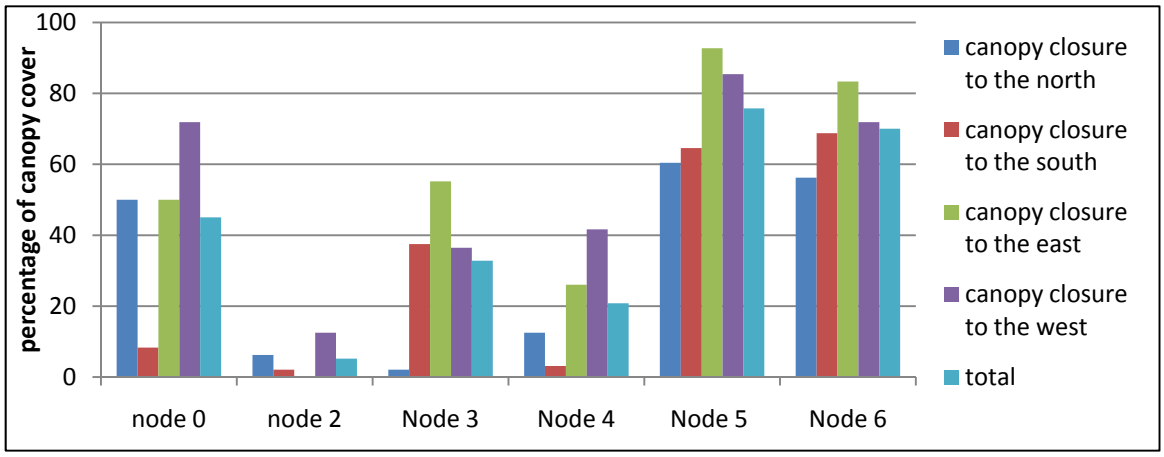

Figure 16: Canopy closure percentages at each node paired with aspect.

Canopy closure values at the nodes are presented below, in figure 20.

Manual SWE and SD sampling

The SWE and SD measurements were collected weekly from the 18th of January to the 29th of April 2010 and are included in appendix C.

Snow pillow verification

The snow pillow measurements of SWE were compared with manual measurements and are included in appendix C. Due to initial calibration errors with the snow pillow, there was a systematic bias of -0.807 inches. Therefore all snow pillow data was reduced by 0.807 inches (Figure 21).

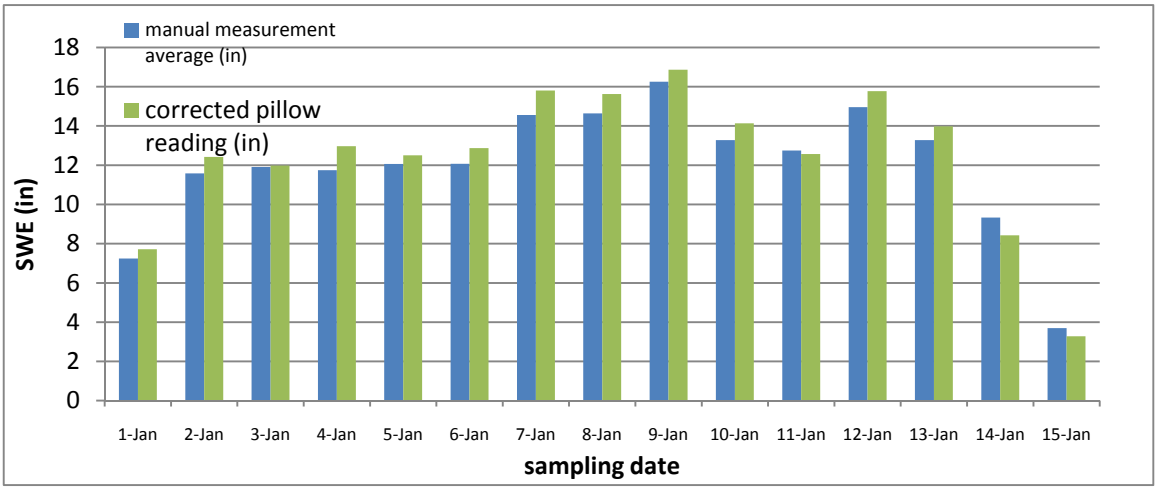

Figure 17: Comparison of manual SWE measurements to snow pillow output

Correspondence analysis

Correspondence analysis (CA) was performed on all tower one data, the manual SWE and SD measurements at each Snowcloud node, and the site characterization at each Snowcloud node to arrive at a set of potential predictors of SWE. The weekly, monthly and seasonal running average data series from tower one were utilized for the initial analysis. However, the large amount of input variables limited visualization within the CA charts. Due to this, these data series were disaggregated according to elevation of sensor location on tower one. The tower has instrument clusters of 15 feet, 25 feet and 100 feet above the ground surface. Only data measured at 25 feet and lower were used to mimic data collection at Snotel and RAWS sites, which generally have towers less than 25 feet in height.

Despite increased resolution using only data collected at 25 feet and lower, many of the potential predictors continued to plot closely and inhibited visual analysis (Figure 22).

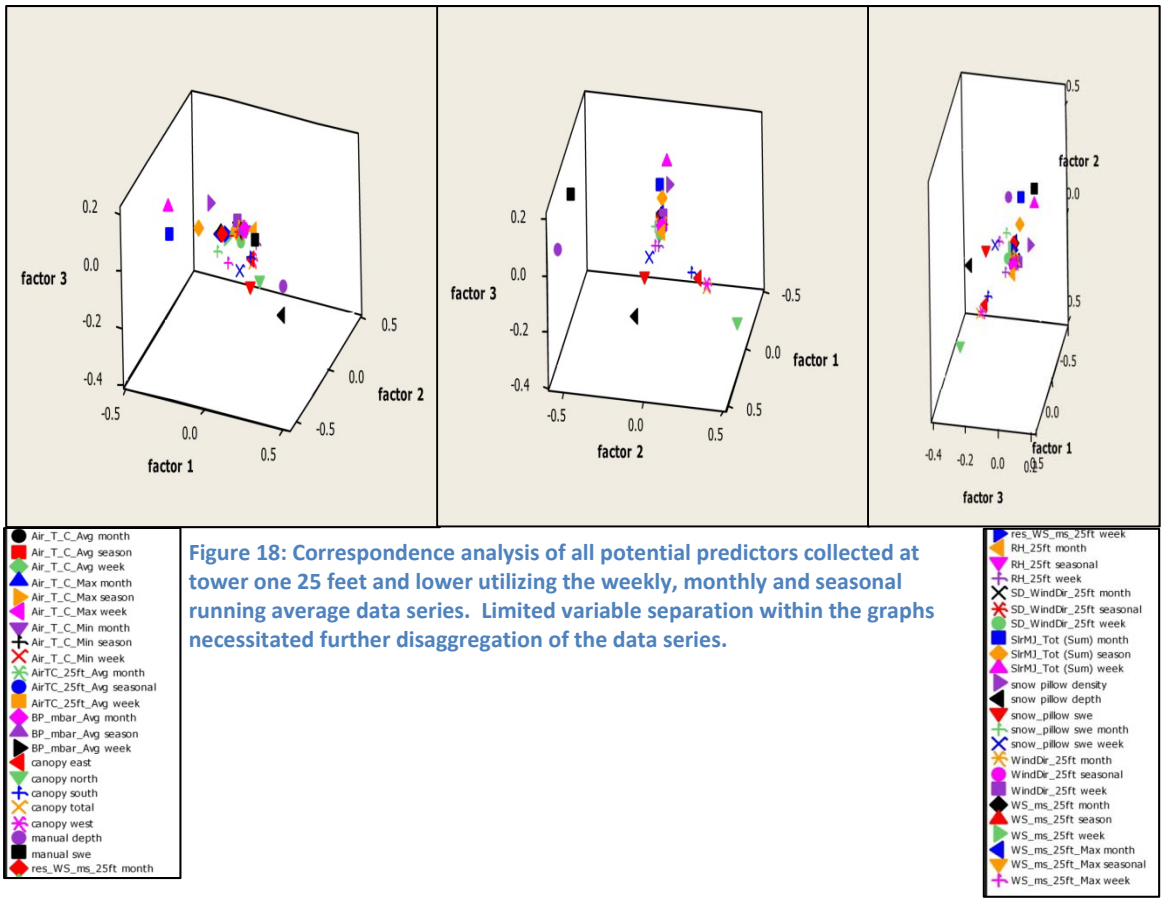

Figure 18: Correspondence analysis of all potential predictors collected at tower one 25 feet and lower utilizing the weekly, monthly and seasonal running average data series. Limited variable separation within the graphs necessitated further disaggregation of the data series.

Due to this, the grouped weekly, monthly and seasonal running average data series at 25 feet and lower were further disaggregated to individual data as: (1) weekly averaged data, (2) monthly average data and (3) seasonal running average data.

As a majority, the weekly averaged data collected at 25 feet and lower demonstrated the greatest separations between potential predictors within the correspondence analysis graphs (Figures 23-25). The monthly and seasonal data series correspondence analyses can be found within appendix D. A list of potential predictors was created from this data set along with temperature data within the monthly average data set.

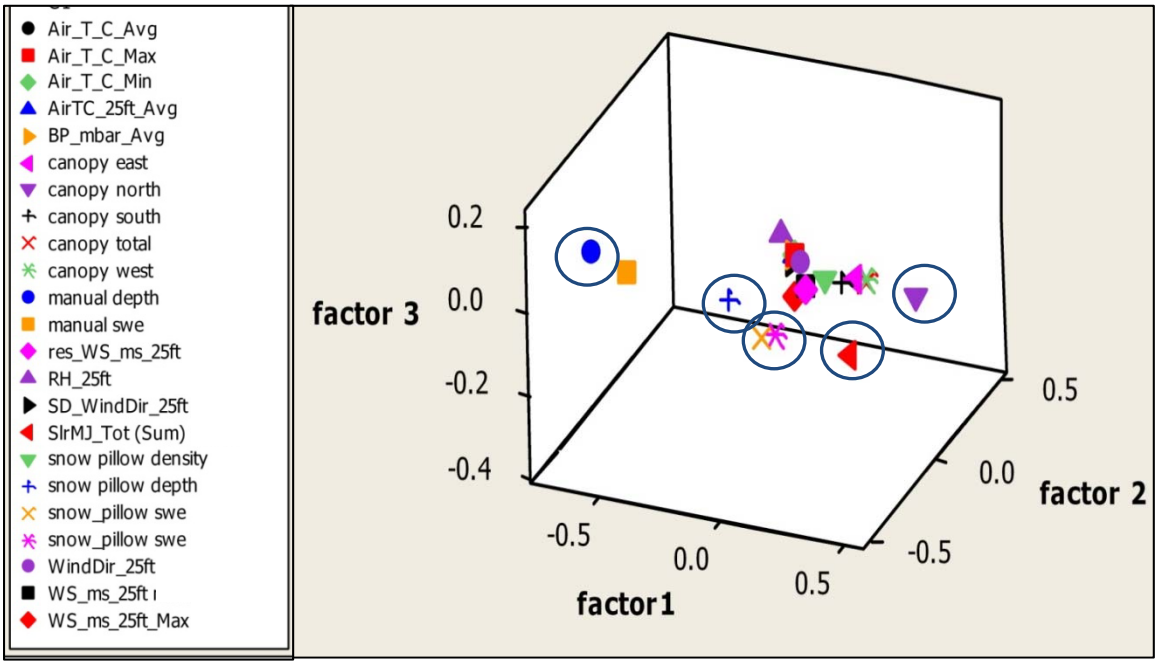

Figure 19: All weekly averaged data collected 25 feet and lower. Blue circles denote independent groupings. Factor one contains 82 percent of the variability within the data set, factor two contains 10% and factor three contains 5%.

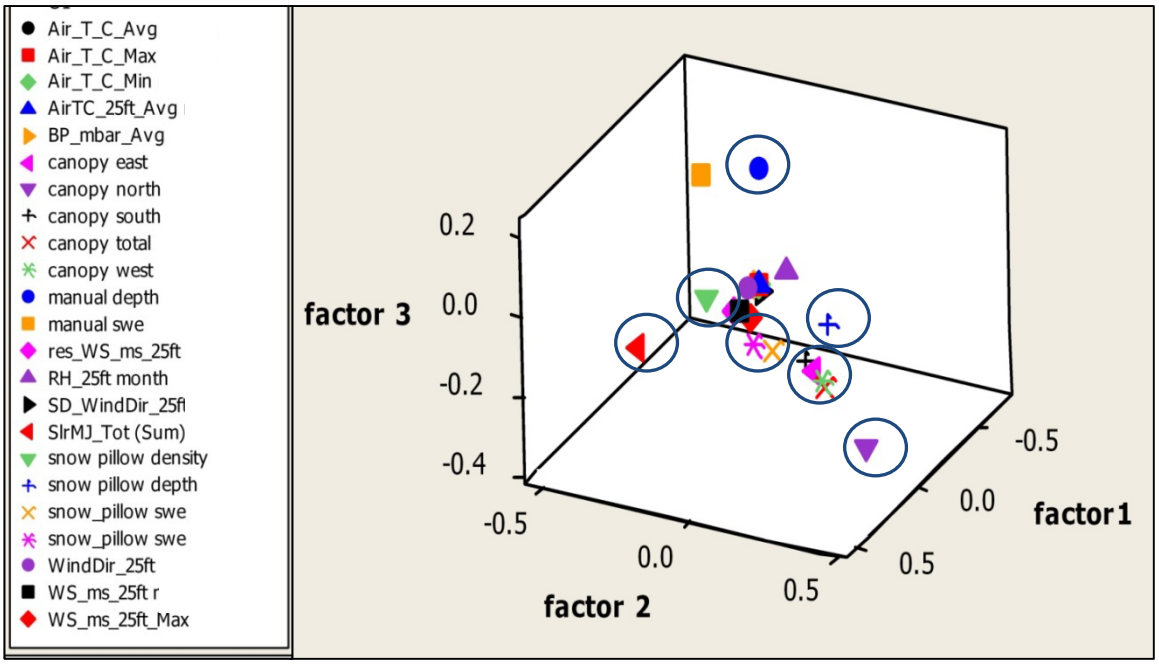

Figure 20: All weekly averaged data collected 25 feet and lower with factor 2 rotated to the front. Blue circles denote independent groupings. Factor one contains 82 percent of the variability within the data set, factor two contains 10% and factor three contains 5%.

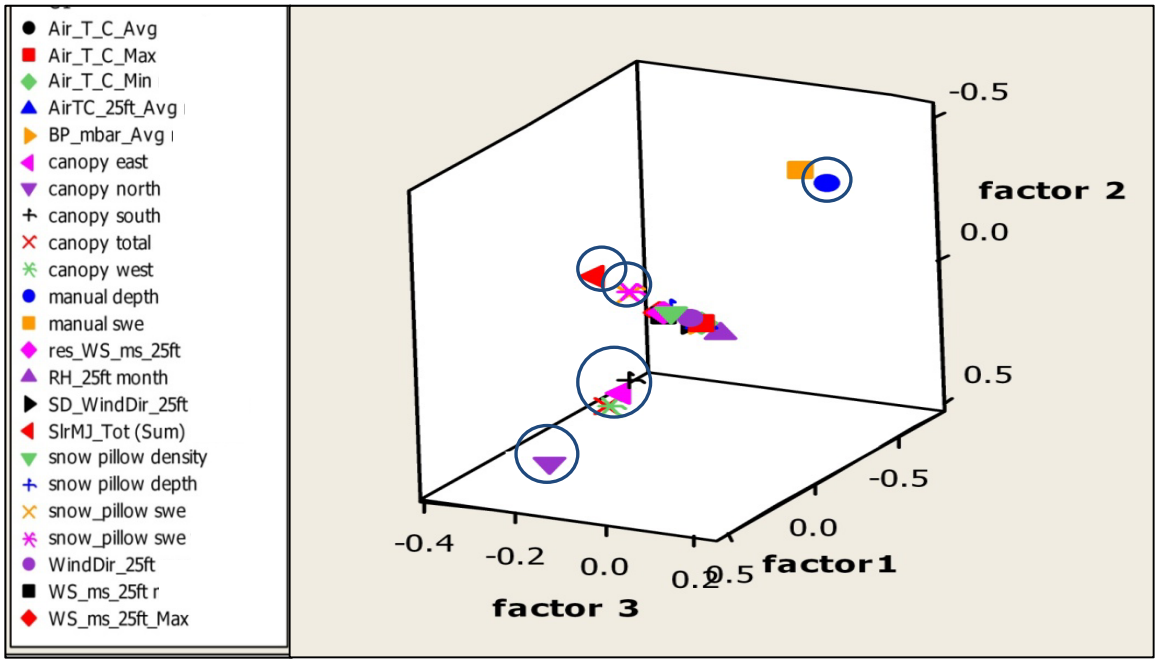

Figure 21: All weekly averaged data collected 25 feet and lower with factor 3 rotated to the front. Blue circles denote independent groupings. Factor one contains 82 percent of the variability within the data set, factor two contains 10% and factor three contains 5%.

Some potential predictors plotted in groupings within unique grid spaces on the charts. If the groupings contained separate state variables, additive composites were created. For example, if a grouping contained 3 temperature values (such as maximum temperature, minimum temperature, average temperature, etc), only one temperature was used as a potential predictor from the grouping. However, if 3 separate variables plotted together such as wind speed, relative humidity and average temperature, then a composite was created by adding the values of the variables together. The individual values within the composites were also kept as potential predictors and compared against composite values from the regression results.

The potential predictors identified from correspondence analysis were:

1. Canopy cover with a northern aspect (%)
2. Canopy cover with a southern aspect (%)
3. Snow depth (manual snow depth or Snowcloud generated snow depth, in)
4. Snow depth at the snow pillow (in)
5. SWE at the snow pillow (in)
6. Snow density at the snow pillow (lb/in^3)
7. Weekly incoming solar radiation (megajoules)
8. Monthly average temperature (°C)
9. A composite of average weekly temperature, relative humidity and wind direction

Regression analysis

SWE* equation 1 (SWE^*_{Snotel})

The initial SWE equation tested the feasibility of estimating SWE in an area surrounding a Snotel site with SD information from wireless sensor networks and environmental data measured at tower one, including snow density from the snow pillow and snow depth. The regression analyses used variations of the potential predictors from the correspondence analysis and the best model was analyzed by regression of the actual vs. predicted SWE values at the node sites and at all transects (Equation 7, figures 26-29 and table 3).

Figure 26 compares observed and estimated SWE values at each Snowcloud node. The average difference between observed and estimated SWE at the Snowcloud nodes was 1.6×10^{-5} inches, with a standard deviation of 1.661. The differences were approximately normally distributed, with the exception of one outlier. A probability plot of the residuals along with a histogram and graph of the residuals can be seen in Figure 27. Based on the assumption of normality the slope of the regression line was 0.89 (±0.07) and the intercept was 0.88 (±0.60), with the values in parentheses representing the bounds of a 95% confidence interval based on the T statistic for this regression. Figures 28 and 29 compare observed and estimated SWE on each transect.

Eq. 7: *(F statistic = 2571.2, Correlation coefficient = 0.93, P statistic = 0.000+)*

$$SWE^*_{Snotel} = 164.1785 - 2.247406X_1 + 1.645053X_2 + 0.268118X_3 + 0.7505726X_4 - 0.03315234X_5 - 0.2170932X_6 - 0.5985992X_7$$

Variable	Descriptor	P value
X_1	Canopy closure to the north	0.000
X_2	Canopy closure to the south	0.168
X_3	Manual or Snowcloud generated snow depth	0.000
X_4	SWE at the snow pillow	0.000
X_5	Weekly total incoming solar radiation	0.0014
X_6	Snow depth at the snow pillow	0.001
X_7	Monthly average temperature	0.001

Table 3: P values of independent variables within the SWE*$_{Snotel}$ equation.

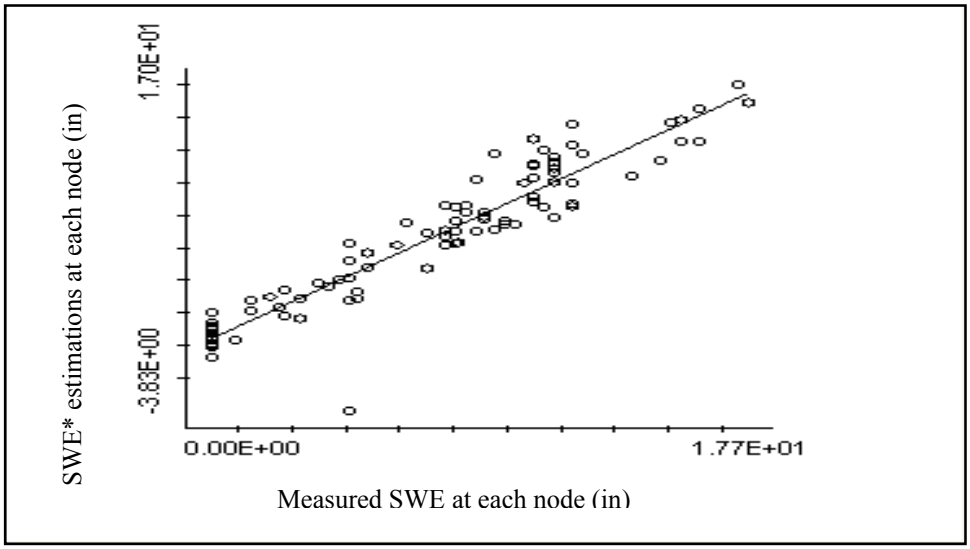

Figure 22: Regression of actual vs. predicted values from use of SWE*$_{Snotel}$ equation which tests the applicability of extending Snotel sites with WSN SD data. The slope of this regression was 0.89 (±0.07) and the intercept was 0.88 (±0.60), with the values in parentheses representing the bounds of a 95% confidence interval. The correlation coefficient of the regression was 0.94 with an F statistic of 656.3, a T statistic of 25.62 and a Spearman rank coefficient of 0.94.

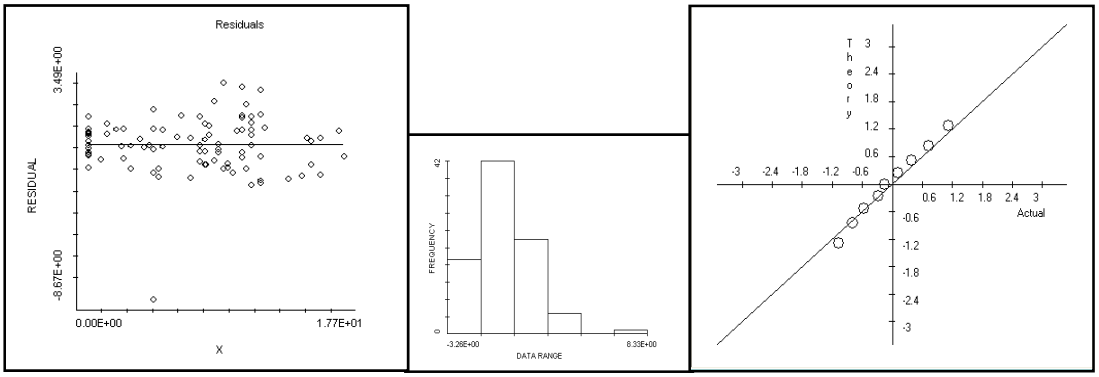

Figure 23: Residuals of SWE*$_{Snotel}$, histogram analysis of residuals and a probability plot of the residuals. The outlier within the residual plot can be seen within the far right class on the histogram plot.

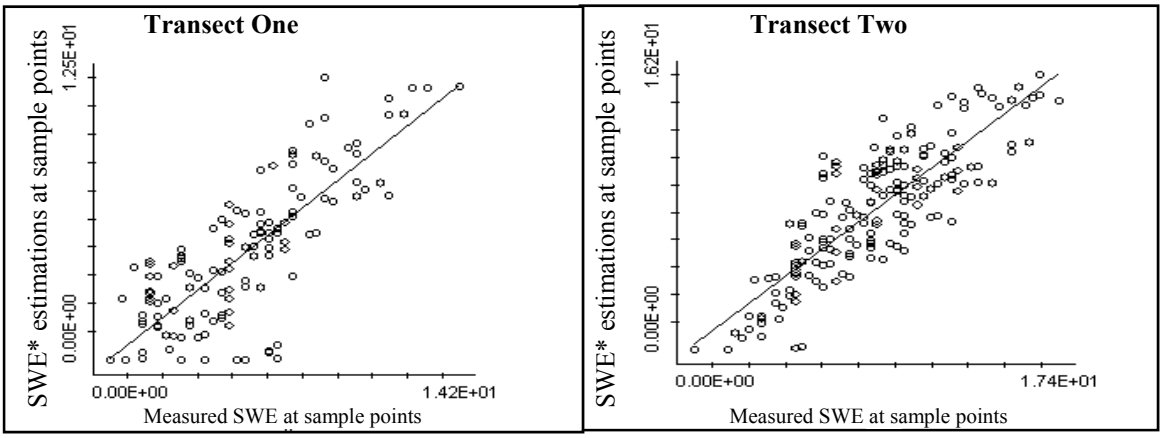

Figure 24: Regression of actual vs. predicted SWE values (in inches) from SWE*$_{SNOTEL}$ equation along sample points on transects one and two.

Transect One
- Slope: 0.92 (±0.08*) , Intercept: 0.37(±0.72*)
- Correlation coefficient: 0.87
- F statistic: 531.75
- T statistic : 23.1
- Spearman rank coefficient: 0.83

**denotes bounds of a 95% confidence interval*

Transect Two
- Slope: 0.85 (±0.07*), Intercept: 0.094 (±0.35*)
- Correlation coefficient: 0.88
- F statistic: 614.5
- T statistic : 24.8
- Spearman rank coefficient: 0.88

**denotes bounds of a 95% confidence interval*

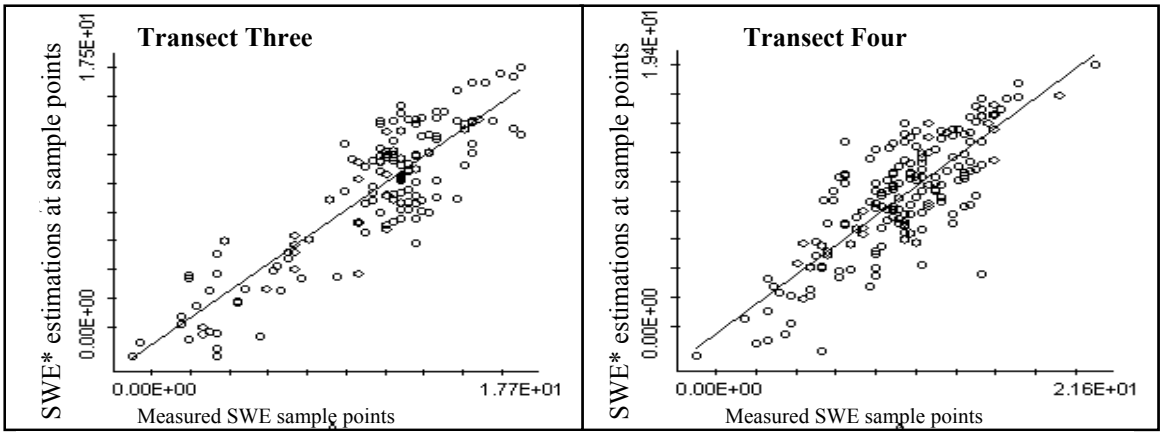

Figure 25: Regression of actual vs. predicted SWE values (in inches) from SWE*$_{SNOTEL}$ equation along sample points on transects three and four.

Transect Three
- Slope: 0.92 (±0.05*) , Intercept: -0.08 (±0.35*)
- Correlation coefficient: 0.94
- F statistic: 1409.2
- T statistic : 37.54
- Spearman rank coefficient: 0.84

**denotes bounds of a 95% confidence interval*

Transect Four
- Slope: 0.91(±0.09*), Intercept: 0.57 (±1.14*)
- Correlation coefficient: 0.81
- F statistic: 331.75
- T statistic : 18.1
- Spearman rank coefficient: 0.74

**denotes bounds of a 95% confidence interval*

SWE* equation 2 ($SWE^*_{general}$)

The second SWE equation tested the applicability of extending wireless sensor networks to Snotel sites using only SD from Snowcloud and snow density from the onsite snow pillow and no state variables from tower one. The $SWE^*_{general}$ equation was generated to compare a generalized SWE extrapolation technique to the more time and resource intensive SWE^*_{Snotel} equation.

Snow density at the snow pillow was determined as SWE divided by snow depth. The Judd sonar sensor at tower one was not properly calibrated during the 2010 field season. Due to this, SD at the Snowcloud node 3 (15 meters to the south of the snow pillow) was used as a surrogate for this measurement. Snow depths at node 3 corresponded reasonably well with those observed at the snow pillow on each sampling week with the exception of sampling week 2 (January 25, 2010). See figure 30 below. The average difference between SD measurements at the snow pillow and those reported at node three from all sampling weeks was ±7.4." Further Snow pillow to node SD comparisons can be found within Appendix C.

The best model was analyzed by regression of the actual vs. predicted SWE values. See equation 8 and figures 31-34.

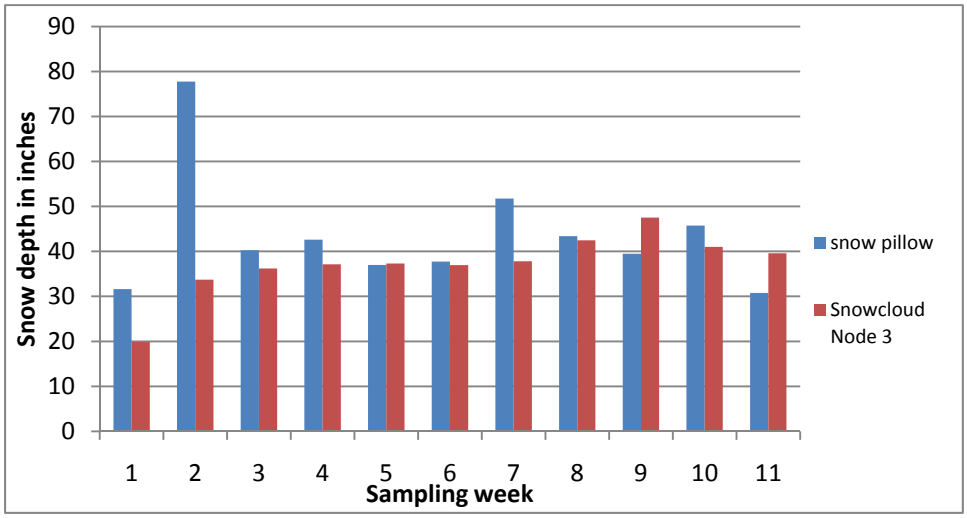

Figure 26: Comparison of manual SD measurements around the snow pillow to Snowcloud node 3 SD, where week one represents 18-Jan 2010 and week 11 represents 29- Mar 2010.

Figure 31 compares observed and estimated SWE values at each Snowcloud node. The comparison of the observed and estimated values by regression yielded a slope estimate of 1.01 (±0.05), and an intercept value of 0.11(±0.45), with the values in parentheses representing the bounds of a 95% confidence interval based on the T statistic for this regression. The regression comparison was highly significant with a P statistic of 0.000+ and an F statistic of the regression of 1582.13. The average difference between observed and estimated SWE at the Snowcloud nodes was -1.20 x 10^{-8} inches, with a standard deviation of 1.16. The differences were approximately normally distributed. A probability plot of the residuals along with a histogram and graph of the residuals can be seen in Figure 32. Figures 33 and 34 compare observed and estimated SWE on all points on each transect.

Eq. 8: $$SWE^{*}_{general} = \rho * sd$$

in which ρ= generalized snow density, calculated from:

$\left[\left(\frac{SWE\ at\ snow\ pillow}{SD\ at\ Snowcloud\ Node\ 3}\right) * density\ of\ water\right]$ and sd= snow depth from the Snowcloud nodes.

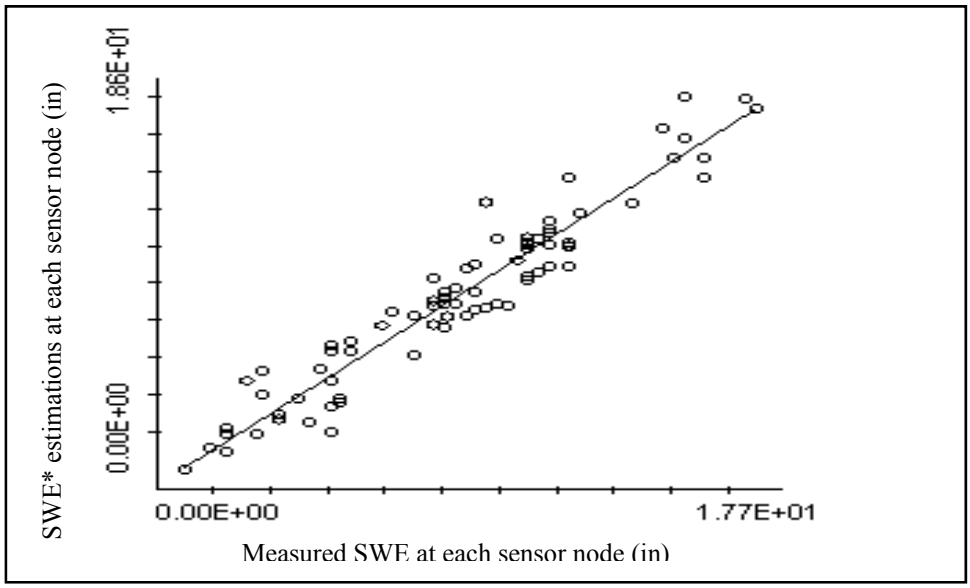

Figure 27: Regression of actual vs. predicted values from use of SWE*$_{general}$ equation which tests the applicability of extending Snotel sites with WSN SD data using only a generalized density multiplier with the Snowcloud estimated depths. The slope of this regression was 1.01 (±0.05) and the intercept was 0.11 (±0.45), with the values in parentheses representing the bounds of a 95% confidence interval. The correlation coefficient of the regression was 0.97 with an F statistic of 1582.13, a T statistic of 39.87 and a Spearman rank coefficient of 0.96.

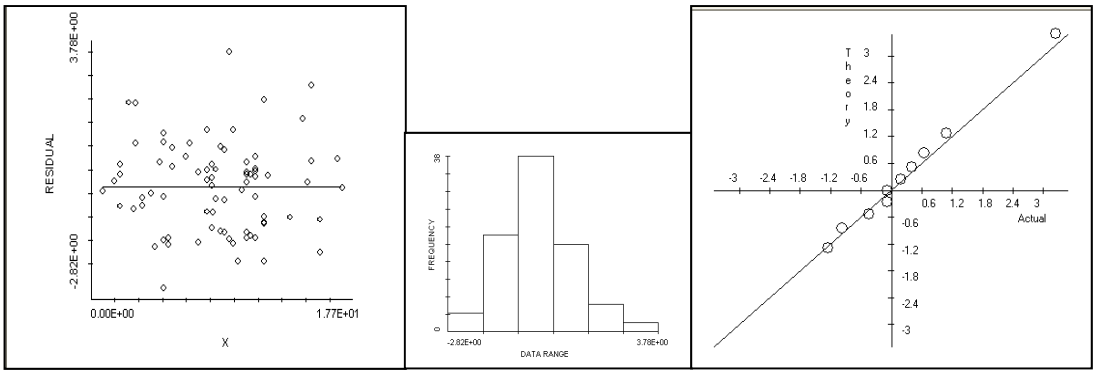

Figure 28: Residuals of SWE*$_{general}$ equation, histogram analysis of residuals and a probability plot of the residuals.

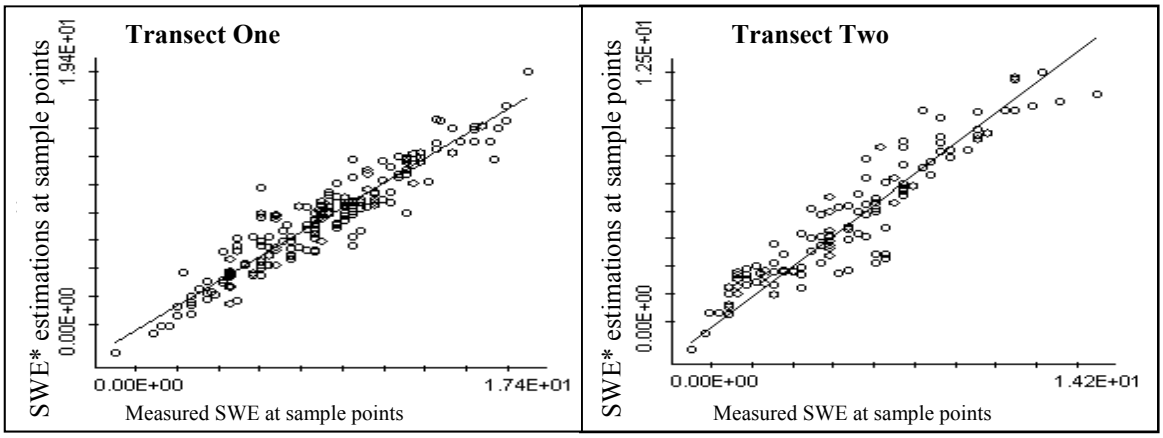

Figure 29: Regression of actual vs. predicted SWE values (in inches) from SWE*$_{general}$ equation along sample points on transects one and two.

Transect One
- Slope: 0.98 (±0.04*), Intercept: 0.69 (±0.43*)
- Correlation coefficient: 0.95
- F statistic: 1746.7
- T statistic : 41.8
- Spearman rank coefficient: 0.94

**denotes bounds of a 95% confidence interval*

Transect Two
- Slope: 0.96 (±0.04*) , Intercept: 0.37 (±0.43*)
- Correlation coefficient: 0.97
- F statistic: 2669.0
- T statistic : 51.7
- Spearman rank coefficient: 0.98

**denotes bounds of a 95% confidence interval*

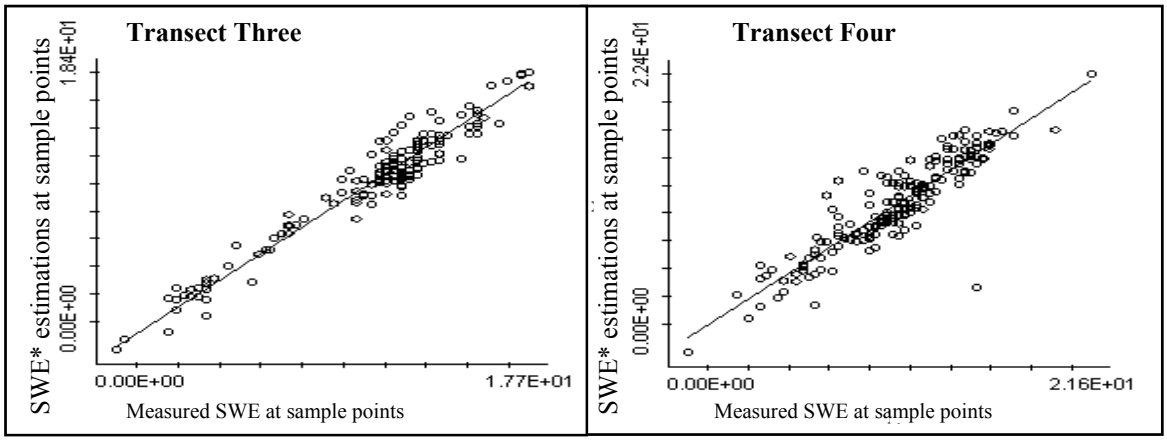

Figure 30: Regression of actual vs. predicted SWE values (in inches) from SWE*$_{general}$ equation along sample points on transects three and four.

Transect Three
- Slope: 1.00 (±0.02*), Intercept: 0.17 (±0.24*)
- Correlation coefficient: 0.99
- F statistic: 7175.8
- T statistic : 84.7
- Spearman rank coefficient: 0.94

**denotes bounds of a 95% confidence interval*

Transect Four
- Slope: 0.96 (±0.07*), Intercept: 1.21 (±0.79*)
- Correlation coefficient: 0.9
- F statistic: 774.3
- T statistic : 27.8
- Spearman rank coefficient: 0.89

**denotes bounds of a 95% confidence interval*

SWE* Equation 3 (SWE^*_{RAWS})

The final SWE equation (SWE^*_{RAWS}) was generated to test the applicability of extending wireless sensor networks to RAWS sites, which are not equipped with snow pillows. All snow pillow data were removed from the initial SWE^*_{Snotel} equation. The best model was analyzed by regression of the actual vs. predicted SWE values. See equation 9, figures 35-38 and table 4.

Figure 35 compares observed and estimated SWE values at each Snowcloud node. The comparison of the observed and estimated values by regression yielded a slope estimate of 0.78 (±0.09), and an intercept value of 1.63(±0.76), with the values in parentheses representing the bounds of a 95% confidence interval based on the T statistic for this regression. The regression comparison was significant with an F statistic of the regression of 315.88. The average difference between observed and estimated SWE at the Snowcloud nodes was 9.74×10^{-9} inches, with a standard deviation of 1.98. The differences were approximately normally distributed. A probability plot of the residuals along with a histogram and graph of the residuals can be seen in Figure 36. Figures 37 and 38 compare observed and estimated SWE on all points on each transect.

Eq. 9: *(F statistic = 1252.2, Correlation coefficient = 0.89, P statistic = 0.000+)*

$$SWE^*_{RAWS} = 443.33 - 5.12393X_1 + 2.574121X_2 + 0.2098947X_3 + 0.09218068X_4 - 1.632019X_5$$

Variable	Descriptor	P value
X_1	Canopy closure to the north	0.000
X_2	Canopy closure to the south	0.168
X_3	Manual or Snowcloud generated snow depth	0.000
X_5	Weekly total incoming solar radiation	0.0014
X_7	Monthly average temperature	0.001

Table 4: Variables and P values within the SWE^*_{RAWS} equation.

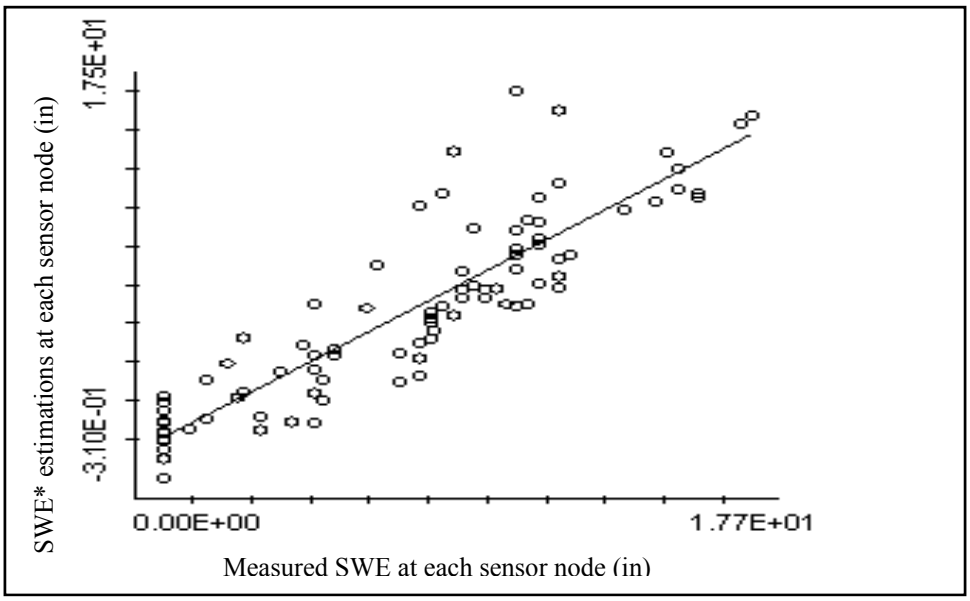

Figure 31: Regression of actual vs. predicted values using SWE^*_{RAWS} which tests the applicability of extending RAWS sites with WSN data. The slope of this regression was 0.78 (±0.09) and the intercept was 1.63 (±0.76), with the values in parentheses representing the bounds of a 95% confidence interval. The correlation coefficient of the regression was 0.89 with an F statistic of 315.88, a T statistic of 17.78 and a Spearman rank coefficient of 0.90.

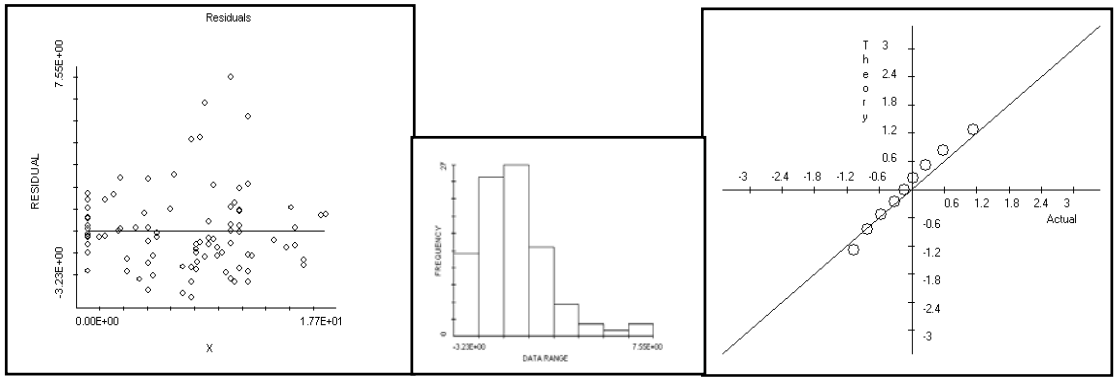

Figure 32: Residuals of SWE^*_{RAWS} equation, histogram analysis of residuals and a probability plot of the residuals.

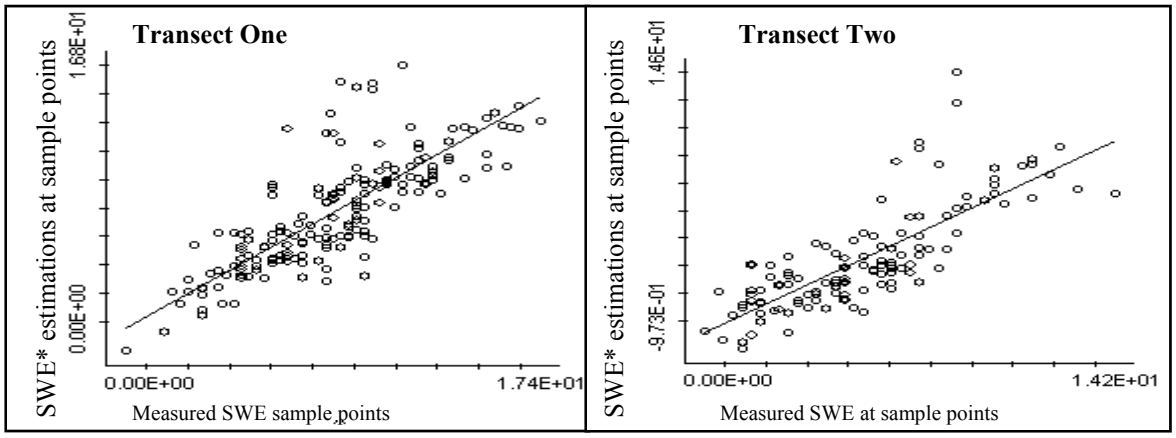

Figure 33: Regression of actual vs. predicted SWE values from SWE*$_{RAWS}$ along sample points on transects one and two.

Transect One
- Slope: 0.78 (±0.08*), Intercept: 1.34 (±0.70*)
- Correlation coefficient: 0.83
- F statistic: 395.26
- T statistic : 19.88
- Spearman rank coefficient: 0.84

**denotes bounds of a 95% confidence interval*

Transect Two
- Slope: 0.77 (±0.06*), Intercept: 0.44 (±0.24*)
- Correlation coefficient: 0.88
- F statistic: 607.53
- T statistic : 24.65
- Spearman rank coefficient: 0.92

**denotes bounds of a 95% confidence interval*

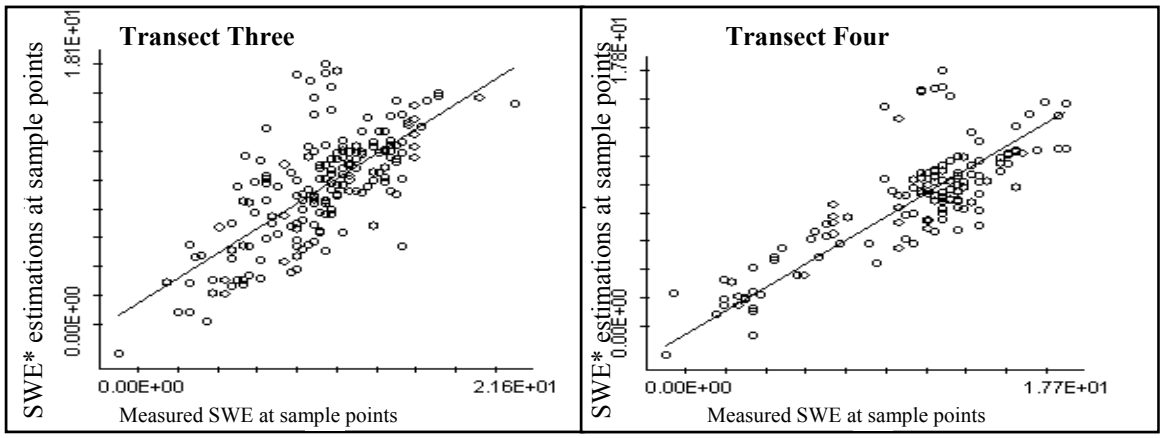

Figure 34: Regression of actual vs. predicted SWE values from SWE*$_{RAWS}$ along sample points on transects three and four.

Transect Three
- Slope: 0.83 (±0.04*), Intercept: 0.62 (±0.51*)
- Correlation coefficient: 0.93
- F statistic: 1110.91
- T statistic : 33.33
- Spearman rank coefficient: 0.83

**denotes bounds of a 95% confidence interval*

Transect Four
- Slope: 0.72 (±0.10*), Intercept: 2.56 (±1.19*)
- Correlation coefficient: 0.72
- F statistic: 188.98
- T statistic : 13.75
- Spearman rank coefficient: 0.69

**denotes bounds of a 95% confidence interval*

SWE estimates through time at the Snowcloud nodes

Measurements of SWE at the Snowcloud nodes from January 18th to March 31st 2010 were compared with estimates from the SWE models (SWE*Snotel, SWE*$_{general}$, SWE*$_{RAWS}$). Figure 39 includes comparisons at all Snowcloud nodes (node1 – node 6) in which the blue line represents manual SWE measurements taken underneath the node, the red line represents the SWE*$_{general}$ estimates under the respective node, the green line represents SWE*$_{Snotel}$ estimates under the respective node and the purple line represents the SWE*$_{RAWS}$ estimates under the respective node. Figure 40 compares average SWE from each of the equations with the averaged manual SWE measurements taken underneath each node using the same colorings as those in figure 39.

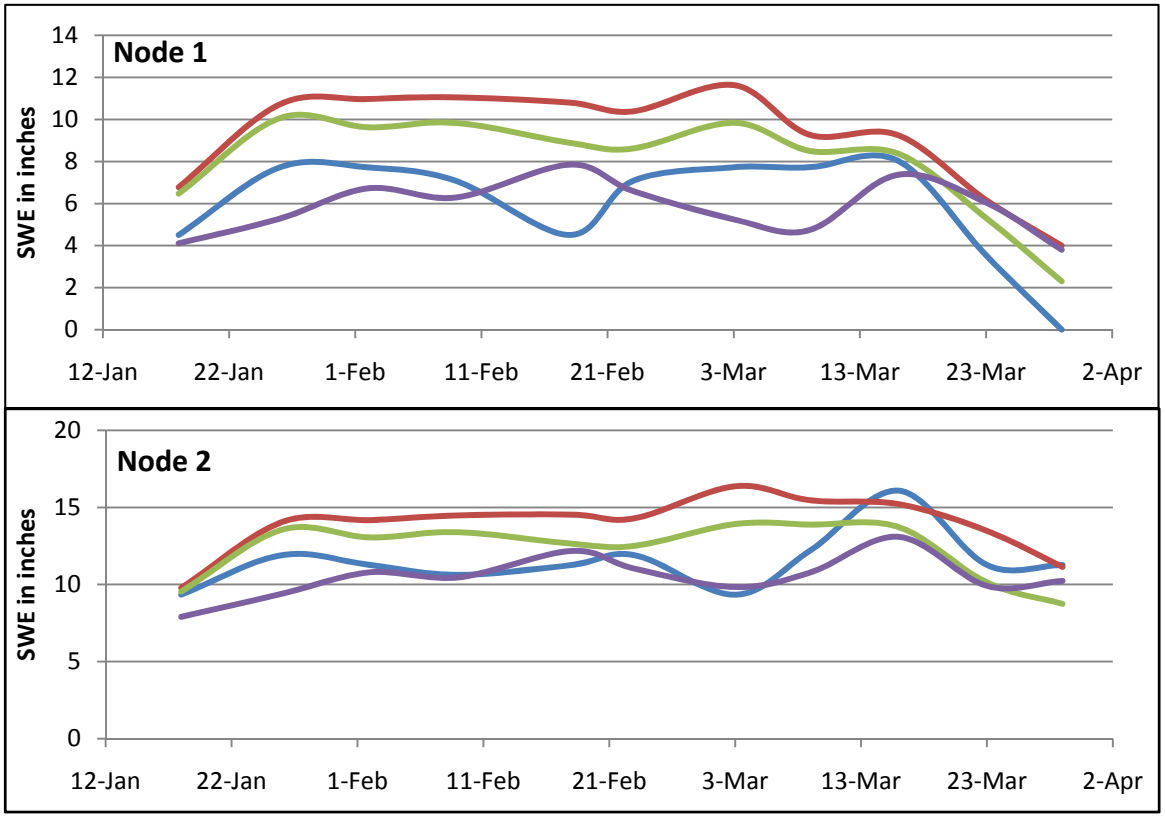

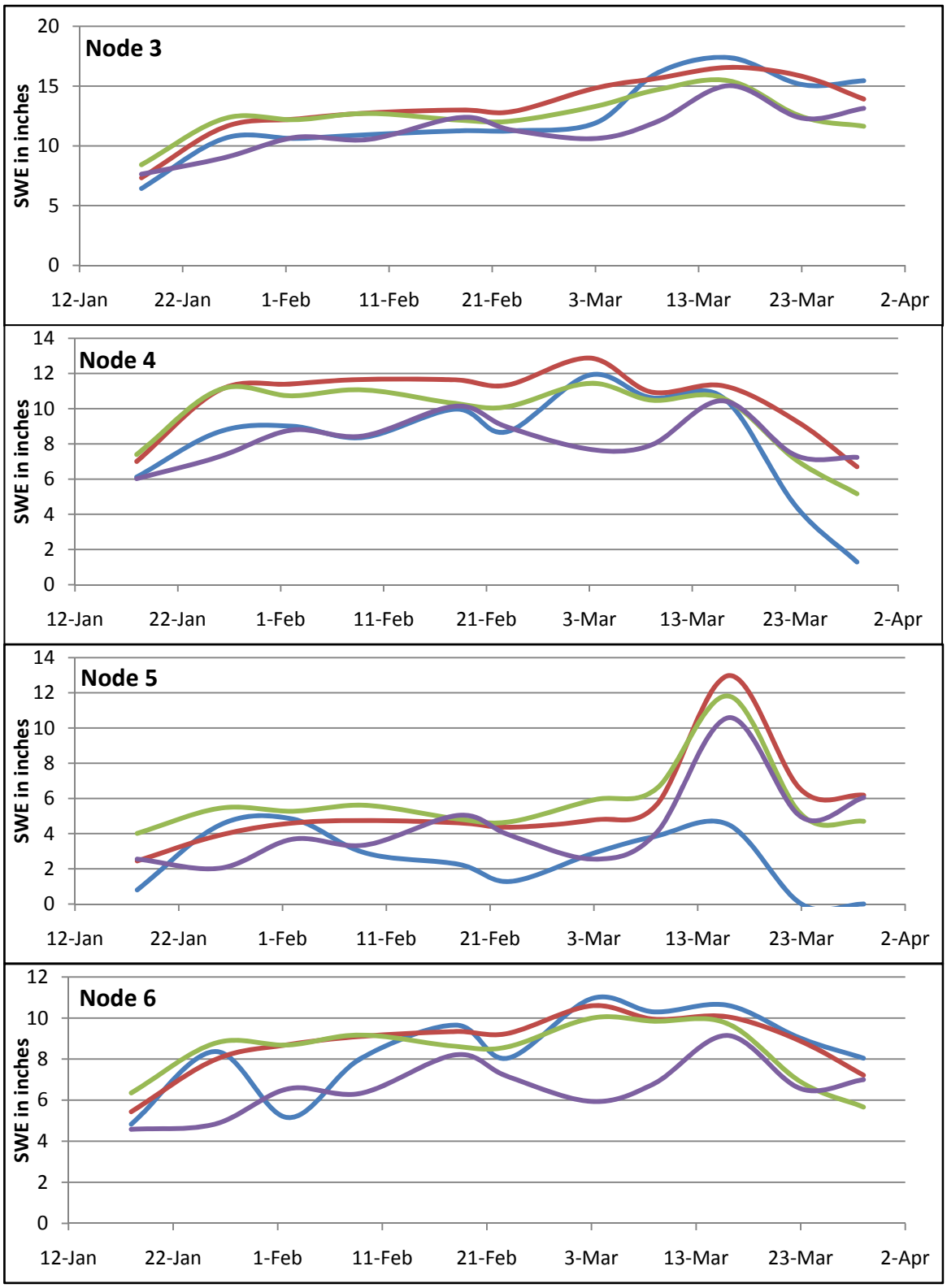

Figure 35: Comparisons of SWE estimates at Snowcloud nodes generated from the application of the $SWE^*_{general}$ (red line), the SWE^*_{Snotel} (green line) and the SWE^*_{RAWS} (purple line) equations at the node sites to manual SWE measurements taken underneath each node on a weekly basis (blue line).

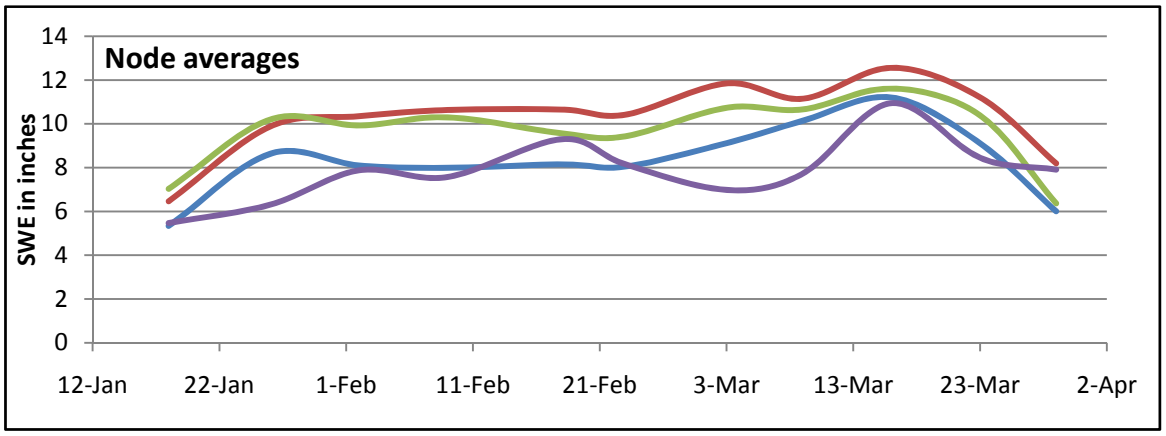

Figure 36: Comparisons of SWE estimates at Snowcloud nodes (node 1- 6) averaged together from the application of the $SWE^*_{general}$ (red line), the SWE^*_{Snotel} (green line) and the SWE^*_{RAWS} (purple line) equations at the node sites to manual SWE measurements taken underneath each node on a weekly basis and averaged together (blue line).

Data Interpolation

Variogram Analysis

Two variograms were created for SD and SWE using the Snowcloud data series from January 18th to March 31st 2010 paired with the $SWE^*_{general}$ equation. The Gaussian model was chosen for both variograms due to the concave upward trend within the data series trend starting when h=0. The Gaussian Model is (eq. 10):

$$\gamma h = Exp(\frac{-h^2}{range})$$

in which γh= variogram model, h= the lag distance and the range= the range of the variogram.

The SWE variogram captured the most variability of SWE in the field area with a class size of 5 x 10^{-5} decimal degrees (8 meters). The range chosen from use of the Gaussian model was 4 x 10^{-4} decimal degrees (63 meters) with a sill of 16 and a nugget of 4.

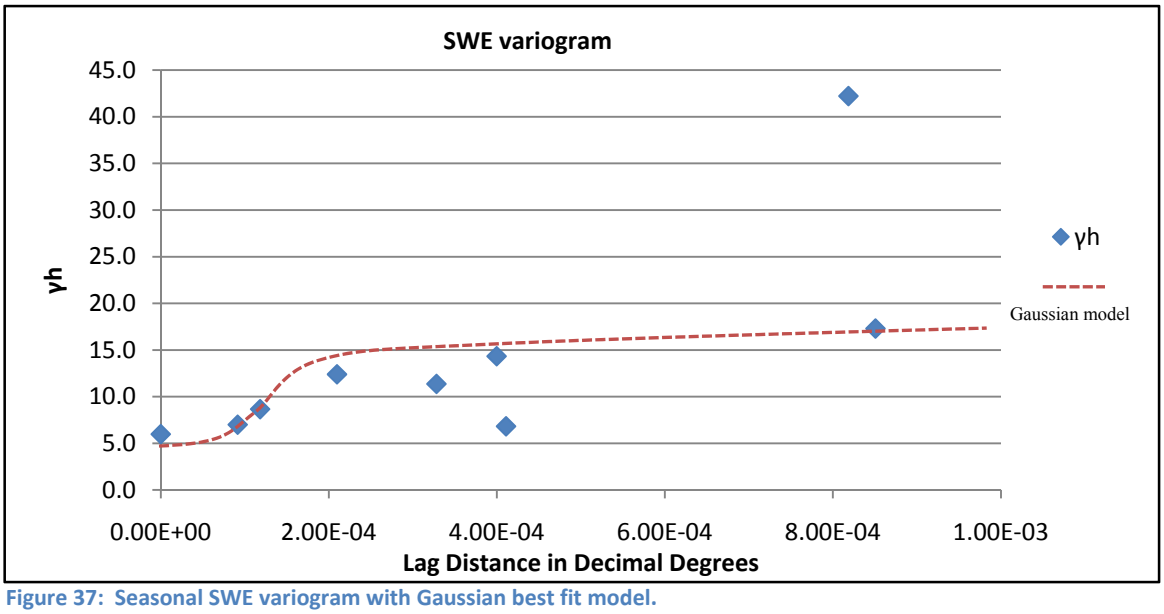

Figure 37: Seasonal SWE variogram with Gaussian best fit model.

The SD variogram captured the most variability of SD in the field area with a class size of 5 x 10^{-5} decimal degrees (8 meters). The range chosen from use of the Gaussian model was 4.3 x 10^{-4} decimal degrees (69 meters) with a sill of 110 and a nugget of 40.

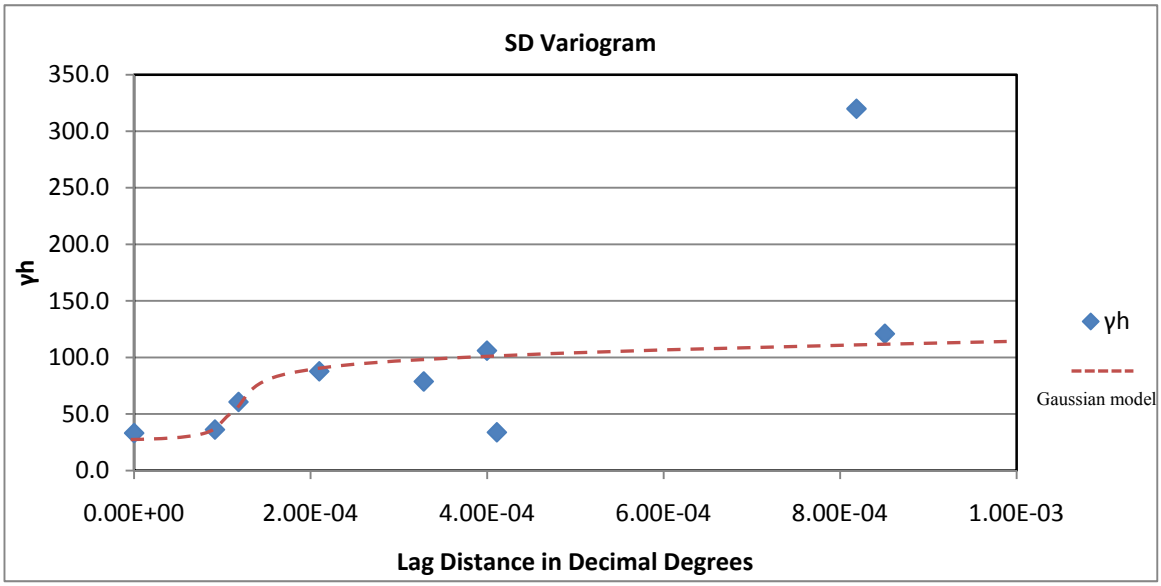

Figure 38: Seasonal SD variogram with Gaussian best fit model.

SD and SWE Kriging

The python script commands for creating a kriged time series can be found within appendix D. Screen shots of the SD and SWE kriging animations from the 18th of January to the 31st of March 2010 are included in figures 43 and 44. The links to the animations can be found below each screen shot.

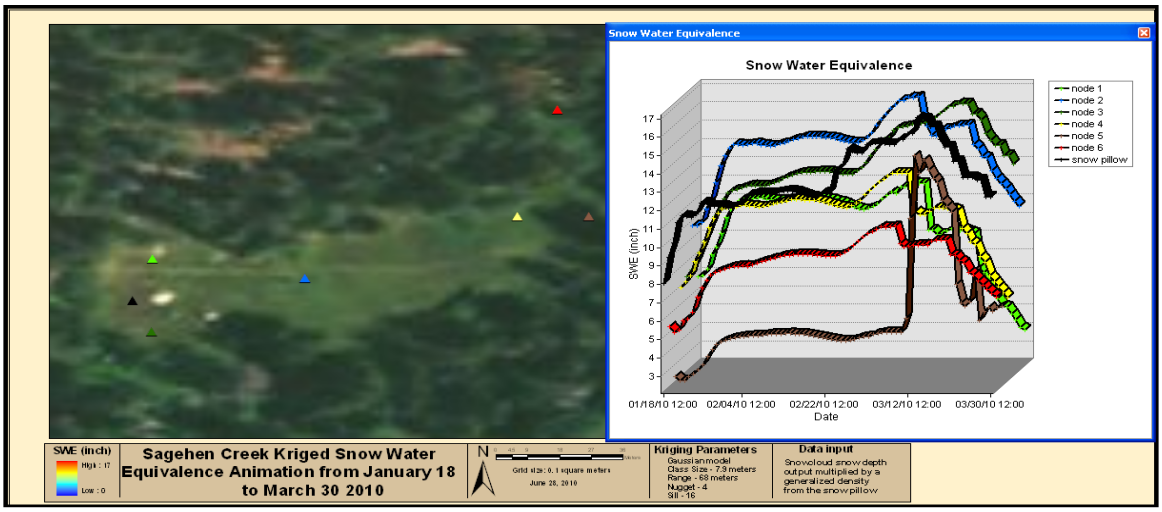

Figure 39: Screen shot of the SWE kriging animation, click on the link below to access the video animation. Higher definition animations can be requested via email at cdmoeser@yahoo.com.

http://www.youtube.com/watch?v=RBSD_6bN7Jc

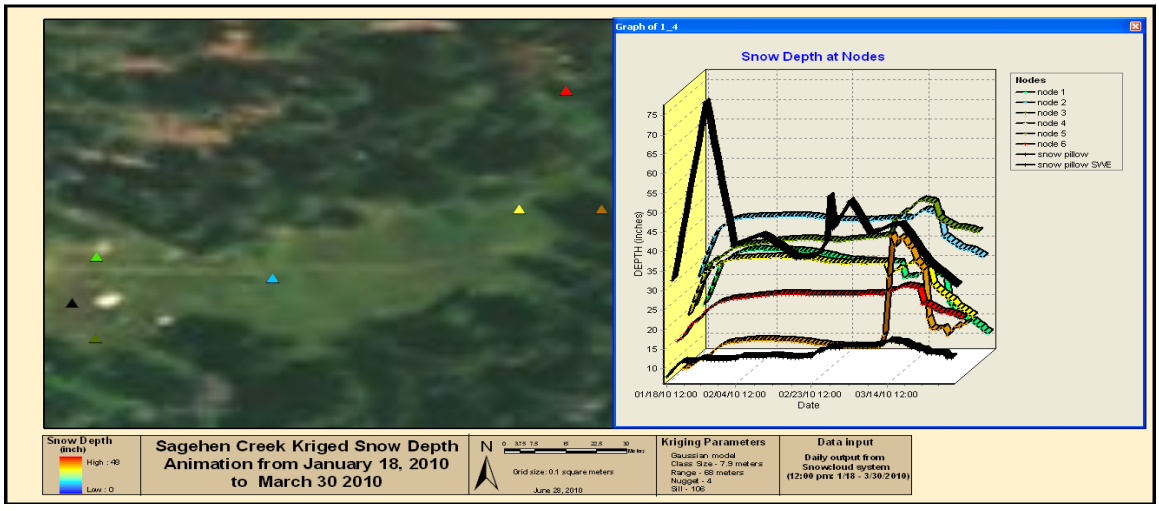

Figure 40: Screen shot of the SD kriging animation, click on the link below to access the video animation. Higher definition animations can be requested via email at cdmoeser@yahoo.com.

http://www.youtube.com/watch?v=OoqvrqDobhM

Kriging verification

Figure 45 compares the measured maxima, minima and mean SWE at all sample points within the field area to the kriged maxima, minima and mean estimates of SWE.

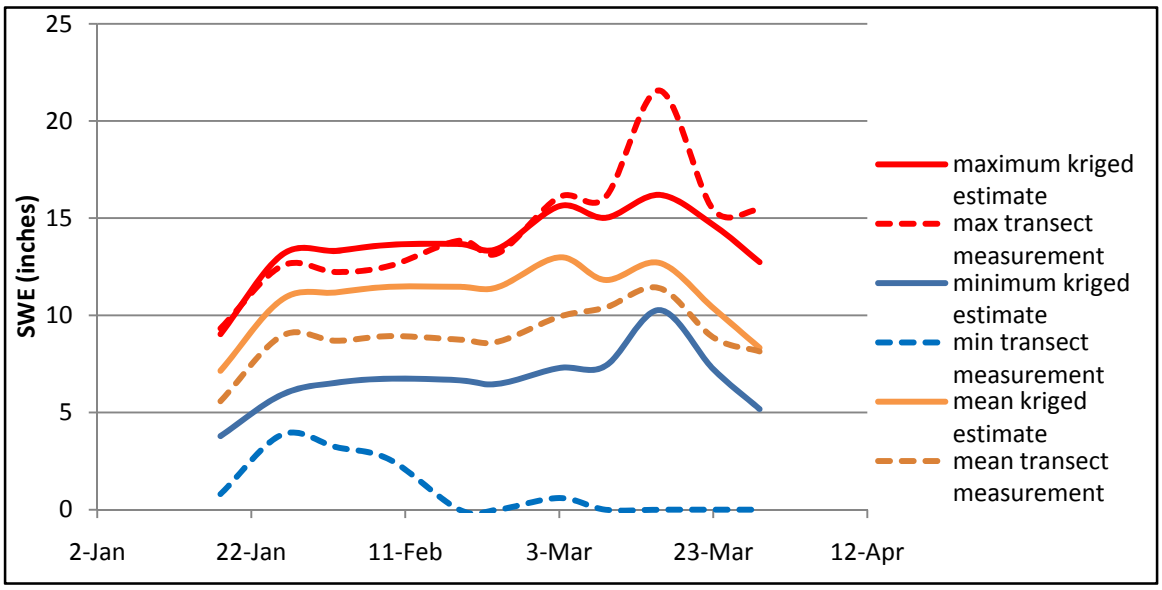

Figure 41: Comparison of maximum, minimum and averaged raster values from kriging to maximum, minimum and weekly manual SWE measurements for the field area.

Comparison of areal interpolation to snow pillow measurements

Figure 46 compares the daily kriged maxima, minima and mean estimates of SWE for the field area to daily measurements of SWE from the snow pillow. Figure 47 compares the weekly manual maxima, minima and mean measurements of SWE at all sample points within the field area to the snow pillow SWE measurements.

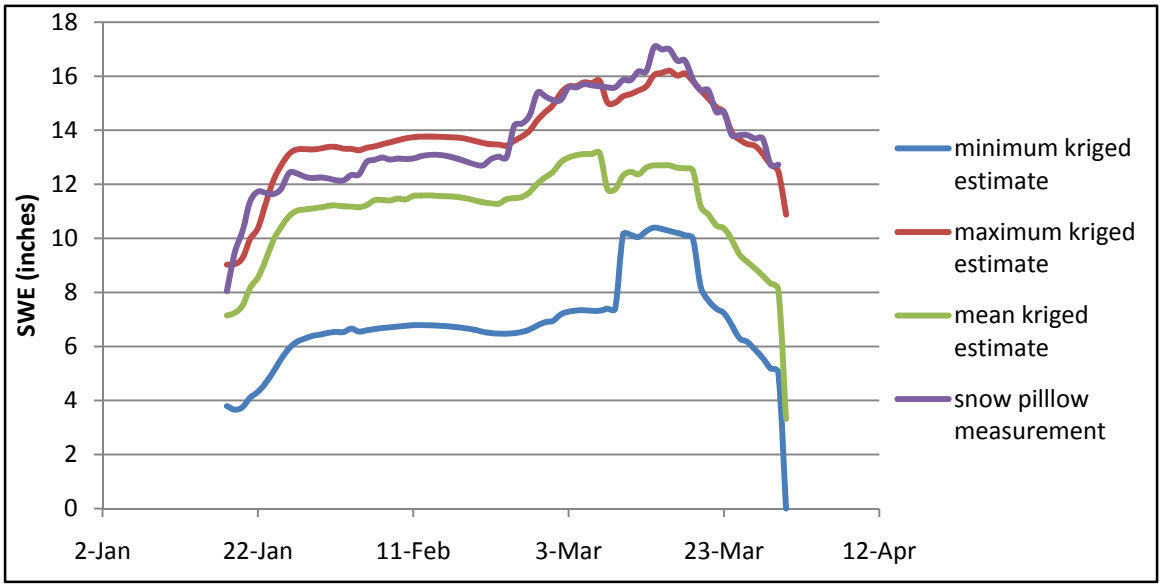

Figure 43: Comparison of maximum, minimum and averaged raster values from kriging to snow pillow measurements on a daily basis.

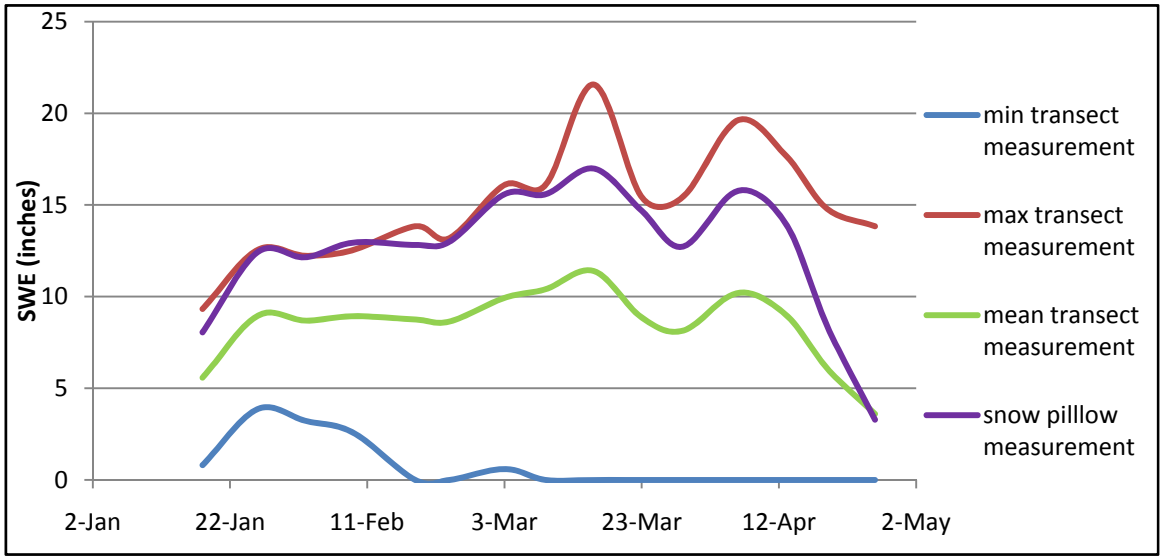

Figure 42: Comparison of maximum, minimum and averaged SWE measurements at each sample point along each transect to snow pillow SWE estimates on a weekly basis.

Discussion

Snowcloud function and accuracy

Sonar

Infield calibration results provided more accurate estimates of sonar emitter to snow and subsequent SD readings than the initial calibration. The initial distances from the ground surface to the sonar emitter measurements (D_{gs}) used in calibration one (indoors) were found to be inaccurate after a final infield verification measurement. Although these inaccurate measurements contributed to the initial calibration failure (calibration one), they do not explain the majority of the initial calibration trial disparity.

Calibration one took place inside a concrete walled room with a calibration height of 4 feet. Most sonar emitters project soundings in a 22° cone from the emitter (Ryan, et al., 2008) (Figure 48). However the angle of emission was not found in the MaxBotic® supplementary specifications material. If the emission cone projection were 22°, then the maximum allowable projection distance would have been less than 21 feet for no interference from the floor, adjacent walls or items within the emission path. During calibration trial one, no precautions were taken to avoid interference from items located within the cone of influence. The MaxBotic® product guide

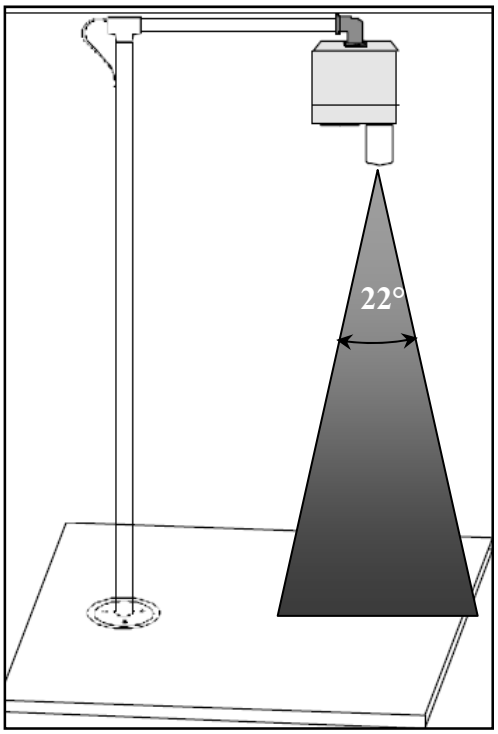

Figure 48: Schematic of a sonar node with a 22° emission cone.

states that best operation is obtained when surrounding noise levels are low, though no specific threshold was provided by the manufacturer. It is possible that noise interference within the concrete walled room affected the initial sonar emitter calibrations. Given the potential for interference, *in situ* calibration is a more reliable method for sonar emitter calibration.

The infield calibration (calibration trial two), was performed on the Snowcloud system tower. This limited noise interference and allowed calibration in the sampling environment in which measurements took place.

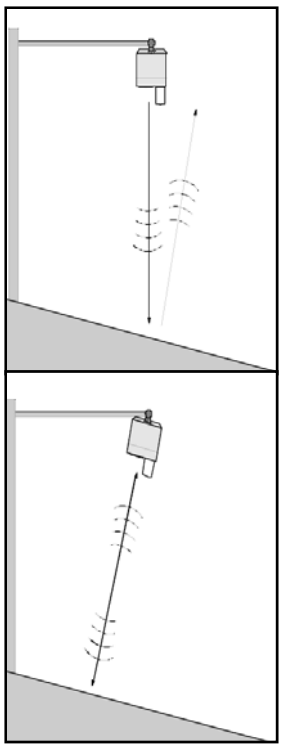

Figure49: Schematic of a wireless sonar node with a correct position (bottom) and incorrect position (top) in reference to the ground surface (Judd, 2010).

Each node's SD sensing accuracy was unique. No systematic errors were seen throughout the sensor suite or at individual times between nodes. Node 6 performed the best, with an average difference between observed and sensed SD of 3.6 inches, a standard deviation of 2.6 and a root mean squared error (RMSE) of 4.14%. Node 5 performed the worst with an average difference of 7 inches, a standard deviation of 10 and a RMSE of 12.95%. The average range of difference between measured and observed values for all Snowcloud nodes was 5.54 inches with a standard deviation of 3.9 and a RMSE of 7.0%. (See appendix A). It is possible that some of the error was from movement of the Snowcloud platform induced by frost heaving. Frost heaving can potentially change both the sonar height above the ground surface and alter the initial perpendicular sensor placement relative to the ground surface, altering the sensed SD (Judd, 2010, Ryan, et al., 2008) (Figure 49).

Unfortunately, the Judd brand sonar sensor on the fixed based tower was inaccurate, precluding the potential to compare accuracy of the Maxbotic® and the Judd sensors. However, if performance of the sonar is measured against the snow pillow, one can get an idea of the utility of the sensor. At the snow pillow, differences between reported and manually measured SWE ranged from 0.47 to 1.24 inches. If this is divided by the average snow density at the snow pillow (measured manually on a weekly basis) then the range of accuracy in SD sensing from the snow pillow was from 1.6 to 4.5 inches with an average difference of 2.4 inches.

Current meteorological sites maintained by the National Weather Service (NWS) utilize either Campbell scientific ultrasonic snow depth sensors or Judd Communications depth sensors. Preliminary studies from the NWS state average error ranges of 2 cm (0.8 in) with variation being as high as 10 cm (4 in) from Campbell sensors and slightly higher variations from the Judd brand sensors (0.2 cm higher than the Campbell sensors) (Ryan, Doesken and Fassnacht, 2008, Ryan, Doesken and Fassnacht, 2008). The less expensive Snowcloud nodes (approximately $1/10^{th}$ the cost of a Campbell scientific sensor and $1/7^{th}$ the cost of a Judd sensor) showed a range of error comparable to the snow pillow and provided information about the entire field area.

Data output from the Maxbotic® sonar emitter performed as programmed for the majority of the sampling season. However, the MaxBotic® sonar did not output voltage readings at some intervals. These data pauses were more common both at night and at the beginning of the season. It is typically much colder within the field area at night and the temperatures were also much lower on average at the beginning of the season. This may mean that the MaxBotic® cannot perform under certain temperature regimes. No information regarding the influence of temperature on sonar performance is available from

the manufacturer. More research is needed to quantify working temperature regimes for the MaxBotic® sonar sensor.

Structure

Periodic communication failure from all nodes occurred during the sampling season. These outages occurred primarily during cold temperatures and high snow accumulation typical of the colder storm cycles seen in the early portion of the Sagehen Creek field season. It is most likely that these lapses were due to snow buildup on the solar panels during prolonged periods of time which led to power failure. The cold temperatures created ice layers on the panels at night, which allowed snow to accumulate and prevented battery recharge from the blockage of sunlight.

Field work

Each transect and the 12 corresponding sample points were created to establish a sampling grid within the field area and to mimic snow courses found throughout the Western United States. Each snow course had completely different average, maximum, and minimum accumulations and different ablation rates. No single transect was representative of the spatial mean of the field site. Transect one had comparatively large measured canopy closure values on each aspect (north, south east and west) and had the lowest accumulation values and slow ablation rates. Transect two, with high canopy closure values to the north and low canopy closure to the south (north edge of the canopy- open area interface), maintained moderate accumulation rates with the fastest ablation rate within the field area (Figure 50).

Figure 50: Looking east along transect two at the canopy open area interface. Transect three is located within the visible large open field to the south (right). Transect one is located within the thick canopy cover to the north (left).

Transect three had low canopy closure values on all aspects and had the highest accumulation mid winter and moderate ablation. Transect four had low canopy closure values to the north and high canopy closure values to the south (southern edge of the canopy open area interface) and maintained very high accumulation along with very slow ablation rates, giving many points along this transect the highest SD values during the ablation phase.

Regression analysis

Site characterization techniques

Percent canopy closure with aspect proved to have a significant association with SWE. Much lower significance was found using total canopy closure. Canopy closure to the north was the most significant predictor of SWE within the regression equations in addition to SD and generalized snow density, with a P value of 0.000+. Correspondence analysis also showed clear independence between all other potential predictors, including the remaining canopy closure qualifiers. Canopy closure to the south had reduced significance within the regression equations. Canopy closure to the south qualifier maintained an 83.2 percentage of significance within the equations. While this is below the $P \leq 0.05$ standard threshold for significance, this qualifier was retained due to a reduction of 282 from the F statistic (when compared to a regression of estimated vs. observed SWE without this qualifier) along with clearly demonstrated independence within the initial correspondence analysis.

SWE equations for augmentation of Snotel sites

The regression models based on the use of Snotel data (SWE^*_{Snotel}, $SWE^*_{general}$) were able to accurately estimate SWE at the nodes and at all sampling points within each transect. However the $SWE^*_{general}$ had increased accuracy of prediction at both the node points and at all transect points. The slope of the $SWE^*_{general}$ regression of actual vs. predicted values at the node sites was 1.01 (±0.05 bounds for a 95% confidence interval) with a correlation coefficient of 0.97, an F statistic of 1582.13 a T statistic of 39.78 and a root mean squared value (RMSE) of 1.2%. $SWE^*_{general}$ also accurately predicted SWE on each transect, with the most accurate predictions along transect three. This is most likely

due to homogenous SD on transect three, in part because the site and canopy characteristics were very similar to those surrounding the snow pillow. The regression of predicted vs. actual values at transect three give a slope of 1.00 (±0.02 bounds for a 95% confidence interval), a correlation coefficient of 0.99 and RMSE of 1.27%. Transect one and transect two comparisons of actual vs. predicted values also generated similar results with a slope ranging from 0.96-0.98 respectively (±0.04 bounds for a 95% confidence interval for both transects), a correlation coefficient range of 0.95 to 0.97 respectively and a RMSE of 0.9-1.3% respectively. Finally, the comparisons of actual vs. predicted values at transect four had the lowest accuracy with a slope of 0.96 (±0.07 bounds for a 95% confidence interval), a correlation coefficient of 0.9 and a RMSE of 1.8%. While lower than the others, these values coupled with an F statistic of 774.3 and a T statistic of 27.8 indicate that a generalized SWE* equation could be used within the entire Sagehen Creek field area. The differences in SWE variance between actual transect measurements vs. predicted values identified areas of lower correlation between a generalized density multiplier and SD. These results suggest a lower correlation between generalized density and SD within the southern canopy-open area interface sample points. However, correlation between observed and predicted SD and SWE on all transects indicates that six Snowcloud nodes in tandem with snow density information from an onsite snow pillow was sufficient to accurately estimate SWE in the field area, despite large SD variances.

Throughout this site, these findings demonstrate the utility of a WSN that measures SD to effectively extend SWE information using SD at multiple locations around fixed based snow sensing equipment. The field wide variability also suggests that a single point measurement such as the onsite snow pillow or an individual Snowcloud node does not represent SWE for an area, especially one in which canopy cover varies significantly. Given

that most Snotel sites are located in open areas; this suggests that the information from a WSN could be very beneficial, especially if used as an input to spatially distributed simulations of SWE and annual stream outflow.

SWE equation for augmentation of RAWS sites

The final SWE* equation (SWE^*_{RAWS}) was able to predict SWE at the node points and along all transect points within the field area, but with reduced accuracy compared to the SWE* equations discussed above. The slope of the SWE^*_{RAWS} regression of actual vs. predicted values at the 6 nodes was 0.78 (±0.09 bounds for a 95% confidence interval) with a correlation coefficient of 0.89, a RMSE of 2.25%, a T statistic of 17.78 and an F statistic of 315.88. Like the $SWE^*_{general}$, this equation had the greatest predictive power along transect three, the lowest on transect four and performed reasonably well along transects one and two. Transect three comparisons of actual vs. predicted SWE gave a slope of 0.83 (±0.04 bounds for a 95% confidence interval), a correlation coefficient of 0.93 and a RMSE of 2.5%. Transect one and two ranged in slope, correlation coefficient and RMSE values from 0.77 (±0.06 bounds for a 95% confidence interval) – 0.78 (±0.08 bounds for a 95% confidence interval), 0.83- 0.88 and 1.9-2.2% respectively. Transect four had a slope of 0.72 (±0.10 bounds for a 95% confidence interval), a correlation coefficient of 0.72 and a RMSE of 2.7%.

Despite the lower accuracy of the SWE^*_{RAWS} equation compared with the $SWE^*_{general}$ equation, SWE could be estimated without onsite snow sensing equipment within the Sagehen Creek field area with a markedly high accuracy, based only on SD and site factors. This suggests the potential for SWE estimations within areas where SWE has not been measured on the ground. The ability to estimate SWE around meteorological stations without snow sensing equipment, even with a diminished accuracy, could greatly enhance areal estimations of SWE for water budget analyses. No previous research has evaluated

the potential for integrating WSN's with established meteorological sites without snow sensing equipment for the purpose of extrapolating SWE. There are currently 1,700 SWE measurement locations within the Western United States and there are about 2,200 RAWS sites within the United States (USFS, 2010). Adding SWE estimates to the suite of measurements obtained from RAWS sites could more than double the information about SWE within the United States, and increase the spatial representativeness of SWE for an area and reduce reliance on point based estimations for a fraction of the price of snow pillows and new Snotel sites. Excluding maintenance costs, the introduction of a 3 to 8 node Snowcloud system would range from 19- 50% the cost of a single snow pillow, without the supporting Snotel infrastructure.

These results suggest that it is feasible to model SWE* on a small scale, and that accuracy of SWE* estimates could be improved. The transect based comparisons lend insight into which areas within the Sagehen Creek field site may have been undersampled by the wireless sensor network. In this case and similar to the results of the $SWE^*_{general}$ predictions, transect four (transect four is located predominantly on the southern edge of the canopy- open area interface) provided the lowest accuracy of estimation. The addition of sensor nodes within this zone of the field area could greatly increase the resolution of the SWE^*_{RAWS} output estimations.

Data interpolation

It was initially unclear whether kriging was appropriate for spatial analysis of SD and SWE from only 6 points (the Snowcloud nodes). However, the generalized SD and SWE variograms provided an accurate representation of the field-wide variability and gave accurate kriged model outputs of SWE and SD. Kriging animations allowed for visualization of spatial and temporal trends. They effectively demonstrated the snow accumulation and

ablation dynamics of the Sagehen Creek field site. Python scripting reduced the time involved for manual kriging at each time step.

The generalized SD and SWE variograms were sufficient to supply general nugget, range, and sill values for the kriged data sets. The maximum and averaged kriged SWE values were similar to the observed maximum and average values from the manual SWE sampling data set. However, the minimum kriged values were higher than the minimum observed values.

The average difference between maximum kriged SWE estimates and maximum observed SWE measurements at all sample point locations was 1.25 inches (standard deviation of 0.89) with a minimum of 0.17 inches (standard deviation of 0.12) to a maximum of 2.7 inches of SWE (standard deviation of 1.9). The average difference between the mean kriged SWE estimates and observed SWE measurements at the sample point locations ranged an average of 1.95 inches (standard deviation of 1.38) with a minimum of 0.19 inches (standard deviation of 0.13) and a maximum of 3.06 inches (standard deviation of 2.16). See figure 46.

While these kriging estimates are not exact, this technique allowed reasonable approximations at all areas within the field area. The kriging process was performed using only the six node Snowcloud generated field data. It is possible that with the addition of more nodes the increased resolution of the initial variogram analysis would increase the kriged raster output accuracy.

The visualization of snow dynamics within a field site also lends insight into identifying under- and over-sampled areas. These animations can also be used for an analysis of both node placement and number of nodes needed per site in order to increase the spatial representativeness of SWE for an area.

Data comparison

The snow pillow within the field area was not representative of average areal SWE values (average kriged SWE values). If the data are compared to the kriging interpolation the snow pillow provides an overestimate of SWE within the field area by an average of 2.58 inches (18.4 % overestimate) with a maximum of 5.1 inches (37% overestimate) of SWE from the 18th of January to March 31st 2010.

In fact, this estimation is most likely conservative for the season. If the snow pillow is compared to the average manual transect SWE values, the snow pillow overestimated SWE within the field area an average of 4.12 inches (30% overestimate) with a maximum overestimation of 5.8 inches (40% overestimate). The maximum overestimation of this field site alone would account for an overestimation of 43500 ft^3 or ~1 acre foot of water.

The snow pillow measurements corresponded most closely to both the maximum observed SWE measurements and the maximum kriged SWE estimates, demonstrating that the snow pillow placement is in an area representative of maximum SWE, not average SWE. The snow pillow measurements differed from maximum kriging interpolation has an average absolute error of 0.35 or 1% error (standard deviation of 0.24) with a maximum of 0.98 or 12 % error and a minimum absolute error of 0 inches.

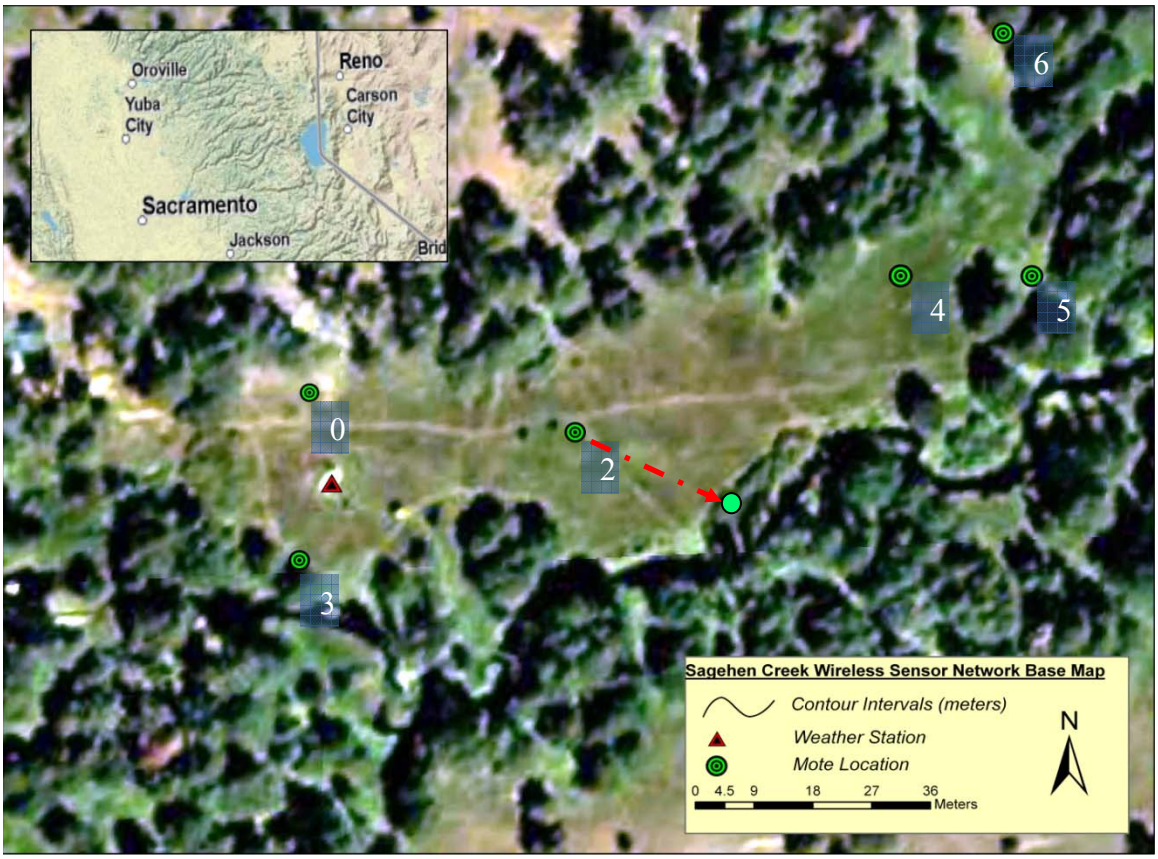

Figure 51: The field area and location of nodes within the Sagehen Creek Experimental Field Station. The red dotted line shows the preferred placement of Snowcloud node 2 for increased SWE* estimation potential.

Despite accurate SWE* estimations within the field area, the regression and kriging analysis could have been improved by either increasing the number of Snowcloud nodes, or changing the location of nodes. Specifically, the SWE* regression equations demonstrated that transect four was undersampled, due to reduced accuracy of the SWE* equations (SWE^*_{RAWS}, SWE^*_{Snotel}, $SWE^*_{General}$) on this transect. Transect four was located in an area predominantly on the southern edge of the canopy-open area interface (figure 9). In comparison, transect three provided SWE* estimates most similar to observed SWE. This transect was located in a predominantly canopy-free zone within a large open meadow, similar to the area surrounding the onsite snow pillow. Two Snowcloud nodes were also situated within this area (transect three). It is possible that relocation of one Snowcloud node from this canopy regime (area surrounding transect three) into the southern edge of

the canopy open area interface regime seen on the majority of transect four could increase areal and point-based SWE* estimations while maintaining a high level of SWE* estimation accuracy on transect three. Figure 51 shows the previous Snowcloud node placement, and shows the recomended movement of Node 2 south from transect three to the southern edge of the open area canopy interface on transect four.

Future study

This pilot study applied statistical techniques to evaluate the utility of WSN's for meteorological station augmentations. This approach could be expanded upon to develop guidelines for WSN deployment. This study was limited in scope by the number of available Snowcloud nodes, the field area and duration. An extension to several seasons of study and larger field areas would allow for development of a protocol and to answer several key questions about factors important for establishing WSN's around meteorological stations, with and without snow sensing equipment. These include, the maximum allowable node placement distance from meteorological stations which would determine the maximum area SWE can accurately be extrapolated from WSN's and a local meteorological station, the appropriate placement of nodes around meteorological stations and the minimum number of nodes needed to best estimate SWE on an areal basis.

Also, multiyear data sets could increase accuracy of SWE estimates. Significant predictors of SWE* may not be properly characterized or found from the analysis of a single year data set (Erickson, etal., 2005). Multiyear SWE variation should be accounted for to apply SWE* equations with WSN platforms within any field area.

The small field area within Sagehen Creek did not allow for all topographic variables to be properly characterized with respect to SD and SWE. The majority of the field was either flat or less than 10% in slope. Slope and slope with respect to aspect have previously

been used as predictors of SWE and SD (Anderton, et al., 2004, Cline, et al., 1998, Elder, et al., 1991, Erickson, et al., 2005, Golding et al., 1986, Jost, et al., 2007, Molotch, et al., 2005). The inclusion of these factors could enhance SWE predictions from basic WSN measurements in all topographic conditions. It is currently unclear how Snowcloud and other networks would perform in areas with large slopes. More research should be dedicated to analysis of SWE extrapolation under all topographic conditions.

Conclusion

At the Sagehen Creek field site, neither the onsite snow pillow nor the manual snow course transects represented the spatial mean of SWE in the field area. The snow pillow overestimated SWE values an average of 30% with a maximum overestimation of 40%.

Data from six Snowcloud SD measurement nodes in conjunction with regression and kriging effectively captured the spatial and temporal variability of SWE within the field site. The Snowcloud nodes were tested to extrapolate SWE from SD around a meteorological station (1) with snow sensing equipment and (2) without snow sensing equipment. Both techniques accurately estimated SWE at the node sites and at all points along a 4 by 12 sampling grid which uniformly covered the 0.77 ha site, with a maximum RMSE of 2.7%. A general density multiplier was used solely with SD for SWE* prediction around meteorological stations with snow sensing equipment and predicted SWE* with greater accuracy than using state variables from tower one and site characterizations (RMSE of 1.2%).

Aspect with percent canopy closure pairings was an important predictor of SWE* at meteorological stations without snow sensing equipment, much more so than generalized canopy closure. The prediction accuracy of the best model was not increased by the addition of a generalized canopy closure qualifier. Within the prediction equation (SWE^*_{RAWS}), percent canopy closure to the north held equal importance with SD for SWE*prediction. Both qualifiers maintained an equivalent P value of 0.000+ within the SWE^*_{RAWS} equation.

The ability to sense SD under canopy and at the canopy – open area interface could supplement data acquired by satellite and aerial imagery sensing platforms. These remote

sensing techniques allow for SD sensing only in canopy-free areas. While the utility of satellite and areal sensing over large areas at high resolutions is clearly valuable, these methods cannot capture much of the snow variability in terrestrial systems with mixed cover. Within Sagehen Creek, the maximum snow variability was seen under canopy and at the canopy-open area interface where the both the minima and maxima of snow depth were sensed, along with the slowest and fastest ablation rates.

Wireless snow depth sensors should be used to augment existing meteorological stations with and without snow sensing equipment to increase potential SD and SWE measurement points and reduce the influence of point-based biases on a watershed scale. The incorporation of these devices has the ability to revolutionize current SWE estimation techniques with start up costs considerably lower than current technology (A three to eight node Snowcloud system would range from 19- 50% the cost of a single snow pillow). Satellite and other remotely sensed data paired with WSN's could reduce major sensing deficiencies under canopy and at the open area- canopy interface. Furthermore, accurate estimations of SWE around meteorological stations without snow sensing equipment would increase potential SWE estimation resolution within runoff models and could more than double the number of sites that provide SWE information in the Western United States. Increased areal and point SWE estimations are integral for increased water runoff forecasting resolution in both normal precipitation years and in years that deviate from the historical mean for precipitation.

References

Anderton SP, White SM, Alvera B (2004) Evaluation of spatial variability in snow water equivalent for a high mountain catchment. Hydrological Processes 18: 435-453

Carr JR (2002) Data visualization in the geological sciences. Prentice Hall, Upper Saddle River, NJ

Clark I (1979) Applied geostatistics. Elsevier Applied Science Publishers, London, UK

Cline DW, Bales RC, Dozier J (1998) Estimating the spatial distribution of snow in mountain basins using remote sensing and energy balance modeling. Water Resources Research 34: 1275-1285

Elder K, Dozier J, Michaelsen J (1991) Snow accumulation and dstribution in an alpine watershed. Water Resources Research 27: 1541-1552

Elder K, Rosenthal W, Davis RE (1998) Estimating the spatial distribution of snow water equivalence in a montane watershed. Hydrological Processes 12: 1793-1808

Erickson TA, Williams MW, Winstral A (2005) Persistence of topographic controls on the spatial distribution of snow in rugged mountain terrain, Colorado, United States. Water Resources Research 41

ESRI (2010) Using kriging in 3D analyst. ArcGIS online manual http://resources.esri.com/help/9.3/arcgisdesktop/com/gp_toolref/geoprocessing_with_3d_analyst/using_kriging_in_3d_analyst.htm. last accessed July, 2010

Fiala ACS, Garman SL, Gray AN (2006) Comparison of five canopy cover estimation techniques in the western Oregon Cascades. Forest Ecology and Management 232: 188-197

Golding DL, Swanson RH (1986) snow distribution patterns in clearings and adjacent forest. Water Resources Research 22: 1931-1940

Haenselmann T (2005) Sensor networks. online book, http://pi4.informatik.uni-mannheim.de/~haensel/sn_book/, last accessed October, 2010

Hydrologic Engineering Center (2010) Hydrologic modeling system manual. http://www.hec.usace.army.mil/software/hec-hms/ last accessed August, 2010

Jindal A, Psounis K (2006) Modeling spatially correlated data in sensor networks. ACM Transactions on Sensor Networks 2

Jonas T, Marty C, Magnusson J (2009) Estimating the snow water equivalent from snow depth measurements in the Swiss Alps. Journal of Hydrology 378: 161-167

Jost G, Weiler M, Gluns DR, Alila Y (2007) The influence of forest and topography on snow accumulation and melt at the watershed-scale. Journal of Hydrology 347: 101-115

Judd Communications (2010) Judd Communications online manual. http://wwwjuddcomcom/ds2manualpdf. last accessed July, 2010

Korhonen L, Korhonen KT, Rautiainen M, Stenberg P (2006) Estimation of forest canopy cover: A comparison of field measurement techniques. Silva Fennica 40: 577-588

Leavesley GH, Lichty, R.W., Troutman, B.M., Saindon, L.G. (1983) Precipitation-runoff modeling system: user's manual. US Gelogical Survey Water Resources investigations report 83-4238, pp. 207

Lundquist JD, Cayan DR, Dettinger MD (2003) Meteorology and hydrology in yosemite national park: A sensor network application. Information Processing in Sensor Networks, Proceedings 2634: 518-528

Molotch NP, Colee MT, Bales RC, Dozier J (2005) Estimating the spatial distribution of snow water equivalent in an alpine basin using binary regression tree models: the impact of digital elevation data and independent variable selection. Hydrological Processes 19: 1459-1479

Musselman KN, Molotch NP, Brooks PD (2008) Effects of vegetation on snow accumulation and ablation in a mid-latitude sub-alpine forest. Hydrological Processes 22: 2767-2776

NSIDC (National Snow and Ice Data Center) (2004) snow data assimilation center (SNODAS) data products page. http://nsidc.org/data/g02158.html. last accessed August, 2010

Nagpaul PS (1999) Guide to advanced data analysis using IDAMS sofware. http://www.unesco.org/webworld/idams/advguide/TOC.htm. last accessed July, 2010

NRCS (Natural Resources Conservation Service) (2010) Snowcourses. www.wcc.nrcs.usda.gov/snowcourse/. last acccessed January, 2010.

PRISM (Parameter-elevation Regresions on Independent Slopes Model) Climate Group (2010) PRSIM information page. http://www.prism.oregonstate.edu/. last accessed August, 2010

Rice R, R.C. Bales. (2010) Embedded Sensor Network Design fo Snowcover Measurements around Snow-Pillow and Snow-Course Sites in The Sierra Nevada of California. Water Resources Research 46

Ryan WA, Doesken NJ, Fassnacht SR (2008) Evaluation of ultrasonic snow depth sensors for U.S. snow measurements. Journal of Atmospheric and Oceanic Technology 25: 667-684

Ryan WA, Doesken NJ, Fassnacht SR (2008) Preliminary results of ultrasonic snow depth sensor testing for National Weather Service (NWS) snow measurements in the US. Hydrological Processes 22: 2748-2757

Shi JC, Dozier J (2000) Estimation of snow water equivalence using SIR-C/X-SAR, part II: Inferring snow depth and particle size. Ieee Transactions on Geoscience and Remote Sensing 38: 2475-2488

Sommer Mess (2010) - Systemtecknik Hydrologie www.sommer.at/en/home.html. last accessed January, 2010

EPA (2010) National Environmental Monitoring Initiative http://www.epa.gov/cludygxb/. last accessed July, 2010

RAWS (Remote Automated Weather Stations) (2010) Remote Automated Weather Stationsinformation page. http://www.fs.fed.us/raws/. last accessed July, 2010

Veatch W, Brooks PD, Gustafson JR, Molotch NP (2009) 'Quantifying the effects of forest canopy cover on net snow accumulation at a continental, mid-latitude site. Ecohydrology 2: 115-128

Woods SW, Ahl R, Sappington J, McCaughey W (2006) Snow accumulation in thinned lodgepole pine stands, Montana, USA. Forest Ecology and Management 235: 202-211

Appendix A: Snowcloud calibration data

Snowcloud calibration constants for calibration trials

Node 1

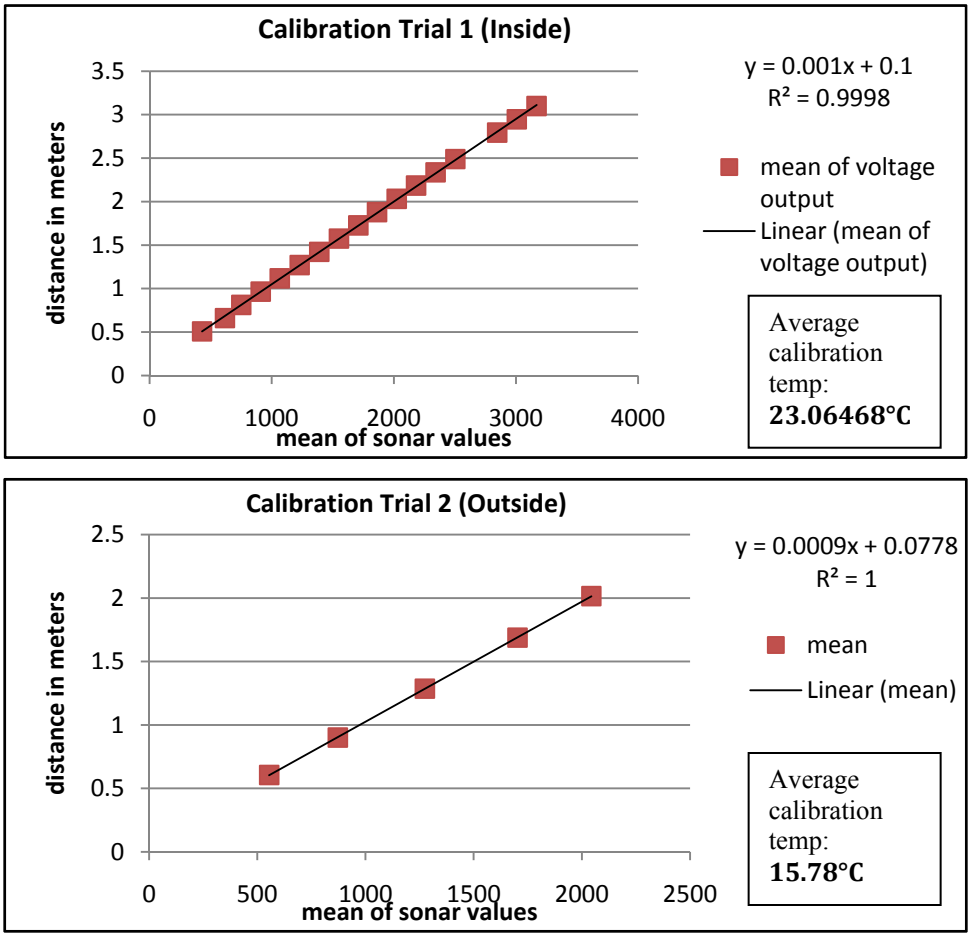

Figure 52: Regression of sonar mean values vs. distance of sonar emitter for calibration equation input.

$$SD_{cal\ trial\ one} = 2.241 - \left\{\left[\frac{\mathrm{Vr}}{\mathrm{Vr} * \sqrt{1 + \frac{\bar{T}}{278.15}}}{0.001\mathrm{Vr} + 0.1}\right]\left(331.3\sqrt{1 + \frac{\bar{T}}{278.15}}\right)\right\}$$

$$SD_{cal\ trial\ two} = 2.291 - \left\{\left[\frac{\mathrm{Vr}}{\mathrm{Vr} * \sqrt{1 + \frac{\bar{T}}{278.15}}}{0.0009\mathrm{Vr} + 0.0778}\right]\left(331.3\sqrt{1 + \frac{\bar{T}}{278.15}}\right)\right\}$$

Node 2

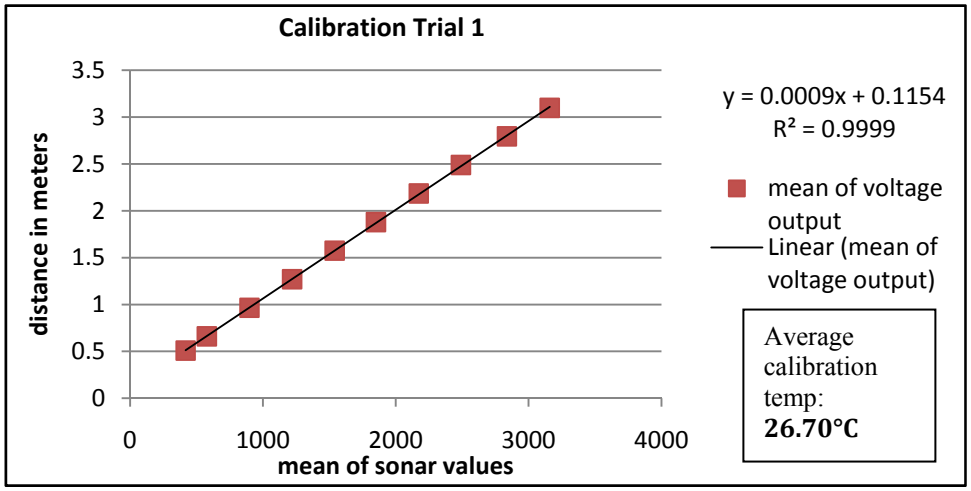

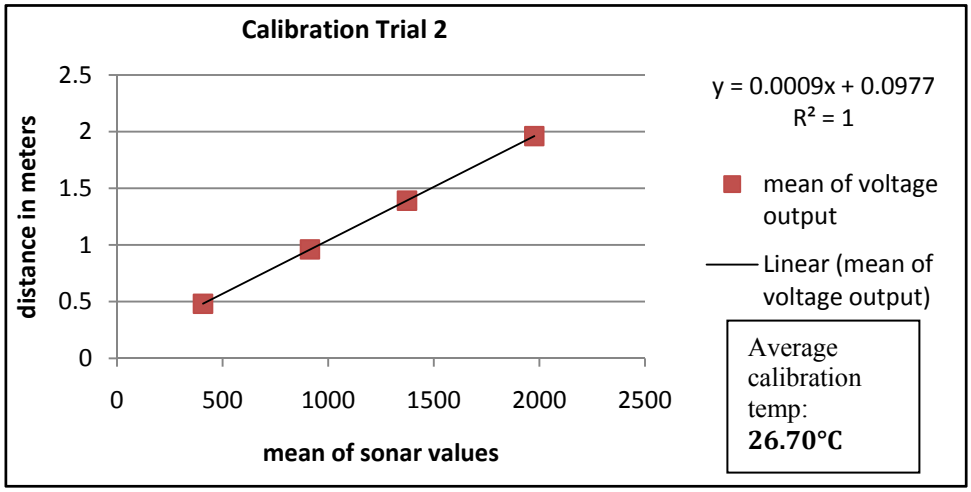

Figure 53: Regression of sonar mean values vs. distance of sonar emitter for calibration equation input.

$$SD_{cal\ trial\ one} = 2.299 - \left\{\left[\frac{\mathrm{Vr}}{\mathrm{Vr} * \sqrt{1 + \frac{\bar{T}}{278.15}}}{0.0009\mathrm{Vr} + 0.1154}\right]\left(331.3\sqrt{1 + \frac{\bar{T}}{278.15}}\right)\right\}$$

$$SD_{cal\ trial\ two} = 2.271 - \left\{\left[\frac{\mathrm{Vr}}{\mathrm{Vr} * \sqrt{1 + \frac{\bar{T}}{278.15}}}{0.00009\mathrm{Vr} + 0.0977}\right]\left(331.3\sqrt{1 + \frac{\bar{T}}{278.15}}\right)\right\}$$

Node 3

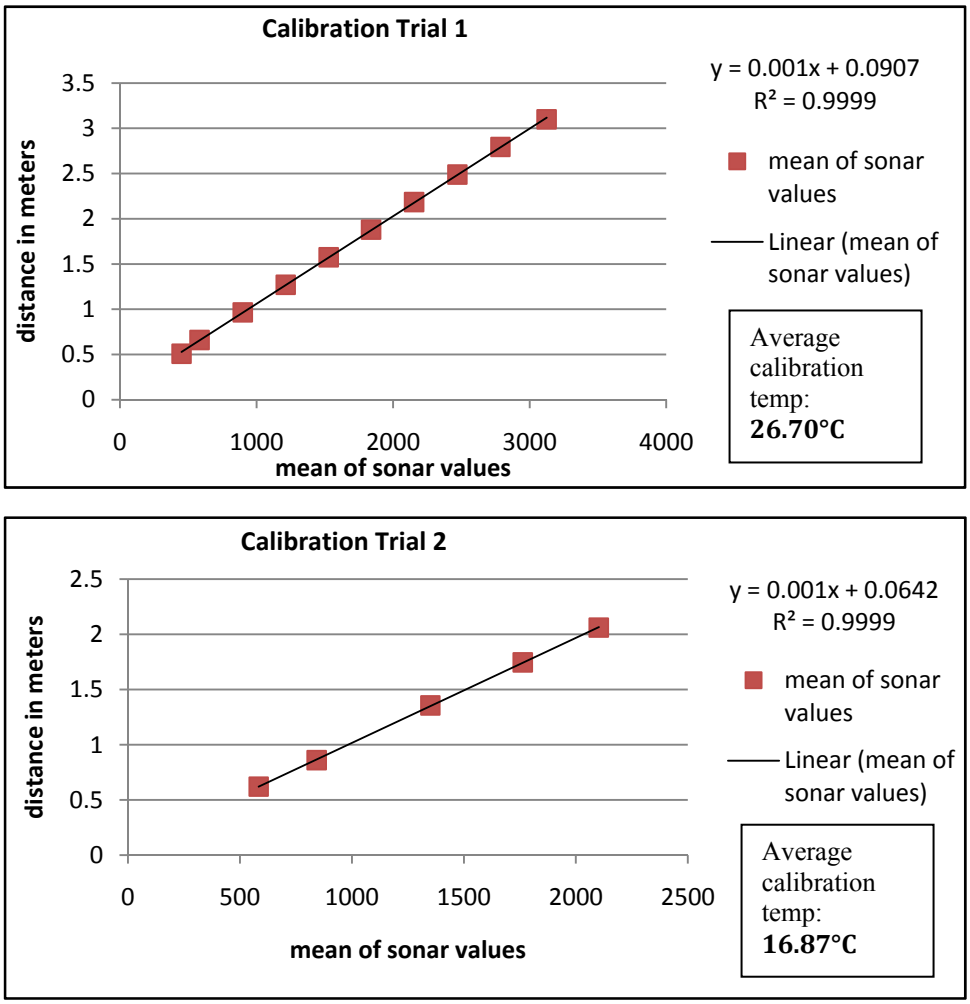

Figure 54: Regression of sonar mean values vs. distance of sonar emitter for calibration equation input.

$$SD_{cal\ trial\ one} = 2.217 - \left\{\left[\frac{\mathrm{Vr}}{\dfrac{\mathrm{Vr} * \sqrt{1 + \dfrac{\overline{T}}{278.15}}}{0.001\mathrm{Vr} + 0.0907}}\right]\left(331.3\sqrt{1 + \frac{\overline{T}}{278.15}}\right)\right\}$$

$$SD_{cal\ trial\ two} = 2.217 - \left\{\left[\frac{\mathrm{Vr}}{\dfrac{\mathrm{Vr} * \sqrt{1 + \dfrac{\overline{T}}{278.15}}}{0.001\mathrm{Vr} + 0.0642}}\right]\left(331.3\sqrt{1 + \frac{\overline{T}}{278.15}}\right)\right\}$$

Node 4

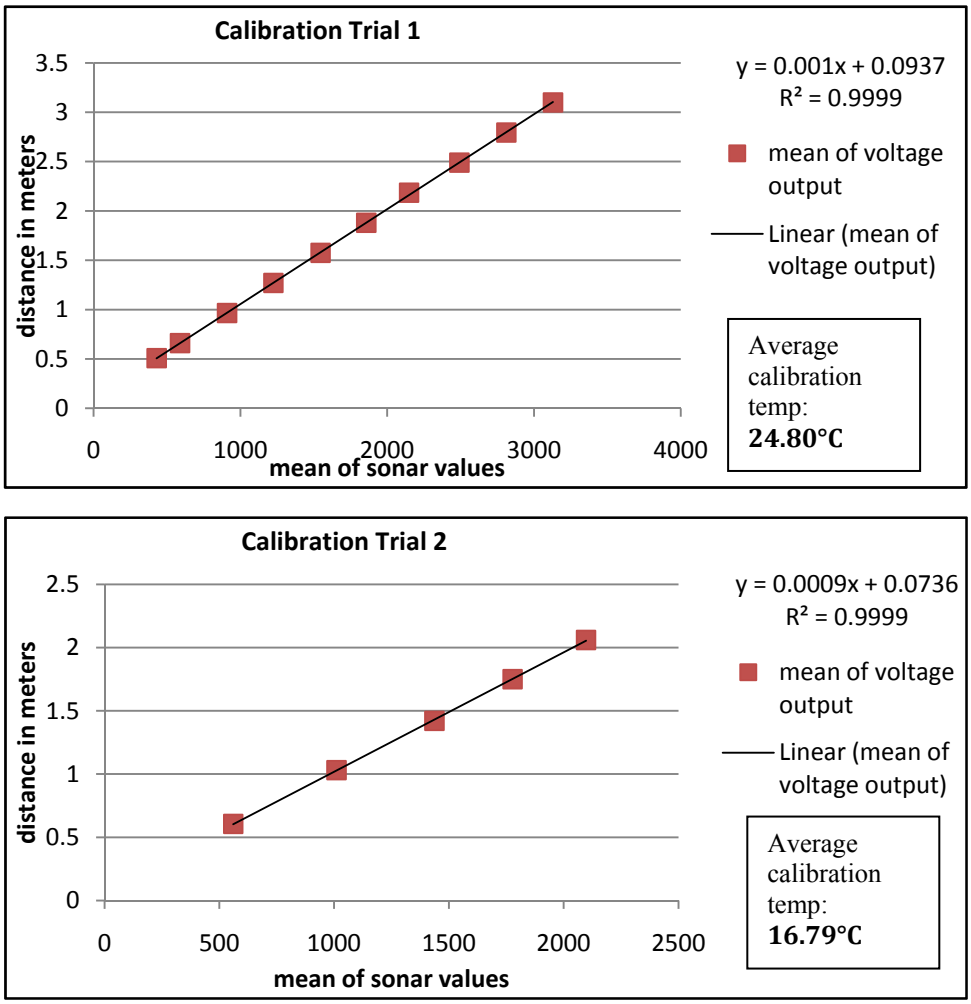

Figure 55: Regression of sonar mean values vs. distance of sonar emitter for calibration equation input.

$$SD_{cal\ trial\ one} = 2.216 - \left\{\left[\frac{\mathrm{Vr}}{\mathrm{Vr} * \sqrt{1 + \frac{\overline{T}}{278.15}}}{0.001\mathrm{Vr} + 0.0937}\right]\left(331.3\sqrt{1 + \frac{\overline{T}}{278.15}}\right)\right\}$$

$$SD_{cal\ trial\ two} = 2.211 - \left\{\left[\frac{\mathrm{Vr}}{\mathrm{Vr} * \sqrt{1 + \frac{\overline{T}}{278.15}}}{0.0009\mathrm{Vr} + 0.0736}\right]\left(331.3\sqrt{1 + \frac{\overline{T}}{278.15}}\right)\right\}$$

Node 5

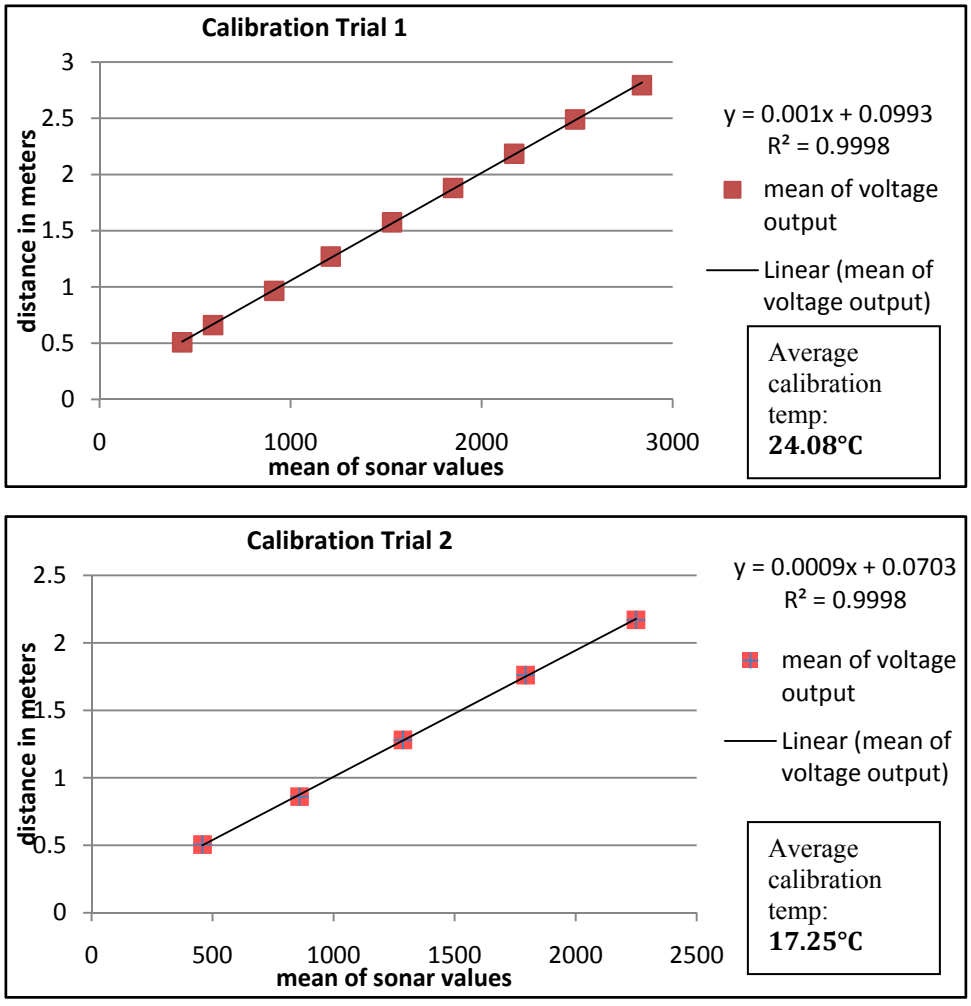

Figure 56: Regression of sonar mean values vs. distance of sonar emitter for calibration equation input.

$$SD_{cal\ trial\ one} = 2.256 - \left\{\left[\frac{\mathrm{Vr}}{\mathrm{Vr} * \sqrt{1 + \frac{\overline{T}}{278.15}}}{0.001\mathrm{Vr} + 0.0993}\right]\left(331.3\sqrt{1 + \frac{\overline{T}}{278.15}}\right)\right\}$$

$$SD_{cal\ trial\ one} = 2.271 - \left\{\left[\frac{\mathrm{Vr}}{\mathrm{Vr} * \sqrt{1 + \frac{\overline{T}}{278.15}}}{0.0009\mathrm{Vr} + 0.0703}\right]\left(331.3\sqrt{1 + \frac{\overline{T}}{278.15}}\right)\right\}$$

Node 6

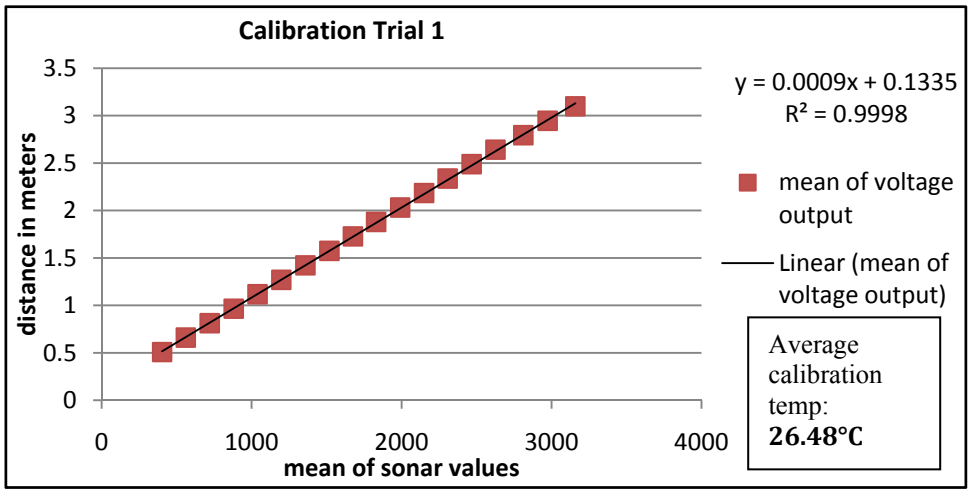

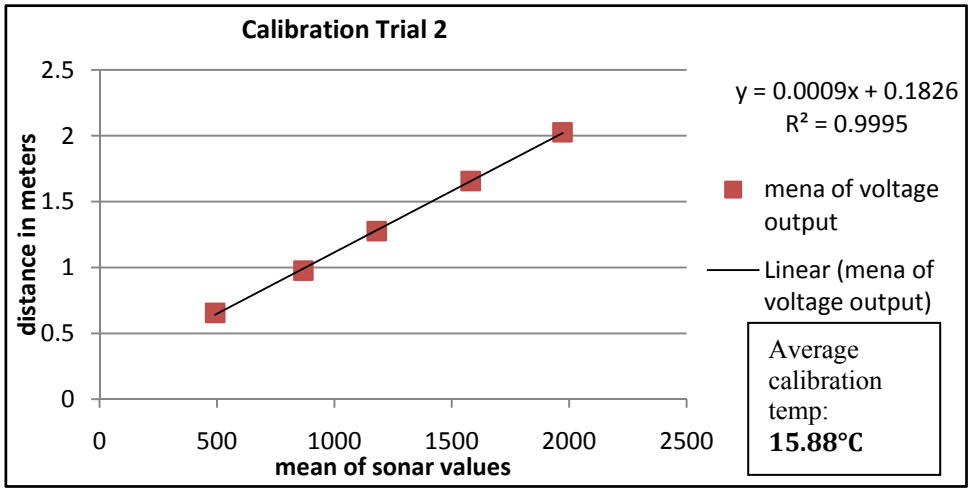

Figure 57: Regression of sonar mean values vs. distance of sonar emitter for calibration equation input.

$$T_{c\ sonar\ one} = 2.285 - \left\{\left[\frac{\mathrm{Vr}}{\mathrm{Vr} * \sqrt{1 + \frac{\overline{T}}{278.15}}}{0.0009\mathrm{Vr} + 0.1335}\right]\left(331.3\sqrt{1 + \frac{\overline{T}}{278.15}}\right)\right\}$$

$$T_{c\ sonar\ two} = 2.321 - \left\{\left[\frac{\mathrm{Vr}}{\mathrm{Vr} * \sqrt{1 + \frac{\overline{T}}{278.15}}}{0.0009\mathrm{Vr} + 0.1836}\right]\left(331.3\sqrt{1 + \frac{\overline{T}}{278.15}}\right)\right\}$$

Manual SD and snow surface to sonar measurements

Manual snow depth measurements in inches

nodes	18-Jan	26-Jan	2-Feb	9-Feb	18-Feb	23-Feb	3-Mar	9-Mar
1	17.32	35.82	29.52	28.74	20.07	19.68	30.70	22.44
2	24.40	46.85	39.37	35.43	35.43	35.43	39.76	39.76
3	28.74	35.82	39.37	42.51	35.43	39.37	51.96	42.91
4	18.89	25.19	31.10	33.07	25.98	26.77	41.33	31.49
5	4.72	12.40	11.81	9.84	5.11	3.14	8.66	4.52
6	13.38	26.77	23.22	16.53	24.40	21.25	32.67	25.59

nodes	16-Mar	23-Mar	29-Mar	6-Apr	13-Apr	19-Apr	26-Apr
1	22.44	9.44	0	5.12	0	0	0
2	39.76	31.49	26.37	39.37	26.37	11.02	0
3	45.27	40.55	24.40	41.33	44.09	36.22	27.55
4	28.74	20.27	3.93	20.07	0	0	0
5	7.08	0	0	11.81	0	0	0
6	28.34	21.25	16.53	14.17	18.89	12.20	2.75

Table 5: Manual measurements of snow depth underneath each sonar emitter.

Manual snow surface to sonar measurements in inches

nodes	18-Jan	26-Jan	2-Feb	9-Feb	18-Feb	23-Feb	3-Mar	9-Mar
1	70.47	51.97	58.66	59.06	67.32	68.11	61.02	65.35
2	57.87	40.94	47.64	44.49	52.36	52.36	47.64	46.85
3	60.63	44.49	50.39	46.85	51.97	50.79	37.01	42.91
4	60.63	47.24	54.33	52.36	59.06	61.02	48.03	55.12
5	81.89	74.80	76.77	76.77	82.68	82.68	78.74	81.89
6	74.02	58.66	62.20	60.63	65.75	66.14	59.06	62.20

nodes	16-Mar	23-Mar	29-Mar	6-Apr	13-Apr	19-Apr	26-Apr
1	66.14	78.74	88.19	74.41	88.19	88.19	88.19
2	44.09	56.30	64.96	48.03	61.81	76.38	87.40
3	39.37	47.24	51.18	34.25	44.09	54.72	62.60
4	56.30	68.90	80.31	66.14	85.04	85.04	85.04
5	81.50	86.61	87.40	75.20	87.40	87.40	87.40
6	62.20	70.47	75.59	62.20	71.65	78.35	86.61

Table 6: Manual measurements of ground surface to sonar measurements underneath each sonar emitter.

Comparison of generated and manual SD and S-S values

Node 1

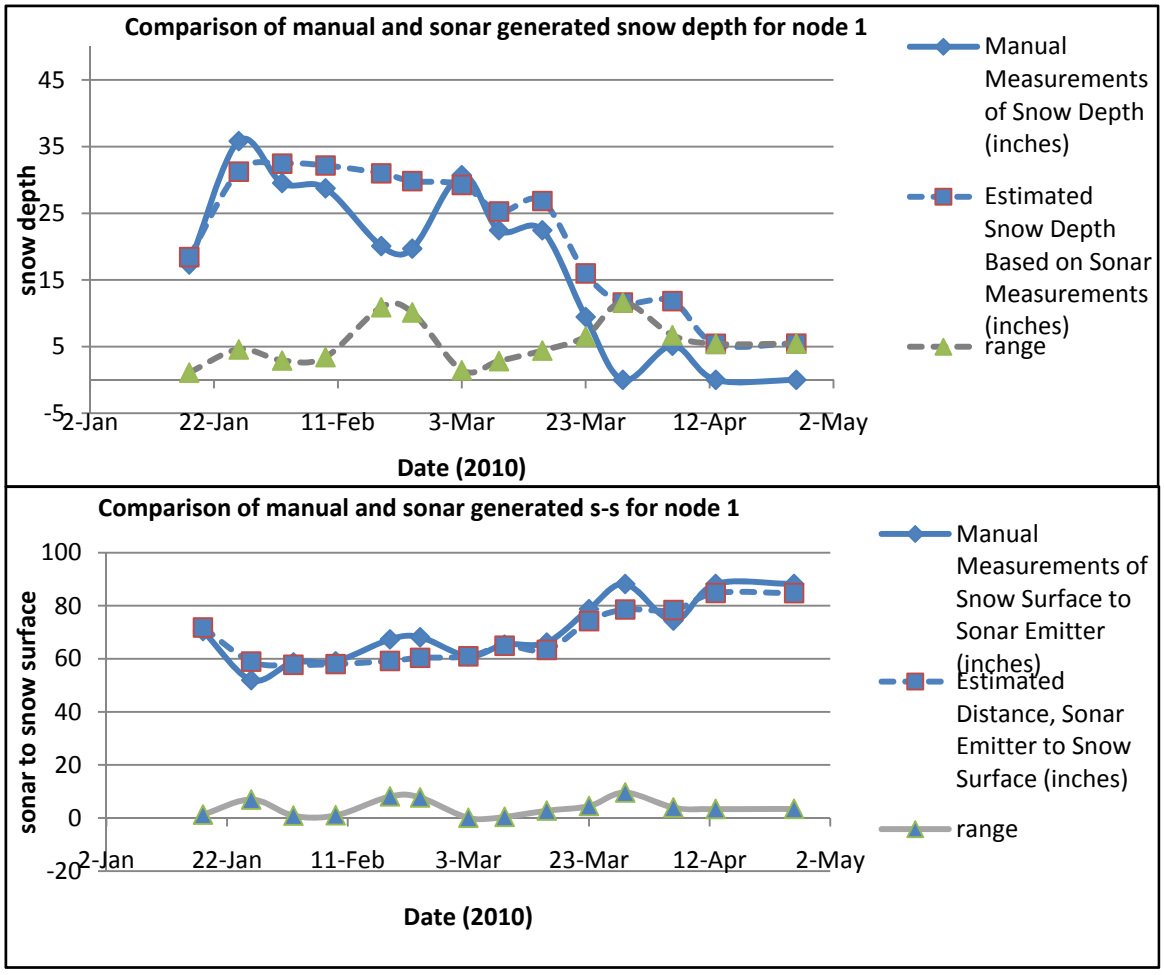

Figure 58: Comparison of manual vs. Snowcloud generated snow depth and s-s for node 1.

Statistics comparing manual to sonar snow depth (inch)	18-Jan	26-Jan	2-Feb	9-Feb	18-Feb	23-Feb	3-Mar	9-Mar	16-Mar	23-Mar	29-Mar	6-Apr	13-Apr	26-Apr
Mean	17.9	33.5	31.0	30.5	25.5	24.8	30.0	23.9	24.6	12.7	5.8	8.5	2.7	2.7
Standard Error	0.55	2.29	1.46	1.71	5.46	5.07	0.73	1.41	2.20	3.27	5.81	3.35	2.71	2.73
Standard Deviation	0.78	3.24	2.06	2.43	7.72	7.17	1.03	2.00	3.11	4.62	8.22	4.74	3.83	3.85
Sample Variance	0.60	10.4	4.24	5.88	59.5	51.3	1.06	4.00	9.68	21.3	67.5	22.4	14.6	14.8
Range	1.10	4.58	2.91	3.43	10.91	10.13	1.46	2.83	4.40	6.53	11.62	6.70	5.41	5.45

Table 7: Descriptive statistics comparing observed SD vs. Snowcloud generated SD (in) node 1.

Node 2

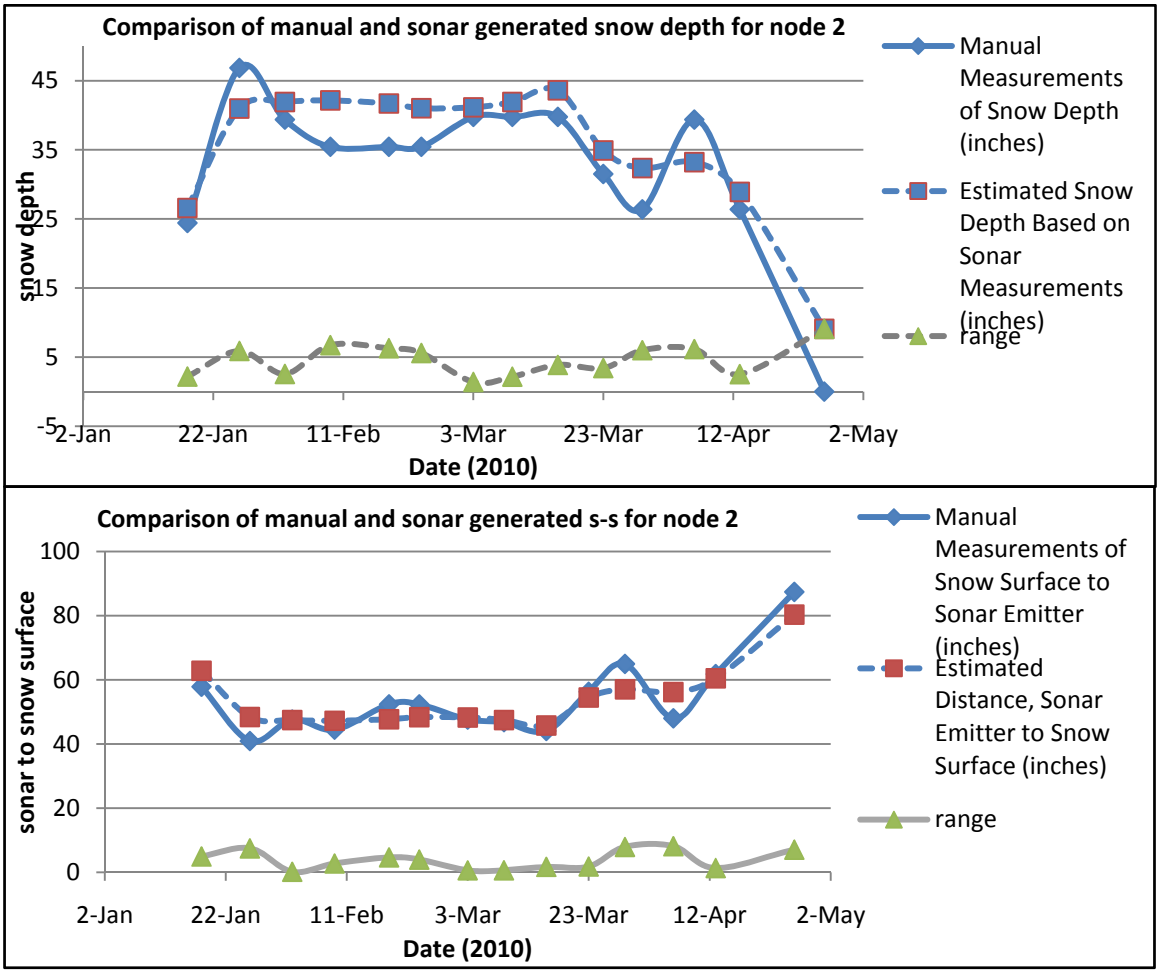

Figure59: Comparison of manual vs. Snowcloud generated snow depth and s-s for node 2.

statistics comparing manual to sonar snow depth (inch)	*18-Jan*	*26-Jan*	*2-Feb*	*9-Feb*	*18-Feb*	*23-Feb*	*3-Mar*	*9-Mar*	*16-Mar*	*23-Mar*	*29-Mar*	*6-Apr*	*13-Apr*	*26-Apr*
Mean	25.4	43.9	40.6	38.8	38.6	38.2	40.5	40.8	41.7	33.2	29.4	36.3	27.6	4.54
Standard Error	1.09	2.94	1.27	3.36	3.13	2.79	0.69	1.08	1.93	1.70	2.99	3.08	1.27	4.54
Standard Deviation	1.53	4.16	1.80	4.75	4.43	3.95	0.98	1.52	2.73	2.41	4.23	4.35	1.79	6.42
Sample Variance	2.36	17.3	3.25	22.6	19.6	15.6	0.96	2.32	7.44	5.79	17.9	18.9	3.21	41.2
Range	2.17	5.88	2.55	6.72	6.27	5.59	1.39	2.16	3.86	3.40	5.98	6.15	2.53	9.08

Table 8: Descriptive statistics comparing observed SD vs. Snowcloud generated SD (in) node 2.

Node 3

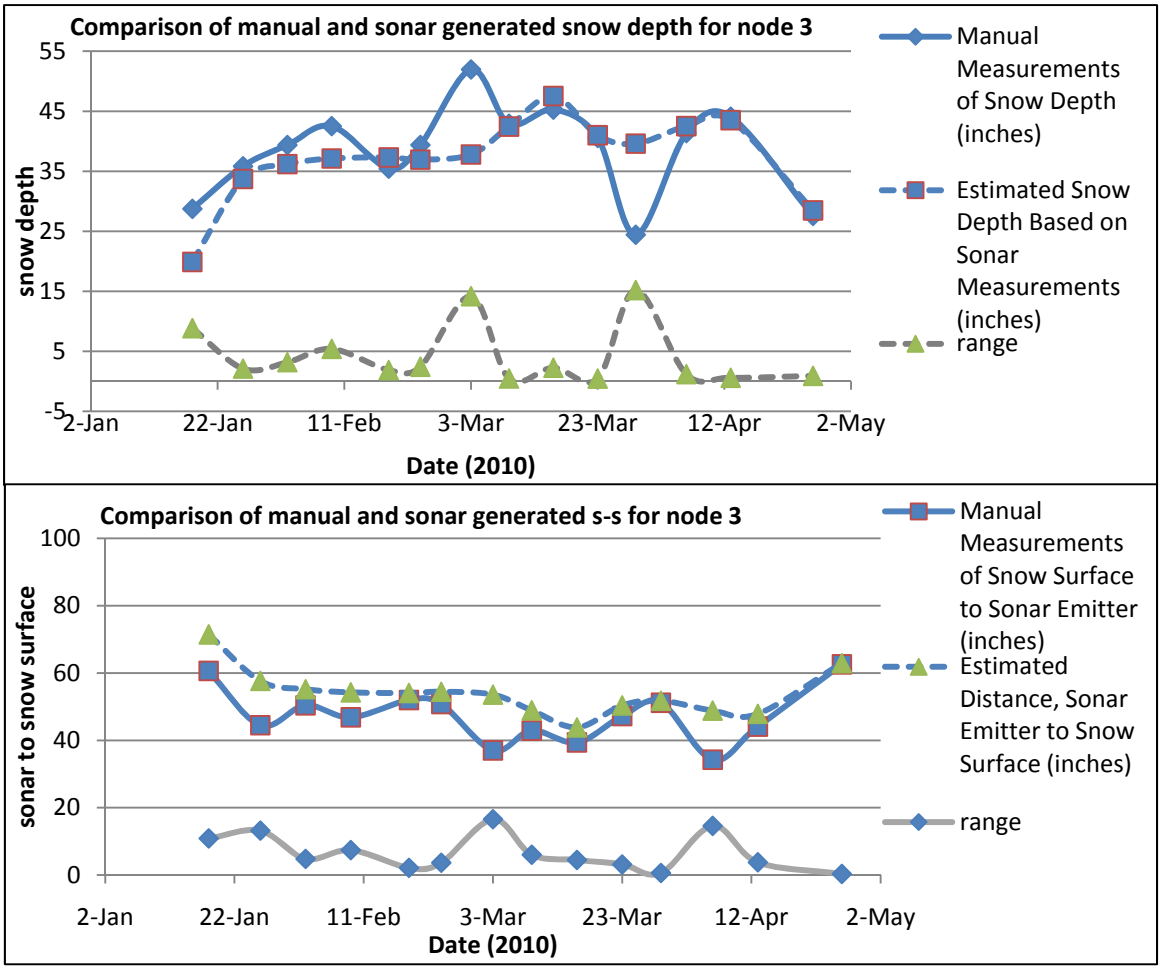

Figure 60: Comparison of manual vs. Snowcloud generated snow depth and s-s for node 3.

statistics comparing manual to sonar snow depth (inch)	*18-Jan*	*26-Jan*	*2-Feb*	*9-Feb*	*18-Feb*	*23-Feb*	*3-Mar*	*9-Mar*	*16-Mar*	*23-Mar*	*29-Mar*	*6-Apr*	*13-Apr*	*26-Apr*
Mean	24.3	34.8	37.8	39.8	36.4	38.2	44.9	42.7	46.4	40.8	32.0	41.9	43.8	28.0
Standard Error	4.43	1.06	1.59	2.70	0.93	1.22	7.09	0.23	1.13	0.22	7.60	0.60	0.29	0.46
Standard Deviation	6.26	1.50	2.25	3.82	1.31	1.72	10.0	0.33	1.59	0.32	10.7	0.84	0.41	0.64
Sample Variance	39.2	2.24	5.06	14.6	1.72	2.95	100.	0.11	2.54	0.10	115.	0.71	0.17	0.41
Range	8.85	2.12	3.18	5.40	1.86	2.43	14.2	0.46	2.25	0.45	15.2	1.19	0.58	0.91

Table 9: Descriptive statistics comparing observed SD vs. Snowcloud generated SD (in) node 3.

Node 4

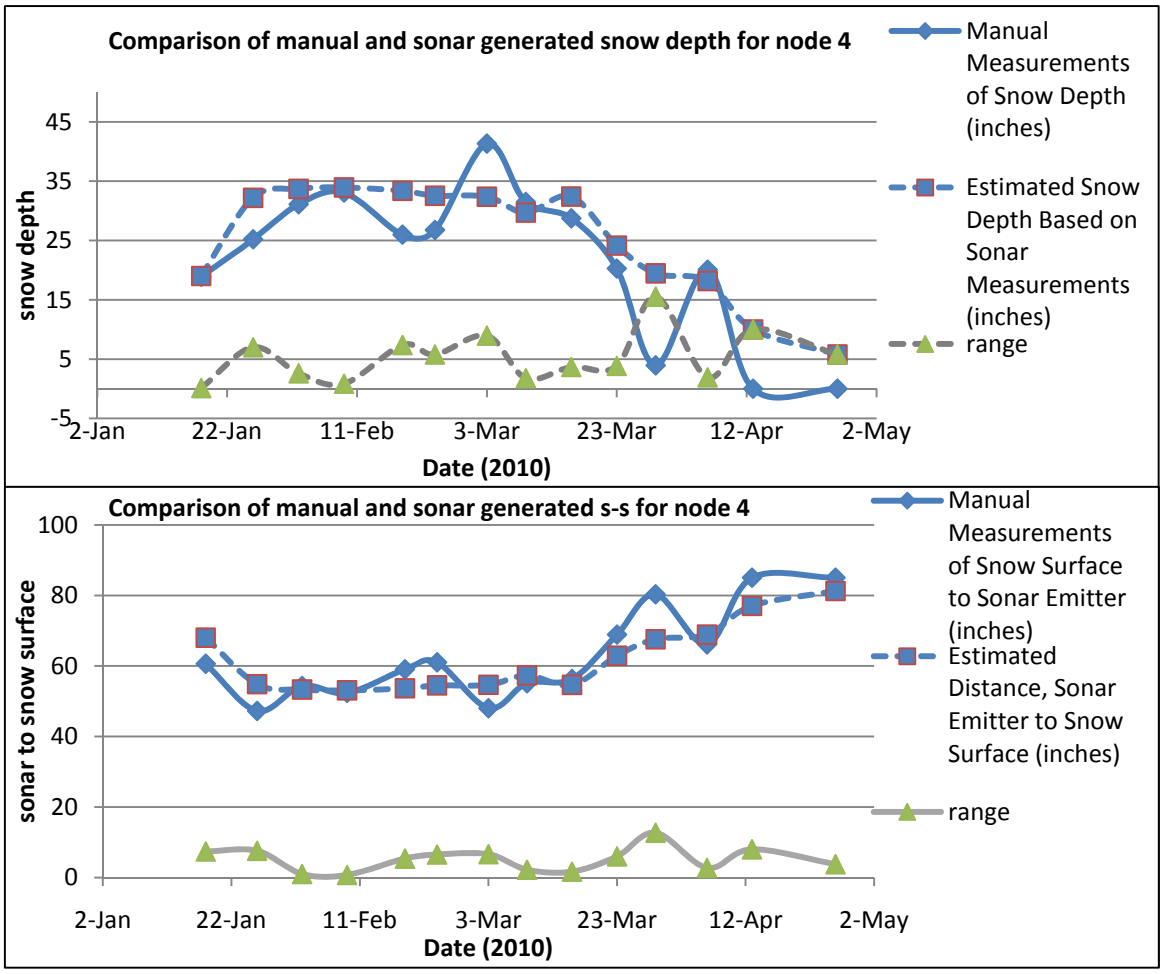

Figure 61: Comparison of manual vs. Snowcloud generated snow depth and s-s for node 4.

statistics comparing manual to sonar snow depth (inch)	18-Jan	26-Jan	2-Feb	9-Feb	18-Feb	23-Feb	3-Mar	9-Mar	16-Mar	23-Mar	29-Mar	6-Apr	13-Apr	26-Apr
Mean	19.0	28.7	32.4	33.5	29.7	29.7	36.9	30.6	30.6	22.2	11.7	19.1	5.01	2.89
Standard Error	0.06	3.50	1.30	0.43	3.69	2.89	4.48	0.90	1.83	1.93	7.76	0.96	5.01	2.89
Standard Deviation	0.09	4.95	1.84	0.61	5.22	4.09	6.33	1.27	2.59	2.73	11.0	1.36	7.08	4.09
Sample Variance	0.01	24.5	3.40	0.38	27.2	16.7	40.1	1.61	6.73	7.47	120.	1.84	50.1	16.7
Range	0.12	7.00	2.61	0.87	7.39	5.78	8.96	1.80	3.67	3.86	15.5	1.92	10.0	5.78

Table 10: Descriptive statistics comparing observed SD vs. Snowcloud generated SD (in) for node 4.

Node 5

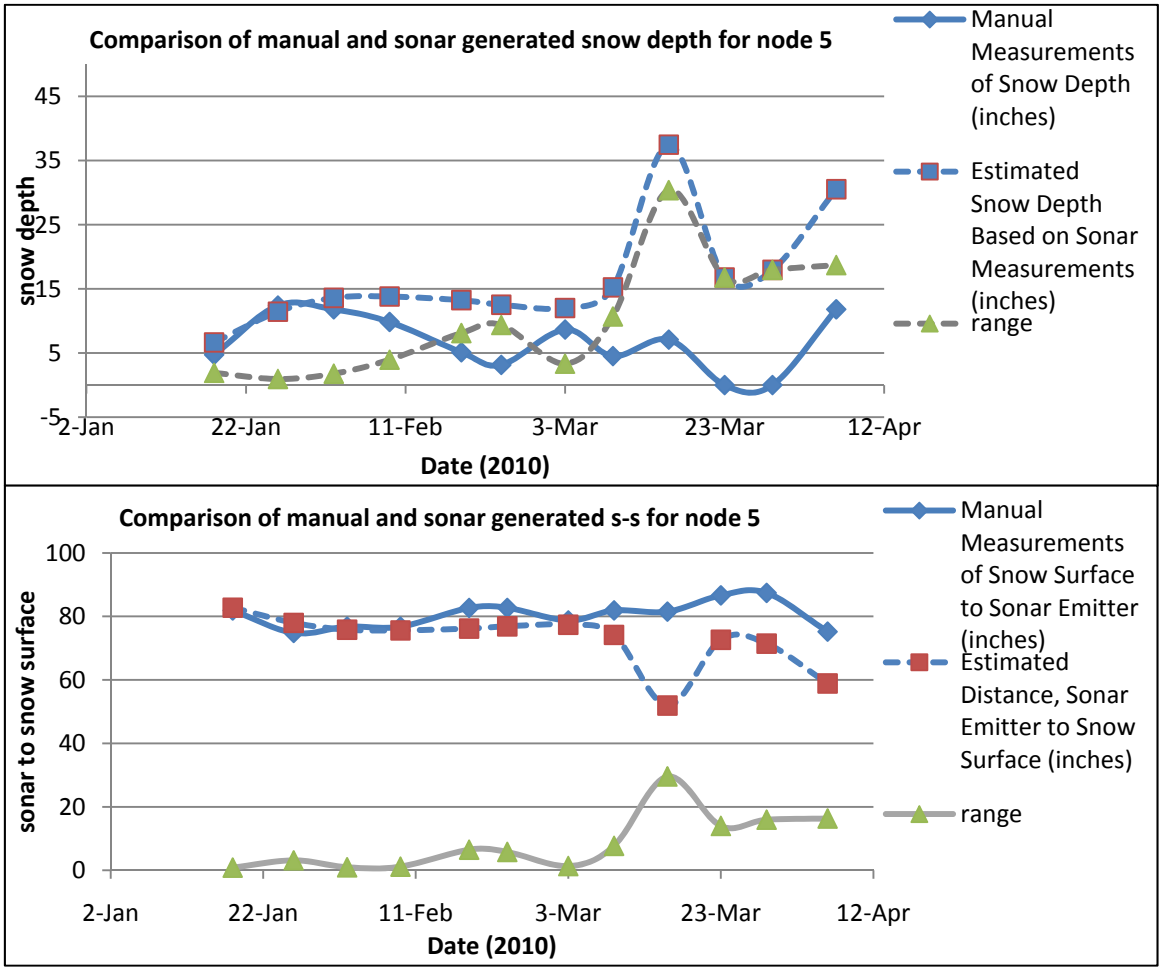

Figure 62: Comparison of manual vs. Snowcloud generated snow depth and s-s for node 5.

statistics comparing manual to sonar snow depth (inch)	18-Jan	26-Jan	2-Feb	9-Feb	18-Feb	23-Feb	3-Mar	9-Mar	16-Mar	23-Mar	29-Mar	6-Apr
Mean	5.69	11.92	12.71	11.83	9.18	7.84	10.34	9.88	22.28	8.39	8.98	21.17
Standard Error	0.96	0.48	0.89	1.98	4.06	4.69	1.67	5.35	15.19	8.39	8.98	9.35
Standard Deviation	1.36	0.68	1.26	2.81	5.74	6.63	2.37	7.57	21.48	11.86	12.70	13.23
Sample Variance	1.85	0.46	1.60	7.87	32.98	44.00	5.61	57.27	461.5	140.6	161.2	175.0
Range	1.93	0.96	1.79	3.97	8.12	9.38	3.35	10.70	30.38	16.77	17.96	18.71

Table 11: Descriptive statistics comparing observed SD vs. Snowcloud generated SD (in) for node 5.

Node 6

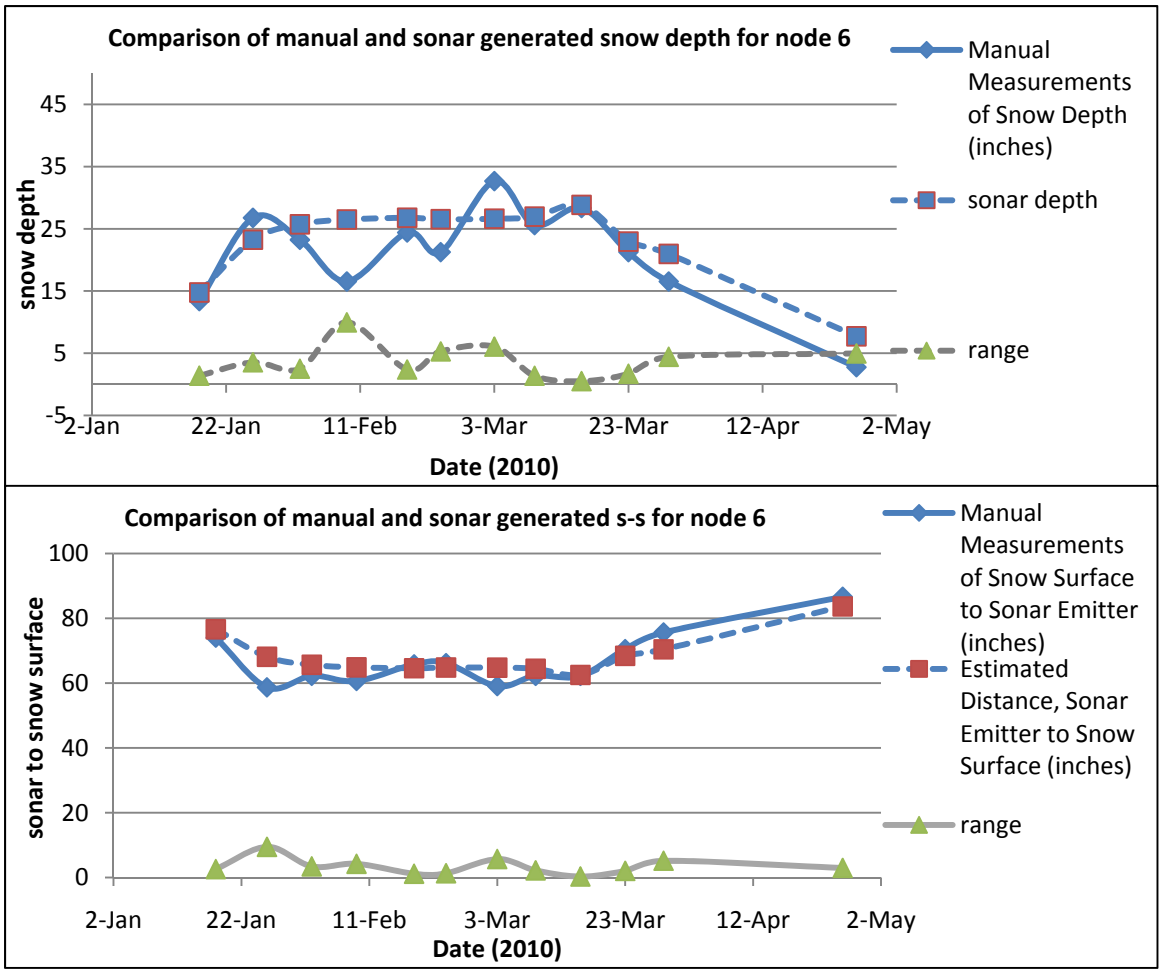

Figure 63: Comparison of manual vs. Snowcloud generated snow depth and s-s for node 6.

statistics comparing manual to sonar snow depth (inch)	18-Jan	26-Jan	2-Feb	9-Feb	18-Feb	23-Feb	3-Mar	9-Mar	16-Mar	23-Mar	29-Mar	26-Apr
Mean	14.08	25.01	24.48	21.52	25.59	23.90	29.65	26.28	28.60	22.10	18.75	5.24
Standard Error	0.69	1.77	1.25	4.98	1.19	2.65	3.03	0.68	0.25	0.85	2.21	2.48
Median	14.08	25.01	24.48	21.52	25.59	23.90	29.65	26.28	28.60	22.10	18.75	5.24
Standard Deviation	0.98	2.50	1.77	7.05	1.68	3.74	4.28	0.97	0.36	1.20	3.13	3.51
Sample Variance	0.96	6.24	3.13	49.65	2.81	13.99	18.34	0.94	0.13	1.43	9.79	12.32
Range	1.38	3.53	2.50	9.96	2.37	5.29	6.06	1.37	0.50	1.69	4.42	4.96

Table 12: Descriptive statistics comparing observed SD vs. Snowcloud generated SD (in) for node 6.

Appendix B: Site characterization

Transect 1	p1t1	p2t1	p3t1	p4t1	p5t1	p6t1	p7t1	p8t1	p9t1	P10t1	P11t1	P12t1
Canopy cover while looking north	77.08	58.3	59.3	48.9	47.9	60.4	58.3	26.0	31.2	22.92	14.58	29.17
Canopy cover while looking south	33.33	76.0	58.3	51.0	52.0	48.9	44.7	73.9	40.6	50.00	35.42	35.42
Canopy cover while looking east	69.79	23.9	41.6	55.2	66.6	60.4	71.8	54.1	68.7	62.50	36.46	36.46
Canopy cover while looking west	59.38	54.1	70.8	68.7	56.2	37.5	53.1	36.4	38.5	10.42	41.67	41.67
total	59.90	53.1	57.5	55.9	55.7	51.8	57.0	47.6	44.7	36.46	32.03	32.03

Table 13: Percentages of canopy closure in relation to aspect at each sampling point along transect 1 where p1t1 is the western most point on transect one and p12t1 is the eastern most point on transect one.

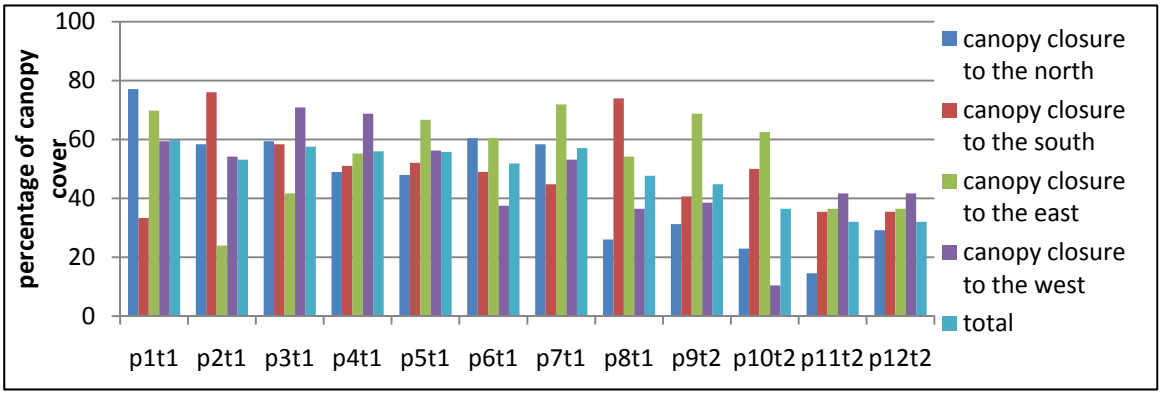

Figure 64: Bar graph comparing canopy closure on each cardinal direction at each point along transect one.

Transect 2	p1t2	p2t2	p3t2	p4t2	p5t2	p6t2	p7t2	p8t2	p9t2	p10t2	p11t2	p12t2
Canopy cover while looking north	64.58	65.6	63.5	78.1	84.3	72.9	56.2	64.5	94.7	45.83	35.41	44.79
Canopy cover while looking south	5.20	3.12	1.04	0	0	4.16	0	36.4	12.5	18.75	23.95	23.95
Canopy cover while looking east	9.37	23.9	50	0	0	14.5	3.12	45.8	3.12	0	0	0
Canopy cover while looking west	73.95	79.1	50	58.3	76.0	78.1	40.6	61.4	62.5	76.04	0	0
total	38.28	42.9	41.1	34.1	40.1	42.4	25	52.0	43.2	35.15	14.84	14.84

Table 14: Percentages of canopy closure in relation to aspect at each sampling point along transect 2 where p1t2 is the western most point on transect two and p12t2 is the eastern most point on transect two.

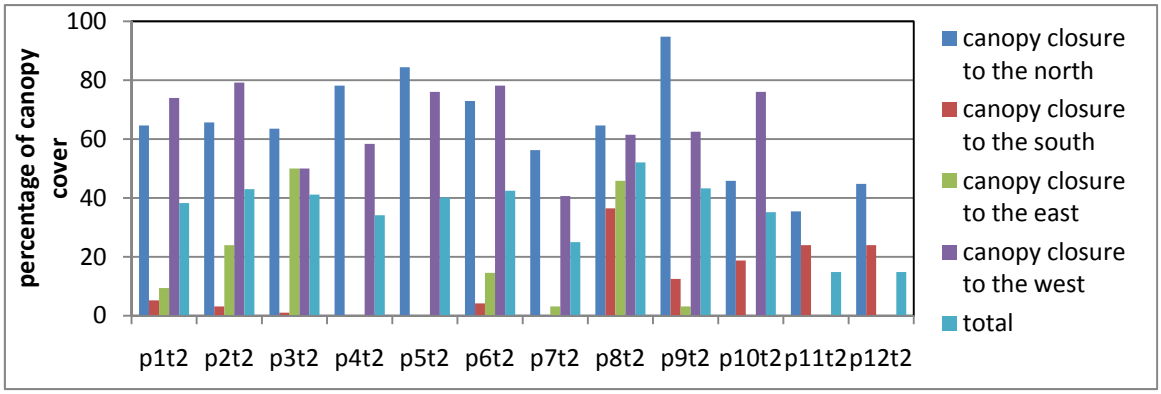

Figure 65: Bar graph comparing canopy closure on each cardinal direction at each point along transect two.

Transect 3	p1t3	p2t3	p3t3	p4t3	p5t3	p6t3	p7t3	p8t3	p9t3	p10t3	p11t3	p12t3
Canopy cover while looking north	54.16	13.5	53.1	0	13.5	10.4	4.16	7.29	19.7	8.333	11.4	3.125
Canopy cover while looking south	52.08	30.2	12.5	21.8	4.16	6.25	0	8.33	0	6.25	3.125	3.125
Canopy cover while looking east	65.62	72.9	47.9	8.33	5.20	0	0	0	0	0	0	0
Canopy cover while looking west	72.91	18.7	0	0	0	0	0	10.4	3.125	4.166	18.75	18.75
total	61.19	33.8	28.3	7.55	5.72	4.16	1.04	6.51	5.72	4.687	8.333	8.333

Table 15: Percentages of canopy closure in relation to aspect at each sampling point along transect 3 where p1t3 is the western most point on transect three and p12t3 is the eastern most point on transect three.

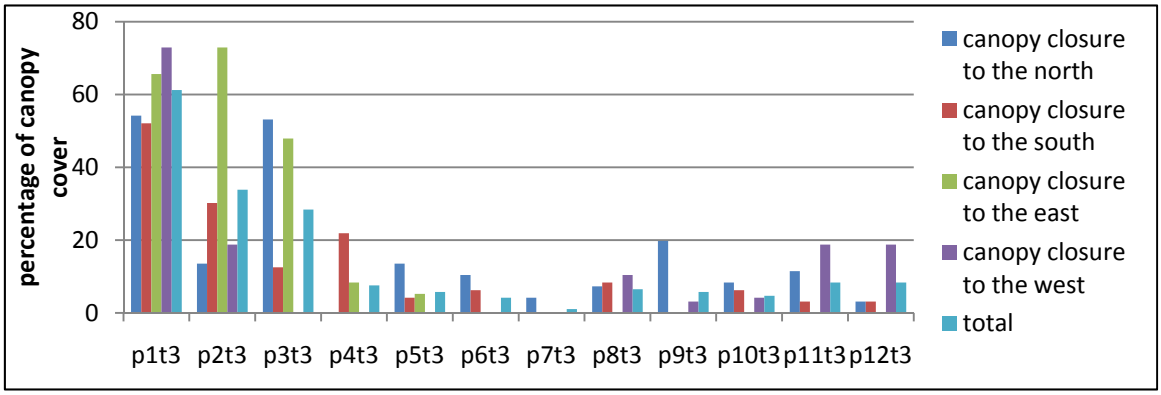

Figure 66: Bar graph comparing canopy closure on each cardinal direction at each point along transect three.

Transect 4	p1t4	p2t4	p3t4	p4t4	p5t4	p6t4	p7t4	p8t4	p9t4	p10t2	p11t4	p12t4
Canopy cover while looking north	1.041	13.5	55.2	6.25	0	0	50	2.08	14.5	25	58.33	63.54
Canopy cover while looking south	27.08	5.20	0	20.8	41.6	26.0	50	83.3	65.6	9.375	45.83	45.83
Canopy cover while looking east	0	1.04	80.2	33.3	7.29	35.4	45.8	20.8	63.5	9.375	76.04	76.04
Canopy cover while looking west	0	1.04	5.20	81.2	6.25	0	4.16	64.5	9.37	3.125	25	25
total	7.031	5.20	35.1	35.4	13.8	15.3	37.5	42.7	38.2	11.71	51.30	51.30

Table 16: Percentages of canopy closure in relation to aspect at each sampling point along transect 4 where p1t4 is the western most point on transect four and p12t4 is the eastern most point on transect four.

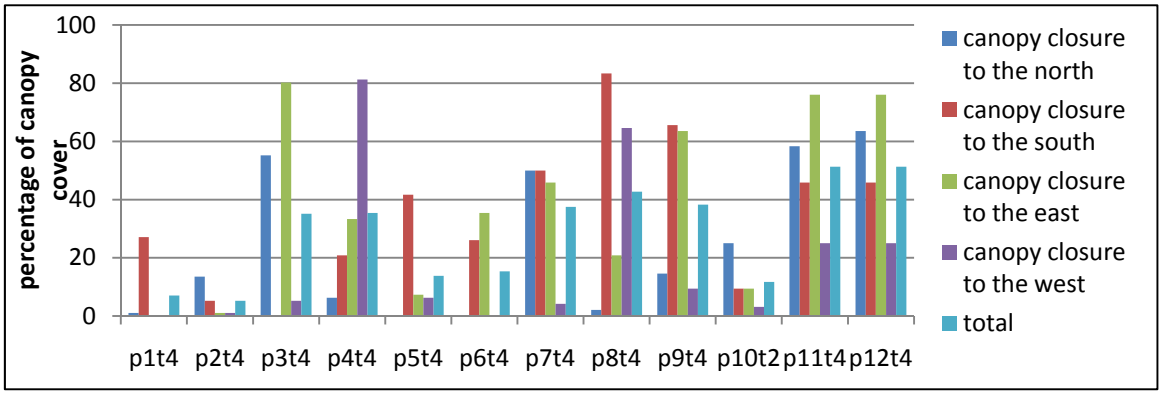

Figure 67: Bar graph comparing canopy closure on each cardinal direction at each point along transect four.

Sensor Nodes	Node 1	Node 2	Node 3	node 4	node 5	node 6
Canopy cover while looking north	50.00	6.25	2.08	12.50	60.42	56.25
Canopy cover while looking south	8.33	2.08	37.50	3.13	64.58	68.75
Canopy cover while looking east	50.00	0.00	55.21	26.04	92.71	83.33
Canopy cover while looking west	71.88	12.50	36.46	41.67	85.42	71.88
total	45.05	5.21	32.81	20.83	75.78	70.05

Table 17: Percentages of canopy closure in relation to aspect at each sensor node.

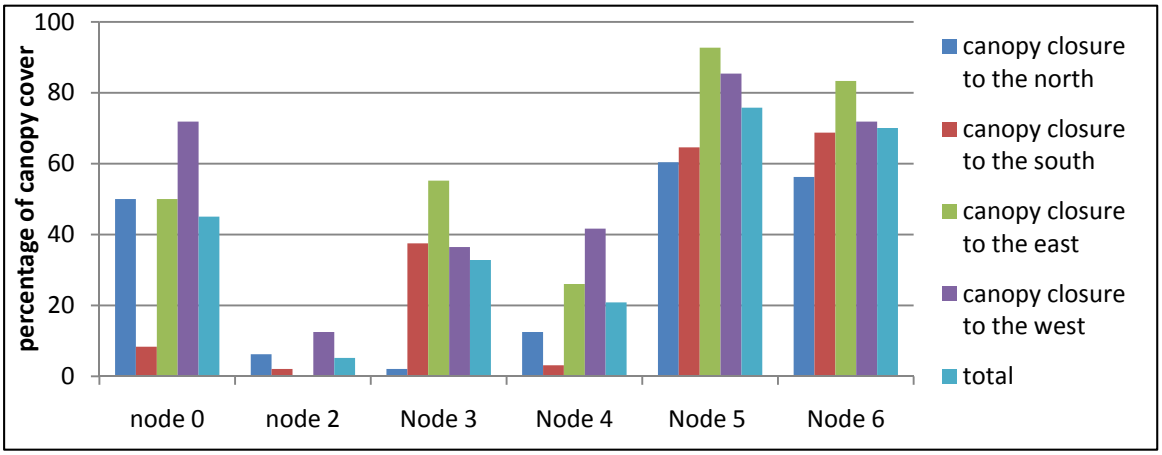

Figure 68: Bar graph comparing canopy closure on each cardinal direction at each sensor node.

Appendix C: Manual SD and SWE measurements

All manual SD and SWE measurements from January 18th 2010 to April 26th 2010 are presented below. The columns represent transects one through four, where transect one is the northern most transect and four is the southernmost transect. The rows represent the sampling points 1 to 12 along each transect where point one is the western most point and point 12 is the eastern most point. The manual SD and SWE data at each node are included after transect and sample point data.

January 18th 2010 Manual SWE Measurements												
SWE in inches	P1	P2	P3	P4	P5	P6	P7	P8	P9	P10	P11	P12
Transect one	6.11	7.40	6.44	5.79	3.86	4.83	3.22	2.57	4.18	6.11	4.83	4.02
Transect two	3.86	4.51	4.18	2.41	4.83	4.51	3.22	3.22	2.90	2.25	7.08	6.11
Transect Three	7.08	7.40	7.08	7.08	7.40	7.40	6.44	8.04	7.40	6.11	6.60	2.57
Transect Four	6.76	5.47	5.79	6.11	7.08	8.04	4.18	6.44	8.69	8.37	6.76	3.22
January 18th 2010 Manual SD Measurements												
Transect one	6.11	7.40	6.44	5.79	3.86	4.83	3.22	2.57	4.18	6.11	4.83	4.02
Transect two	3.86	4.51	4.18	2.41	4.83	4.51	3.22	3.22	2.90	2.25	7.08	6.11
Transect Three	7.08	7.40	7.08	7.08	7.40	7.40	6.44	8.04	7.40	6.11	6.60	2.57
Transect Four	6.76	5.47	5.79	6.11	7.08	8.04	4.18	6.44	8.69	8.37	6.76	3.22

January 26th 2010 Manual SWE Measurements												
SWE in inches	P1	P2	P3	P4	P5	P6	P7	P8	P9	P10	P11	P12
Transect one	9.01	9.65	11.58	10.30	10.30	8.69	5.15	4.83	8.37	6.76	8.53	9.01
Transect two	3.86	6.76	7.40	7.40	6.60	6.44	6.76	5.47	5.15	6.44	8.69	8.69
Transect Three	11.91	11.58	11.26	12.55	11.91	9.65	11.26	12.23	12.23	5.79	10.30	3.86
Transect Four	11.91	11.58	10.30	11.58	10.46	11.26	8.04	9.65	11.26	10.62	6.92	6.76
January 26th 2010 Manual SD Measurements												
Transect one	73.00	68.00	74.50	71.00	67.00	64.50	24.50	23.00	61.50	64.50	66.50	68.00
Transect two	18.50	27.50	61.00	63.00	61.00	29.00	29.00	24.00	23.00	26.00	70.00	64.00
Transect Three	79.00	76.00	74.50	77.00	75.00	70.00	75.50	77.50	77.00	30.00	65.00	15.00
Transect Four	76.00	77.00	70.00	66.50	71.00	78.00	68.00	68.00	74.00	76.00	62.50	25.50

February 2nd 2010 Manual SWE Measurements												
SWE in inches	P1	P2	P3	P4	P5	P6	P7	P8	P9	P10	P11	P12
Transect one	9.65	8.04	6.11	8.69	8.04	9.65	5.79	6.11	5.47	7.40	6.11	9.98
Transect two	3.22	5.79	6.44	6.11	6.44	6.11	6.11	4.83	4.18	6.76	11.91	8.69
Transect Three	12.23	11.26	10.62	11.58	11.26	11.26	9.98	11.26	11.91	9.01	12.23	3.86
Transect Four	12.23	11.91	10.62	9.98	8.04	11.26	9.65	9.65	12.23	9.98	7.08	7.08
February 2nd 2010 Manual SD Measurements												
Transect one	32.00	34.00	32.50	34.50	30.00	32.00	27.00	20.00	20.50	27.00	25.00	25.00
Transect two	12.00	21.00	23.00	26.00	23.00	22.00	22.00	18.00	17.00	18.50	37.00	30.00
Transect Three	42.00	39.00	38.00	42.00	39.00	39.00	40.00	41.00	40.00	34.00	34.50	15.00
Transect Four	39.50	39.50	36.00	34.00	37.00	42.00	34.00	31.00	40.00	37.00	30.00	22.50

February 9th 2010 Manual SWE Measurements												
SWE in inches	P1	P2	P3	P4	P5	P6	P7	P8	P9	P10	P11	P12
Transect one	8.69	9.98	9.65	9.01	6.11	5.47	5.79	6.11	8.69	9.65	7.08	8.04
Transect two	2.57	6.44	6.44	7.08	6.44	7.08	7.40	5.79	5.47	5.47	9.98	9.01
Transect Three	12.55	10.30	12.23	12.55	12.55	11.58	11.26	12.55	11.26	10.62	10.30	3.54
Transect Four	10.94	12.55	10.30	10.30	11.58	10.94	9.98	7.40	12.23	9.65	10.62	6.76
February 9th 2010 Manual SD Measurements												
Transect one	38.00	38.00	39.00	38.00	34.00	22.50	20.00	22.00	28.00	35.00	28.00	31.00
Transect two	12.00	22.50	24.00	28.00	23.00	24.00	27.00	19.00	18.00	20.00	36.00	32.50
Transect Three	45.00	38.00	39.00	42.00	41.00	40.00	41.00	43.00	42.50	37.00	38.00	15.00
Transect Four	40.00	42.00	37.00	39.00	44.00	44.00	37.00	32.50	45.00	43.00	38.00	23.00

February 18th 2010 Manual SWE Measurements												
SWE in inches	P1	P2	P3	P4	P5	P6	P7	P8	P9	P10	P11	P12
Transect one	10.30	11.26	10.94	10.94	9.65	6.44	4.83	4.83	4.83	7.72	9.65	8.37
Transect two	0.00	1.93	4.83	4.83	4.83	4.83	5.79	2.25	2.90	4.51	9.98	9.01
Transect Three	12.23	12.23	10.94	11.58	12.23	11.91	11.58	13.84	12.87	11.58	9.65	2.90
Transect Four	11.58	11.58	9.65	9.98	12.87	12.87	9.01	9.01	12.23	10.62	10.94	7.72

February 18th 2010 Manual SWE Measurements												
SD in inches	P1	P2	P3	P4	P5	P6	P7	P8	P9	P10	P11	P12
Transect one	32.00	32.50	34.00	32.00	31.00	24.50	17.00	16.00	17.50	22.50	28.00	26.00
Transect two	0.00	9.00	15.00	21.00	13.00	14.00	21.50	11.50	9.00	12.00	29.00	26.50
Transect Three	37.00	38.50	33.50	36.00	35.00	35.00	35.00	38.50	39.00	31.50	34.50	11.00
Transect Four	34.00	34.00	28.00	29.00	37.00	41.00	29.50	29.00	39.50	34.00	33.00	20.00

February 23 2010 Manual SWE Measurements												
SWE in inches	P1	P2	P3	P4	P5	P6	P7	P8	P9	P10	P11	P12
Transect one	10.62	10.94	10.94	9.65	10.94	4.83	4.83	6.76	9.98	8.37	9.33	7.40
Transect two	0.00	4.83	3.22	6.11	0.00	3.54	7.72	2.90	1.29	2.90	9.65	7.40
Transect Three	11.58	12.23	11.91	11.91	10.94	12.23	11.58	11.58	12.23	10.94	12.23	2.57
Transect Four	11.58	10.62	9.01	10.62	12.87	11.91	9.33	8.04	12.55	10.62	11.58	6.44
February 23 2010 Manual SD Measurements												
Transect one	31.50	33.00	34.50	32.00	32.00	16.50	17.00	19.00	25.00	29.00	27.00	22.50
Transect two	0.00	16.00	11.00	19.00	0.00	11.00	23.00	11.00	6.00	11.00	28.00	26.00
Transect Three	39.00	37.50	36.00	38.00	30.00	36.50	37.00	38.00	41.00	32.00	34.00	10.50
Transect Four	35.00	34.50	28.00	33.00	40.00	42.00	31.00	29.50	39.00	38.00	37.50	19.00

March 3rd 2010 Manual SWE Measurements												
SWE in inches	P1	P2	P3	P4	P5	P6	P7	P8	P9	P10	P11	P12
Transect one	15.93	11.91	11.58	12.23	12.23	6.11	4.83	7.40	10.30	9.98	13.19	9.98
Transect two	0.60	4.83	4.51	8.04	1.29	1.93	8.69	1.93	1.29	3.86	11.26	9.98
Transect Three	15.12	14.48	13.52	12.87	10.94	12.87	11.26	11.91	13.84	12.23	11.58	2.25
Transect Four	14.48	14.48	11.26	11.26	14.48	13.19	9.98	7.72	14.80	9.33	16.09	7.40
March 3rd 2010 Manual SD Measurements												
Transect one	47.50	44.00	37.00	44.00	47.00	27.50	23.00	23.00	30.00	37.00	42.00	34.00
Transect two	6.00	22.00	21.50	29.00	9.00	13.00	33.00	12.00	10.00	12.00	43.50	38.00
Transect Three	54.00	50.50	48.00	48.50	46.00	47.50	49.00	51.00	54.00	45.00	47.00	12.00
Transect Four	50.00	48.00	37.00	33.50	54.00	56.00	30.00	41.00	52.00	52.00	60.00	45.00

March 9th 2010 Manual SWE Measurements												
SWE in inches	P1	P2	P3	P4	P5	P6	P7	P8	P9	P10	P11	P12
Transect one	12.87	12.87	13.52	12.87	12.23	6.76	8.37	6.44	6.76	9.33	9.33	8.37
Transect two	0.00	5.47	4.51	7.40	0.00	4.83	8.37	0.97	1.61	4.83	12.87	14.16
Transect Three	15.45	14.80	13.84	13.84	12.87	14.16	13.19	12.87	15.45	11.58	14.80	4.18
Transect Four	15.12	13.84	9.65	12.55	15.12	15.45	8.04	12.55	14.80	13.19	15.45	5.79
March 9th 2010 Manual SD Measurements												
Transect one	40.00	40.00	43.00	41.00	40.00	27.50	21.00	20.00	28.00	32.00	26.50	23.50
Transect two	0.00	16.00	15.00	21.50	0.00	15.00	25.00	5.00	10.00	15.00	33.00	34.00
Transect Three	45.00	43.00	42.00	42.00	39.00	42.00	41.00	41.00	47.00	41.00	46.00	14.00
Transect Four	43.00	43.50	28.00	40.00	46.00	49.00	41.00	39.50	43.00	42.00	50.00	17.00

March 16th 2010 Manual SWE Measurements												
SWE in inches	P1	P2	P3	P4	P5	P6	P7	P8	P9	P10	P11	P12
Transect one	16.41	14.48	16.41	13.68	15.45	8.04	8.69	6.11	9.33	9.98	11.26	9.01
Transect two	0.00	0.00	2.90	7.40	0.00	2.57	5.15	0.48	1.93	1.61	12.23	11.26
Transect Three	16.09	16.09	15.45	14.80	15.45	16.41	15.12	15.77	16.09	12.87	17.38	3.86
Transect Four	16.09	15.45	10.94	11.26	16.73	17.38	14.16	15.12	15.77	16.09	21.56	8.04
March 16th 2010 Manual SD Measurements												
Transect one	45.00	41.00	48.00	45.00	44.00	20.00	26.00	32.00	33.00	34.00	33.50	27.00
Transect two	0.00	0.00	11.00	19.50	0.00	10.00	18.00	2.00	9.50	7.00	35.00	34.00
Transect Three	48.50	42.50	42.00	43.50	41.50	42.00	41.50	43.00	49.00	37.50	51.00	13.00
Transect Four	46.50	42.50	29.50	41.00	50.00	54.50	46.00	45.50	43.50	50.00	63.00	24.00

March 23rd 2010 Manual SWE Measurements												
SWE in inches	P1	P2	P3	P4	P5	P6	P7	P8	P9	P10	P11	P12
Transect one	13.52	12.23	10.62	12.23	11.91	5.15	2.90	4.83	8.37	8.69	12.23	7.40
Transect two	0.00	0.00	0.00	2.57	0.00	0.00	3.86	0.00	0.00	0.00	9.98	10.94
Transect Three	15.12	12.23	12.55	11.91	11.26	12.23	12.87	14.80	15.45	13.52	13.52	0.32
Transect Four	14.16	12.55	9.65	13.19	15.45	14.80	11.58	10.62	12.23	13.19	12.87	3.86

March 23rd 2010 Manual SWE Measurements												
SD in inches	P1	P2	P3	P4	P5	P6	P7	P8	P9	P10	P11	P12
Transect one	38.00	34.00	34.00	36.00	36.50	19.00	15.00	14.50	24.00	26.50	26.00	18.00
Transect two	0.00	0.00	0.00	8.00	0.00	0.00	14.00	0.00	0.00	0.00	26.00	29.00
Transect Three	39.00	33.00	35.50	34.50	30.00	32.50	32.50	34.00	42.00	33.50	42.50	2.00
Transect Four	39.50	36.00	22.00	35.00	42.50	44.00	36.00	38.00	35.50	41.50	40.50	19.00

March 29th 2010 Manual SWE Measurements												
SWE in inches	P1	P2	P3	P4	P5	P6	P7	P8	P9	P10	P11	P12
Transect one	14.16	10.62	12.87	12.55	10.62	5.47	3.86	3.86	8.37	9.33	8.37	3.22
Transect two	0.00	0.00	0.00	0.00	0.00	0.00	0.00	0.00	0.00	0.00	8.37	11.26
Transect Three	12.39	9.98	12.55	11.58	10.30	10.62	12.87	12.23	12.23	11.91	15.12	0.00
Transect Four	12.55	11.26	6.11	12.23	14.48	14.80	11.26	10.62	10.94	11.91	15.12	5.15
March 29th 2010 Manual SD Measurements												
Transect one	33.50	27.50	32.00	31.50	30.00	15.00	9.00	10.00	20.00	21.50	17.00	8.50
Transect two	0.00	0.00	0.00	0.00	0.00	0.00	0.00	0.00	0.00	0.00	19.00	26.00
Transect Three	31.00	27.00	30.00	27.00	27.00	25.00	28.00	28.50	36.00	30.50	39.00	0.00
Transect Four	32.00	30.50	16.00	31.50	38.00	41.00	33.00	33.00	33.00	37.50	38.50	14.00

April 6th 2010 Manual SWE Measurements												
SWE in inches	P1	P2	P3	P4	P5	P6	P7	P8	P9	P10	P11	P12
Transect one	14.16	12.55	15.77	16.09	15.12	7.24	5.15	4.51	9.01	9.98	8.69	5.15
Transect two	1.29	1.61	1.61	1.61	0.00	1.61	4.18	2.90	1.93	1.61	8.04	6.11
Transect Three	16.09	13.84	15.12	13.52	11.91	13.19	13.84	13.84	16.73	15.45	17.70	2.57
Transect Four	15.77	13.84	8.69	12.23	17.38	19.63	14.80	13.52	16.09	16.41	15.45	10.94
April 6th 2010 Manual SD Measurements												
Transect one	49.00	37.00	46.00	49.00	46.00	28.00	23.50	22.00	35.00	31.00	32.00	25.00
Transect two	5.00	9.00	10.00	11.00	0.00	9.00	20.00	15.00	10.00	10.00	34.00	27.00
Transect Three	50.00	43.50	45.00	45.00	39.00	43.50	43.00	44.00	56.00	45.00	58.00	13.00
Transect Four	49.50	49.00	32.50	43.00	55.00	56.50	50.00	44.00	53.00	56.00	55.00	30.00

April 13th 2010 Manual SWE Measurements												
SWE in inches	P1	P2	P3	P4	P5	P6	P7	P8	P9	P10	P11	P12
Transect one	12.55	15.12	17.38	15.12	11.91	6.76	4.83	3.54	7.72	6.44	7.40	4.51
Transect two	0.00	0.00	0.00	0.00	0.00	0.00	1.29	0.00	0.00	0.00	10.30	6.76
Transect Three	14.48	11.58	12.87	13.84	10.30	12.87	12.23	13.19	17.70	13.84	17.38	2.25
Transect Four	15.12	13.19	7.72	14.48	16.09	15.45	12.87	11.91	13.84	14.16	13.52	9.65
April 13th 2010 Manual SD Measurements												
Transect one	34.00	38.50	48.00	38.00	30.00	18.00	14.00	11.00	25.00	18.00	19.00	12.00
Transect two	0.00	0.00	0.00	0.00	0.00	0.00	5.00	0.00	0.00	0.00	24.00	18.50
Transect Three	38.00	29.00	34.00	32.00	24.50	31.00	28.00	30.50	43.00	34.00	45.00	3.00
Transect Four	39.00	34.50	20.00	38.50	40.50	13.00	38.50	34.00	41.00	43.00	42.50	23.00

April 19th 2010 Manual SWE Measurements												
SWE in inches	P1	P2	P3	P4	P5	P6	P7	P8	P9	P10	P11	P12
Transect one	9.65	11.58	13.52	9.98	8.37	3.22	2.25	1.93	6.76	0.00	2.57	0.00
Transect two	0.00	0.00	0.00	0.00	0.00	0.00	0.00	0.00	0.00	0.00	5.47	7.40
Transect Three	10.62	8.69	7.40	6.76	4.83	5.15	4.83	7.72	13.19	9.33	12.55	0.00
Transect Four	11.91	9.65	3.86	8.37	11.26	13.84	11.58	10.30	12.23	14.48	14.80	3.86
April 19th 2010 Manual SD Measurements												
Transect one	22.50	28.00	35.00	29.00	21.00	8.50	4.00	4.00	15.50	0.00	7.00	0.00
Transect two	0.00	0.00	0.00	0.00	0.00	0.00	0.00	0.00	0.00	0.00	14.00	15.50
Transect Three	24.00	17.00	19.50	16.00	12.00	15.00	12.00	18.00	31.00	21.00	33.50	0.00
Transect Four	26.00	22.00	8.00	20.00	29.00	33.00	31.00	31.00	28.00	38.00	39.00	13.00

April 26th 2010 Manual SWE Measurements												
SWE in inches	P1	P2	P3	P4	P5	P6	P7	P8	P9	P10	P11	P12
Transect one	7.08	9.98	11.26	9.01	4.51	0.00	0.00	0.00	3.22	1.61	0.00	0.00
Transect two	0.00	0.00	0.00	0.00	0.00	0.00	0.00	0.00	0.00	0.00	0.00	3.54
Transect Three	6.76	0.00	3.22	3.86	0.00	3.54	0.00	3.22	10.30	3.86	12.87	0.00
Transect Four	6.11	5.15	0.00	2.57	6.11	12.23	9.33	11.26	4.51	9.65	13.84	4.83

April 26th 2010 Manual SWE Measurements												
SD in inches	P1	P2	P3	P4	P5	P6	P7	P8	P9	P10	P11	P12
Transect one	19.00	23.00	30.00	22.00	11.50	0.00	0.00	0.00	6.00	3.00	0.00	0.00
Transect two	0.00	0.00	0.00	0.00	0.00	0.00	0.00	0.00	0.00	0.00	0.00	8.00
Transect Three	14.00	0.00	9.00	9.00	0.00	8.00	0.00	8.00	19.50	7.50	27.00	0.00
Transect Four	15.50	11.00	0.00	10.50	16.00	23.00	20.50	26.00	15.00	29.00	37.00	10.00

Table 18: Manual SD and SWE measurements along each point on each transect.

Manual SWE and SD measurements at each node site

	January 18th 2010			January 26th 2010			February 2nd 2010			February 9th 2010		
Measurement in inches	SD	SWE	Time	SD	SWE	Time	SD h	SWE	Time	SD	SWE	Time
Node 1	16.00	4.51	11:15	64	7.72	11:10	28.5	7.72	11:15	28.00	7.08	11:15
Node 2	29.50	9.33	12:00	75	11.91	12:00	40	11.26	12:00	41.00	10.62	12:00
Node 3	28.50	6.44	12:30	74	10.62	12:15	38	10.62	12:30	42.00	10.94	12:30
Node 4	26.00	6.11	1:30	67.5	8.69	1:30	30	9.01	1:30	30.00	8.37	1:30
Node 5	4.00	0.80	11:45	12.5	4.51	1:20	11.5	4.83	11:45	10.00	2.90	11:45
Node 6	13.00	4.83	10:30	61	8.37	10:30	20	5.15	10:00	31.00	8.04	10:00

	February 18th 2010			February 23rd 2010			March 3rd 2010			March 9th 2010		
Measurement in inches	SD	SWE	Time	SD	SWE	Time	SD	SWE	Time	SD	SWE	Time
Node 1	19.00	4.51	10:02	18.00	7.08	10:02	29.00	7.72	1:40	21.50	7.72	11:30
Node 2	34.50	11.26	10:40	35.00	11.91	10:40	47.50	9.33	2:15	38.00	12.23	11:45
Node 3	38.00	11.26	10:45	37.50	11.26	10:45	52.00	11.91	2:20	46.00	16.09	12:00
Node 4	25.00	9.98	11:02	24.00	8.69	11:02	36.00	11.91	2:40	28.00	10.62	11:45
Node 5	5.50	2.25	10:30	5.50	1.29	10:30	9.00	2.90	2:00	7.00	3.86	12:00
Node 6	25.50	9.65	9:35	26.00	8.04	9:35	35.00	10.94	1:15	31.00	10.30	11:00

	March 16th 2010			March 23rd 2010			March 29th 2010			April 6th 2010		
Measurement in inches	SD	SWE	Time	SD	SWE	Time	SD	SWE	Time	SD	SWE	Time
Node 1	20.00	8.04	11:45	9.50	3.54	10:20	0.00	0.00	10:30	12.00	2.41	10:30
Node 2	41.00	16.09	1:15	32.50	11.26	11:40	24.50	11.26	11:00	42.00	13.84	11:15
Node 3	52.00	17.38	1:20	42.00	15.12	12:00	40.00	15.45	12:00	57.00	17.70	12:15
Node 4	27.00	10.62	12:15	16.00	4.51	10:50	5.00	1.29	10:50	15.50	2.41	10:45
Node 5	9.00	4.51	1:00	0.00	0.00	11:20	0.00	0.00	10:55	14.00	1.93	12:00
Node 6	32.50	10.62	11:30	21.50	9.01	10:15	18.50	8.04	10:15	32.50	9.01	10:15

	April 13th 2010			April 19th 2010			April 26th 2010		
Measurement in inches	SD	SWE	Time	SD	SWE	Time	SD	SWE	Time
Node 1	0.00	0.00	12:00	0.00	0.00	12:00	0.00	0.00	12:00
Node 2	28.00	11.91	1:00	11.00	4.18	10:00	0.00	0.00	12:00
Node 3	46.00	15.45	1:20	37.00	14.80	11:30	26.00	9.65	11:00
Node 4	0.00	0.00	12:30	0.00	0.00	12:00	0.00	0.00	12:00
Node 5	0.00	0.00	12:45	0.00	0.00	12:00	0.00	0.00	12:00
Node 6	22.00	8.04	12:00	14.00	5.15	9:30	2.00	1.29	10:00

Table 19: Manual SD and SWE measurements at each sensor node.

Measurements at the snow pillow

January 18th 2010				January 26th 2010			February 2nd 2010			February 9th 2010		
Measurement in inches	SD	SWE	Time	SD	SWE	Time	SD	SWE	Time	SD	SWE	Time
North Side	31.00	7.08	12:30	79.00	11.91	12:20	42.00	12.23	12:30	45.00	12.55	11:00
South Side	31.00	6.76	12:30	77.50	11.58	12:20	39.50	11.91	12:30	43.00	12.23	11:00
East Side	30.50	7.40	12:30	76.00	11.58	12:20	39.00	11.26	12:30	38.00	10.30	11:00
West side	34.00	7.72	12:30	78.50	11.26	12:20	40.50	12.23	12:30	44.50	11.91	11:00
Average	31.63	7.24	12:30	77.75	**11.58**	12:20	40.25	11.91	12:30	42.63	11.75	11:00

February 18th 2010				February 23rd 2010			March 3rd 2010			March 9th 2010		
Measurement in inches	SD	SWE	Time	SD	SWE	Time	SD	SWE	Time	SD	SWE	Time
North Side	37.00	12.23	10:45	39.00	11.58	10:45	54.00	15.12	14:20	45.00	15.45	12:45
South Side	35.00	11.58	10:45	35.00	11.26	10:45	48.50	12.87	14:20	41.50	13.52	12:45
East Side	38.50	12.23	10:45	37.50	12.23	10:45	50.50	14.48	14:20	43.00	14.80	12:45
West side	37.50	12.23	10:45	39.50	13.19	10:45	54.00	15.77	14:20	44.00	14.80	12:45
Average	37.00	12.07	10:45	37.75	**12.07**	10:45	51.75	14.56	14:20	43.38	14.64	12:45

March 16th 2010				March 23rd 2010			March 29th 2010			April 06th 2010		
Measurement in inches	SD	SWE	Time	SD	SWE	Time	SD	SWE	Time	SD	SWE	Time
North Side	48.50	16.09	12:45	39.00	15.12	12:20	31.00	12.39	12:30	50.00	16.09	12:45
South Side	44.00	16.41	12:45	35.00	12.87	12:20	33.50	14.16	12:30	47.00	14.48	12:45
East Side	42.50	16.09	12:45	37.50	12.23	12:20	27.00	9.98	12:30	43.50	13.84	12:45
West side	48.00	16.41	12:45	39.50	12.87	12:20	31.50	14.48	12:30	48.50	15.45	12:45
Average	45.75	16.25	12:45	35.75	**13.27**	12:20	30.75	12.75	12:30	47.25	14.96	12:45

April 13th 2010				April 19th 2010			April 26th 2010		
Measurement in inches	SD	SWE	Time	SD	SWE	Time	SD	SWE	Time
North Side	38.00	14.48	11:00	24.00	10.62	11:30	14.00	6.76	10:30
South Side	35.00	15.12	11:00	18.50	8.04	11:30	9.00	3.54	10:30
East Side	29.00	11.58	11:00	17.00	8.69	11:30	0.00	0.00	10:30
West side	29.00	11.91	11:00	22.00	9.98	11:30	10.00	4.51	10:30
Average	32.75	13.27	11:00	20.38	**9.33**	11:30	8.25	3.70	10:30

Table 20: Manual SD and SWE measurements on each side of the snow pillow.

Descriptive Statistics comparing the averaged manual measurements to the snow pillow corrected for an initial calibration bias (-0.807 in).

	18-Jan	*26-Jan*	*2-Feb*	*9-Feb*	*18-Feb*	*23-Feb*	3-Mar	9-Mar
Mean	7.48	12.00	11.95	12.36	12.28	12.47	15.18	7.48
Standard Error	0.24	0.42	0.04	0.61	0.22	0.40	0.62	0.24
Standard Deviation	0.33	0.60	0.05	0.86	0.31	0.57	0.88	0.33
Sample Variance	0.11	0.36	0.00	0.74	0.10	0.32	0.77	0.11
Range	0.47	0.84	0.07	1.22	0.44	0.80	1.24	0.47

	9-Mar	10-Mar	11-Mar	29-Mar	6-Apr	13-Apr	19-Apr	26-Apr
Mean	15.13	16.56	13.70	12.66	15.37	13.63	8.88	3.69
Standard Error	0.49	0.31	0.43	0.09	0.41	0.35	0.45	0.40
Standard Deviation	0.69	0.43	0.61	0.13	0.57	0.50	0.64	0.57
Sample Variance	0.48	0.19	0.37	0.02	0.33	0.25	0.41	0.33
Range	0.98	0.61	0.86	0.18	0.81	0.71	0.91	0.81

Table 21: Descriptive statistics comparing the averaged manual measurements each week with the snow pillow data output minus 0.807 inches.

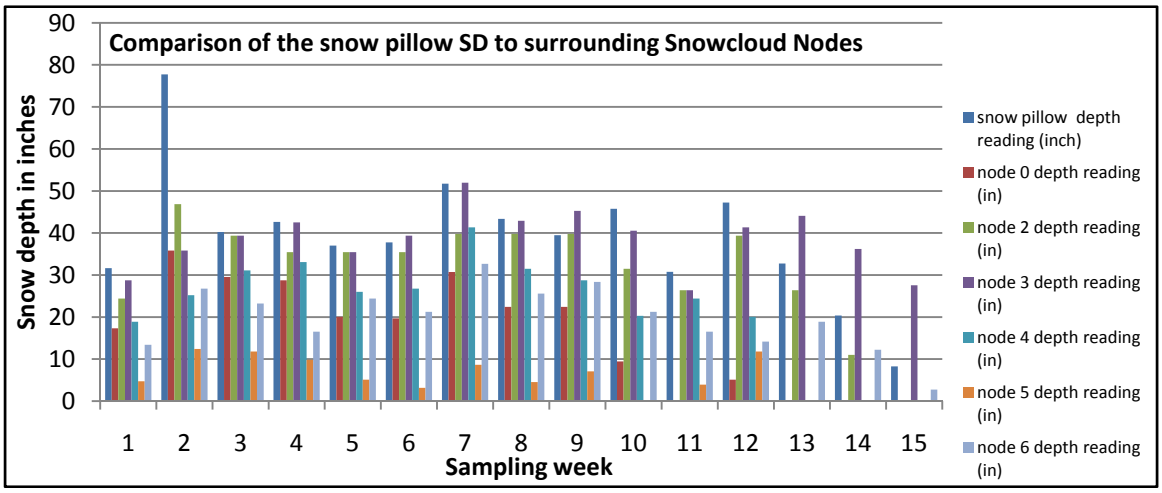

Figure 69: Comparison of manual SD measurements around the onsite snow pillow to the surrounding Snowcloud nodes where sampling week one represents 18-Jan 2010 and sampling week 15 represents 26-Apr, 2010.

Appendix D: Correspondence and regression analysis

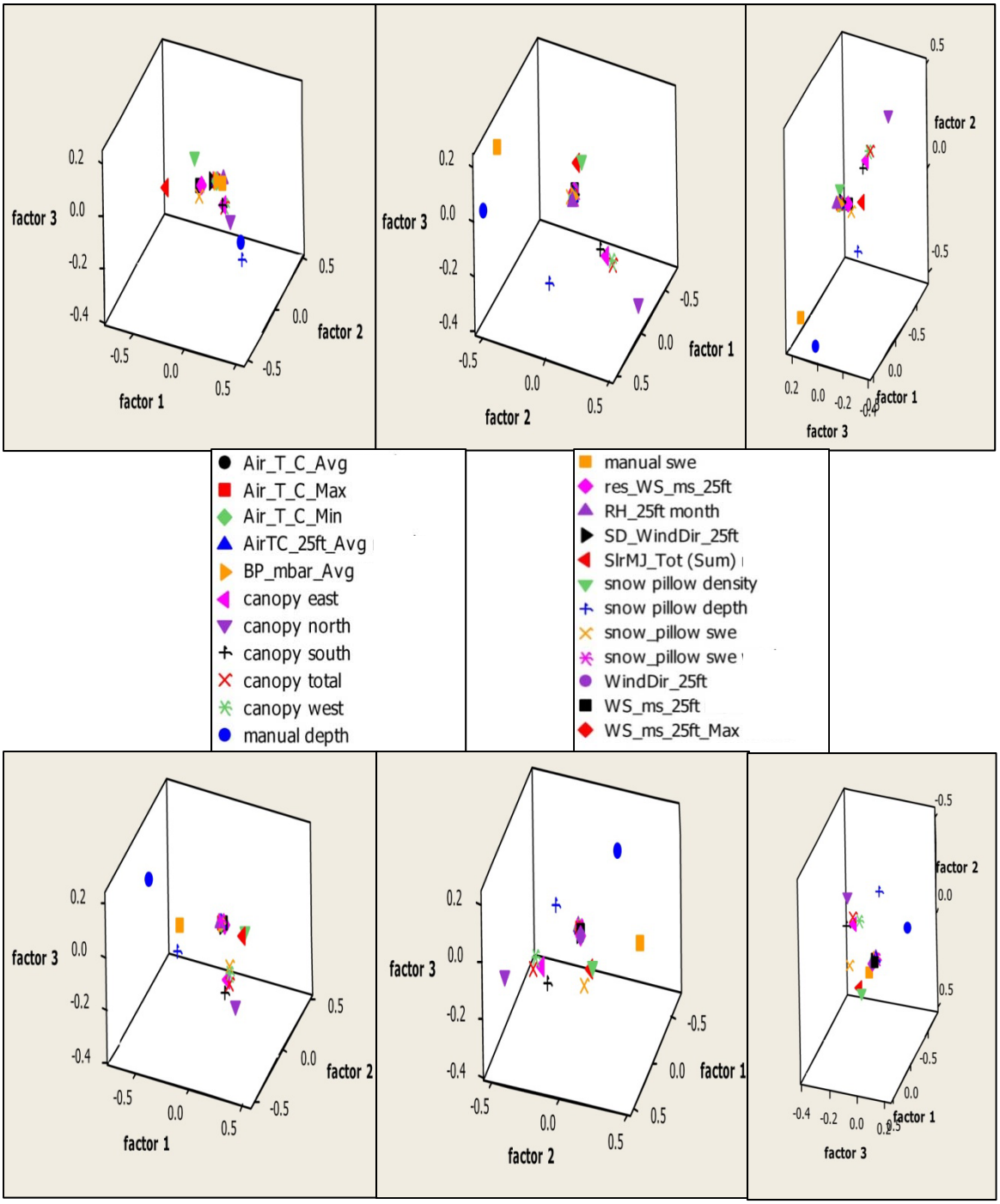

Figure 7: 3- Dimensional correspondence analysis graphs of the monthly seasonal data series (on the top row) and the seasonal running average data series (on the bottom row) with all tower one data collected 25 feet and lower.

Appendix E: Kriging

The below text is Python command script used to run the automation of the ArcGIS kriging processes. These script commands also create confidence intervals from raster variance output files and create contour intervals of desired weights to act as confidence values overlayed on each kriged raster output.

```
import arcgisscripting
gp = arcgisscripting.create()

# Directory that master table is saved at
gp.workspace = "C:\sagehen_creek\sagehen_final\data"
gp.toolbox = "management"

# Make script to overwrite files
gp.overwriteoutput = 1

print "Started processing ...."

## mote's IDs
m1 = str(1)
m2 = str(2)
m3 = str(3)
m4 = str(4)
m5 = str(5)
m6 = str(6)
m7 = str(7)

# Add field to master table
## You may have to change master table file name here
gp.addfield ("SWE_SD_A.dbf", "order", "long", "5")

# For mote 1 "1"
# Query with 1 and make temp table
query1 = '"ID" =' + m1
gp.maketableview("SWE_SD_A.dbf", "temp1.dbf", query1)
# Copy the table view to a new table
gp.copyrows("temp1.dbf", m1 + ".dbf")

# For mote 2 "2"
query2 = '"ID" =' + m2
gp.maketableview("SWE_SD_A.dbf", "temp2.dbf", query2)
gp.copyrows("temp2.dbf", m2 + ".dbf")
```

```
# For mote 3 "3"
query3 = '"ID" =' + m3
gp.maketableview("SWE_SD_A.dbf", "temp3.dbf", query3)
gp.copyrows("temp3.dbf", m3 + ".dbf")

# For mote 4 "4"
query4 = '"ID" =' + m4
gp.maketableview("SWE_SD_A.dbf", "temp4.dbf", query4)
gp.copyrows("temp4.dbf", m4 + ".dbf")

# For mote 5 "5"
query5 = '"ID" =' + m5
gp.maketableview("SWE_SD_A.dbf", "temp5.dbf", query5)
gp.copyrows("temp5.dbf", m5 + ".dbf")

# For mote 6 "6"
query6 = '"ID" =' + m6
gp.maketableview("SWE_SD_A.dbf", "temp6.dbf", query6)
gp.copyrows("temp6.dbf", m6 + ".dbf")

# For mote 7 "7"
query7 = '"ID" =' + m7
gp.maketableview("SWE_SD_A.dbf", "temp7.dbf", query7)
gp.copyrows("temp7.dbf", m7 + ".dbf")

print "Please wait ...."

# Expression for copying OID to new field
expression= "[OID]"

# For mote 1
# Copy ID
gp.CalculateField_management(m1 + ".dbf", "order_", expression, "VB")

# For mote 2
gp.CalculateField_management(m2 + ".dbf", "order_", expression, "VB")

# For mote 3
gp.CalculateField_management(m3 + ".dbf", "order_", expression, "VB")

# For mote 4
gp.CalculateField_management(m4 + ".dbf", "order_", expression, "VB")

# For mote 5
gp.CalculateField_management(m5 + ".dbf", "order_", expression, "VB")

# For mote 6
gp.CalculateField_management(m6 + ".dbf", "order_", expression, "VB")
```

```
# For mote 7
gp.CalculateField_management(m7 + ".dbf", "order_", expression, "VB")

# Merge all seven tables
gp.Merge(m1 + ".dbf;" + m2 + ".dbf;" + m3 + ".dbf;" + m4 + ".dbf;" + m5 + ".dbf;" + m6 +
".dbf;" + m7 + ".dbf", "merged.dbf" , "order")

## Set output folder for mutiple tables to be saved
outspace = "C:\sagehen_creek\sagehen_final\Tables"

print "Processing creating tables now ...."
print "Please wait ....."

#This section will export each table by each time stamp
s = gp.GetCount_management(m1 + ".dbf")
l = range(s)
for n in l:

   if n < 10:
      query = '"order_" = ' + str(n)
      gp.maketableview("merged.dbf", "temp_m.dbf", query)
      output = outspace + "/T0" + str(n) + ".dbf"
      gp.copyrows("temp_m.dbf", output)

   else:
      query = '"order_" = ' + str(n)
      gp.maketableview("merged.dbf", "temp_m.dbf", query)
      output = outspace + "/T" + str(n) + ".dbf"
      gp.copyrows("temp_m.dbf", output)

else:
   print "Table creation is done!!"

#---------------------------------------------------------------------------
# Now below here are the kriging steps

# Check out any necessary licenses
gp.CheckOutExtension("spatial")

# Set the input workspace
# Where the tables are saved
##
## Where each table is saved
gp.workspace = "C:\sagehen_creek\sagehen_final\Tables"

# Python will overwrite exsisting outputfiles
gp.overwriteoutput = 1

print "Now start kriging......."
```

```
# Load required toolboxes...
gp.AddToolbox("C:/Program Files/ArcGIS/ArcToolbox/Toolboxes/Spatial Analyst Tools.tbx")
gp.AddToolbox("C:/Program Files/ArcGIS/ArcToolbox/Toolboxes/Data Management
Tools.tbx")

# Set the output workspace, replace baip by your own username
##
outWorkspaceKriging = "C:\sagehen_creek\sagehen_final\Kriging"
outWorkspaceVariance = "C:\sagehen_creek\sagehen_final\Variance"

try:

   # Get a list of the tables in the input folder
   fcs = gp.ListTables()

   # Loop through the list of dbf tables
   # Do not edit this part
   fcs.Reset()
   fc = fcs.Next()

   while fc:

      print "Processing " + fc.split('.')[0] + "'s Kriging and Variance..."

      # Set the output raster, such as 01_Krig
      outRasterKrig = outWorkspaceKriging + "/K" + fc.split('.')[0]
      outRasterVar = outWorkspaceVariance + "/V" + fc.split('.')[0]

      # Set temporary layer, such as 01_layer
      fc_layer = fc.split('.')[0] + "_layer"

      # Set Spatial reference
      Sp_Ref =
"GEOGCS['GCS_WGS_1984',DATUM['D_WGS_1984',SPHEROID['WGS_1984',6378137.0,29
8.257223563]],PRIMEM['Greenwich',0.0],UNIT['Degree',0.0174532925199433]];IsHighPrecisio
n"
      # Process: Make XY Event Layer...
      gp.MakeXYEventLayer_management(fc, "LONG", "LAT", fc_layer, Sp_Ref)

      # Process: Kriging... change model, size, nugget, class size, range and sill here
      gp.Kriging_sa(fc_layer, "pd", outRasterKrig, "spherical", "0.000001", "0.4496", "2.6185",
"16.05", "VARIABLE 3", outRasterVar)


      fc = fcs.Next()

   print "The Kriging process is successfully completed!"
```

```
except:

    gp.AddMessage(gp.GetMessages(2))
    print gp.GetMessages(2)


#---------------------------------------------------------------------------
# Now make 95% Confidence Interval

print "Now Start making 95% Confidence Interval....."

# Set the input workspace
# where the tables are saved
# ensure you have saved each table for each time frame
##
## Where Variance raster are saved
gp.workspace = "C:\sagehen_creek\sagehen_final\Variance"

# This is the temporary raster output space.  It will be erased on each loop.
##
##
outWSpp = "C:\sagehen_creek\sagehen_final\Temp"

# This is 95% confidence interval raster output directory
##
##
out95per = "C:\sagehen_creek\sagehen_final\ConfiInter"

try:

    #Get a list of the tables in the input folder
    rts = gp.ListRasters("", "GRID")

    #Loop through the list of rasters
    rts.Reset()
    rt = rts.Next()

    while rt:

        print "Processing " + rt + "'s 95% confidence interval..."

        # Set Output raster
        #
        outpp = outWSpp + "/temp"
        out95 = out95per + "/P" + rt.split('v')[1]

        # This calculates 1.96 * squareroot of Variance,
        # which is 95% confidence interval
        gp.SquareRoot_sa(rt, outpp)
```

```
        gp.times_sa(outpp, 1.96, out95)

        # This deletes/cleans temporary raster output
        gp.delete_management(outpp)

        # Move on to next grid in the list
        rt = rts.Next()

    print "The 95% confidence interval process is successfully completed!"

except:

    gp.AddMessage(gp.GetMessages(2))
    print gp.GetMessages(2)


#---------------------------------------------------------------------------
# Then Create Contour lines
##
##  Where the confidence interval raster are saved
gp.workspace = "C:\sagehen_creek\sagehen_final\ConfiInter"

# Set the output workspace, replace baip by your own username
# This is contour line output directory
##
##
outCon = "C:\sagehen_creek\sagehen_final\Contour"

try:

    # Get a list of the tables in the input folder
    rts = gp.ListRasters("", "GRID")

    # Loop through the list of rasters
    rts.Reset()
    rt = rts.Next()

    while rt:

        print "Processing " + rt + "'s contour lines..."

        # Set Output raster
        outContourShape = outCon + "/con" + rt.split('p')[1]

        # Contour List for break points
        ##
        ## change range as you want
        InContourList = "1.0; 2.0; 3.0; 4.0; 5.0"
```

```
        # Process contour lines
        gp.ContourList_sa(rt, outContourShape, InContourList)


        # Move on to next grid in the list
        rt = rts.Next()

    print "The contour line process is successfully completed!"

except:

    gp.AddMessage(gp.GetMessages(2))
    print gp.GetMessages(2)
```